Ref. Ares(2022)7879257 - 15/11/2022

TURNkey - Towards more Earthquake-resilient Urban Societies through a Multi-sensor-based Information System enabling Earthquake Forecasting, Early Warning and Rapid Response actions

This project has received funding from the European Union's Horizon 2020 research and innovation programme under grant agreement No 821046

Towards more Earthquake-resilient Urban Societies through a Multi-sensor-based Information System enabling Earthquake Forecasting, Early Warning and Rapid Response actions

TURNkey

Deliverable D 4.2

Report on recommendations on fragility functions for buildings and infrastructure components to be used in rapid response context

Authors:	Alexandru Tiganescu, Ali G. Ozcebe, Alireza Kharazian, Antonella Di Meo, Antonino Famà, Atefe Darzi, Barbara Borzi, Benedikt Halldórsson, Bjarni Bessason, Caterina Negulescu, Dina D'Ayala, Dragos Toma-Danila, Francesca Bozzoni, Georgia Giannaraki, Li Sun, Mandy Korff, Mario Martinelli, Marta Faravelli, Nikolaos Melis, Pierre Gehl, Rosemary Fayjaloun, Sergio Molina Palacios, Stefan Florin Balan.
Reviewers:	Jochen Schwarz, Lars Abrahamczyk
Responsible Partner:	EUCENTRE
Version:	1.1
Date:	25/10/2022
Distribution level:	Public

This project has received funding from the European Union's Horizon 2020 research and innovation programme under grant agreement No 821046

DOCUMENT REVISION HISTORY

Date	Version	Editor	Comments
25/10/2022	1.1	Final Version Update	Minor Changes
31/03/2021	1.0	Final Version	

LIST OF PARTNERS

Participant	Name	Country
NOR	Stiftelsen NORSAR	Norway
DEL	Stichting Deltares	Netherlands
KNMI	Koninklijk Nederlands Meteorologisch Instituut	Netherlands
BRGM	Bureau de Recherches Géologiques et Minières	France
EMSC	Euro-Mediterranean Seismological Centre	France
UIce	Haskoli Islands (University of Iceland)	Iceland
EUC	Fondazione Eucentre	Italy
UStr	University of Strathclyde	UK
BUW	Bauhaus-Universität Weimar	Germany
UA	Universidad de Alicante	Spain
ARU	Anglia Ruskin University Higher Education Corporation	UK
UNIBG	Università degli Studi di Bergamo	Italy
UCL	University College London	UK
INFP	Institutul National de Cercetare si Dezvoltare pentru Fizica Pamantului	Romania
YET	YetItMoves S.r.l.	Italy
GMP	Gempa GmbH	Germany
NOA	National Observatory of Athens	Greece
NTC	Nutcracker Research Ltd.	UK
B80	Beta 80 SpA	Italy
Sim	Siminn hf.	Iceland
UPat	Panepistimio Patron (University of Patras)	Greece

GLOSSARY

Acronym	Description
TB(s)	Testbeds
RC	Reinforced Concrete
DPMs	Damage Probability Matrices
CSM	Capacity Spectrum Method
MCS	Mercalli-Cancani-Sieberg
MSK	Medvedev–Sponheuer–Karnik
IM	Intensity Measure
PGA_{cond}	Peak Ground Acceleration; "cond" stands for the condition, e.g. PGA_{rock} when the PGA is referred to rock, PGA_{ampl} when PGA is referred to free surface
PGV_{cond}	Peak Ground Velocity; "cond" stands for the condition, e.g. PGV_{rock}
$Sd_{T,\ cond}$	Spectral displacement at the specified period "T"; "cond" stands for the condition, e.g. $Sd_{1sec,\ rock}$
$Sa_{T,\ cond}$	Spectral acceleration at the specified period "x"; "cond" stands for the condition, e.g. $Sd_{1sec,\ rock}$
PGD	Permanent Ground Displacement

This project has received funding from the European Union's Horizon 2020 research and innovation programme under grant agreement No 821046

SDOF	Single Degree Of Freedom
MDOF	Multi Degree Of Freedom
D	Damage level
α	Median of the lognormal distribution
β	Standard deviation of the lognormal distribution
GMPE	Ground Motion Prediction Equation
GIS	Geographical Information System
DLS	Damage Limit State
CLS	Collapse Limit State
NLS	Nonlinear Static Analysis
NLD	Nonlinear Dynamic Analysis
SMM	Simplified Mechanic Method
DPMs	Damage Probability Matrices
CAV	Cumulative Absolute Velocity
SSI	Soil-Structure Interaction
I	Macroseismic Intensity
PEER	Pacific Earthquake Engineering Research
PBEE	Performance-Based Earthquake Engineering
Vs30	Shear wave velocity in the top 30 m of soil
RMS	Root Mean Square

This project has received funding from the European Union's Horizon 2020 research and innovation programme under grant agreement No 821046

INDEX OF CONTENTS

This project has received funding from the European Union's Horizon 2020 research and innovation programme under grant agreement No 821046

This project has received funding from the European Union's Horizon 2020 research and innovation programme under grant agreement No 821046

INDEX OF FIGURES

This project has received funding from the European Union's Horizon 2020 research and innovation programme under grant agreement No 821046

INDEX OF TABLES

This project has received funding from the European Union's Horizon 2020 research and innovation programme under grant agreement No 821046

This project has received funding from the European Union's Horizon 2020 research and innovation programme under grant agreement No 821046

1 INTRODUCTION

Aiming at presenting the main outcomes of Subtask 4.1.2 (*Ranking and enhancement of existing fragility models for buildings and infrastructure components*) of TURNkey project, this document reports an exhaustive state-of-the-art compilation of the most representative seismic fragility and loss estimation models for the buildings and infrastructure components in the testbeds (TBs in the following) of the TURNkey project. Indeed, this activity is included within the Work Package 4, aimed at developing and harmonizing seismic physical vulnerability and loss estimation models for structures and infrastructure components within a rapid loss prediction framework. Within a broader context, it may be stated that the contents of this Deliverable may also be extrapolated as a useful synthesis of the structural vulnerability standing for the entire European territory.

In Chapter 2, first a detailed list of the fragility and loss estimation models adopted for building taxonomies and infrastructure components is tabulated together with their associated publication/reference and a brief description of the corresponding work. Then, futher important information is syntesized in terms of type, structural typology, intensity measure, damage scale, and the region of applicability referring to each individual fragility/loss model under consideration.

In Chapter 3, in-depth information and discussion of the vulnerability and loss estimation models presented in Chapter 2 are provided for each TB. Furthermore, background exposure information is also provided. Organization of this Chapter follows the order of the TB numeration adopted in TURNkey project, hence it is sorted in the respective order of 3.1. TB1-Bucharest (Romania), 3.2. TB2-Pyrenees (France), 3.3. TB3-Hveragerði (Southern Iceland) and Húsavík (Northern Iceland), 3.4. TB4-Patras and Aegio area (Greece), 3.5. TB5-Port of Gioia Tauro (Italy)[1], 3.6. TB6- Groningen (Netherlands). Last but not least, it is worth to note the attention paid in unified representation of the fragility models through the statement of statistical parameters (α median,β standard deviation) of the cumulative density functions used for idealization purposes and clear description of the intensity measure under consideration.

Chapter 4 presents the conclusive summary of the Deliverable.

[1] It is noted that being different than the remaining TBs, TB5 provides vulnerability information of the specific port configuration and overlying crane, the fragility models of which are specifically developed within the TURNkey project.

This project has received funding from the European Union's Horizon 2020 research and innovation programme under grant agreement No 821046

2 LITERATURE REVIEW ON PHYSICAL VULNERABILITY ESTIMATION MODELS

2.1 Fragility models

Fragility functions describe the probability that a structure or an infrastructure component will reach a certain level of damage following a given ground shaking. They are usually represented as two-parameter (media and log-standard deviation) cumulative lognormal distributions. Different methods can be used to develop fragility functions, including empirical, judgmental, analytical and hybrid approaches. Analytical fragility curves adopt damage distributions simulated from the analyses of structural models under increasing earthquake loads as their statistical basis. They become widely used since they are more readily applicable to different structural/infrastructural types and to geographical regions where damage records are insufficient.
A literature review was carried out to identify the fragility models developed for buildings and infrastructure components, which are included in the platform. In this paragraph, the main findings from this review are presented. In particular, §2.1.1 refers to buildings and §2.1.2 refers to infrastructures (bridges and port facilities).

2.1.1 Buildings

In Table 2.1 a list of existing fragility models found in literature for the buildings are described. In Table 2.2 the fragility models related to the SERA Taxonomy are reported.

Table 2.1: Existing fragility models for buildings in the literature.

Reference	Methodology	Building Structural Typology
Whitman (1973)	For each building, designs were prepared using the seismic requirements of the Uniform Building Code. The study was done in two stages. Firstly, an actual existing 13-story steel frame building («pilot building») was redesigned for various levels of earthquake resistance. Then designs were prepared for a series of hypothetical buildings («prototype buildings») having dimensions and layout typical of apartment buildings now being constructed in the Boston area.	The Damage Probability Matrices (DPMs) presented in this report are intended to apply to five - to twenty-story buildings with RC frames or shear walls or steel frames.
Braga et al. (1982)	These are the first DPMs produced in Italy as a result of the statistical treatment of the damage data collected in the municipalities affected by the Irpinia earthquake in 1980. A DPM expresses what will happen to buildings, designed according to some particular set of requirements, during earthquakes of various intensities.	There are three classes of structures: i.e., A, B, C, identified on the basis of vertical and horizontal structural elements. In particular: - Class A: fiel stone/hewn stone/brick masonry and vaults, fiel stone/hewn stone and wooden floors; - Class B: fiel stone/hewn stone and steel floors; - Class C: briek masonry and wooden floors, brick masonry and steel floors, fiel stone/ hewn stone/ brick masonry/reinforced concrete and RC floors.

This project has received funding from the European Union's Horizon 2020 research and innovation programme under grant agreement No 821046

Di Pasquale et al. (1998)	In order to produce DPMs, the Italian National Seismic Service has processed the Irpinia 1980 database. Main differences between Di Pasquale et al. (1998) and the original version of DPMs proposed in Braga et al. (1982) consist in: - The use of dwellings instead of buildings; - The earthquake intensity in terms of MCS (Mercalli–Cancani–Sieberg) scale instead of the MSK (Medvedev–Sponheuer–Karnik) scale; - Different classes of structures.	There are four classes of structures: i.e., A, B, C1, C2, identified on the basis of vertical and horizontal structural elements. In particular: - Class A: fiel stone/hewn stone/brick masonry and vaults, fiel stone/hewn stone and wooden floors; - Class B: brick masonry and wooden floors, fiel stone/hewn stone and steel floors, field stone and RC floors; - Class C1: brick masonry and steel floors, hewn stone/brick masonry and RC floors; - Class C2: reinforced concrete vertical and horizontal structural elements .
Sabetta et al. (1998)	They used post-earthquake surveys of approximately 50000 buildings damaged by destructive Italian earthquakes in order to derive vulnerability curves. The database was sorted into three structural classes and six damage levels according to the MSK macroseismic scale. A mean damage index, calculated as the weighted average of the frequencies of each damage level, was derived for each municipality where damage occurred and each structural class. Empirical fragility curves with a binomial distribution were derived as a function of PGA, Arias Intensity and effective peak acceleration	Three structural classes: i.e., A, B, C. These classes are the same of those in Di Pasquale et al. (1998) but class C1 and class C2 have merged into the only class C.
Lagomarsino and Giovinazzi (2006)	They have developed DPMs from European Macroseismic Scale (EMS98; Grüntal et al., 1998) that provides a model for the estimation of the earthquake impact from the observed damage on buildings considering five levels of damage, besides the absence of damage.	There are ten classes: - M1: Rubble stone - M2: Adobe (earth bricks) - M3: Simple stone - M4: Massive stone - M5: Unreinforced Masonry (old bricks) - M6: Unreinforced Masonry – RC floors - M7: Reinforced/confined masonry - RC1: Concrete Moment Frame - RC2: Concrete Shear Walls - RC3: Dual System.
Rota et al. (2008)	They have used data obtained from post-earthquake damage surveys carried out in various municipalities over the past 30 years in Italy in order to derive typological fragility curves for typical building classes. Observational DPMs were first produced and then processed to obtain lognormal fragility curves that relate the probability of reaching or exceeding a given damage state to the mean PGA defined in the municipality where the damaged buildings were located.	The structural typologies taken into account are: - Masonry (regular and irregular layout, rigid and flexible floors, with or without rods) - RC (seismic and no-seismic designed) - Steel - Mixed.
Singhal and Kiremidjian (1996)	They present a systematic approach for estimating fragility curves and DPMs for different structural systems. This method is based on nonlinear dynamic analysis of the structure. The ground motion level for fragility curves is characterized by spectral acceleration. For damage probability matrices, modified Mercalli intensity is used as the ground motion parameter. The probabilities associated with the different damage states at a specified ground motion level are evaluated using the Monte Carlo-simulation technique. The nonstationary autoregressive moving average model is used for the generation of earthquake time histories.	RC frames. Three different classes of RC frames, based on the number of stories, are considered (Low-rise: 2 floors, Mid-rise: 5 floors, High-rise: 12 floors).

This project has received funding from the European Union's Horizon 2020 research and innovation programme under grant agreement No 821046

HAZUS (FEMA 2003)	The Capacity Spectrum Method (CSM) was proposed for the first time in HAZUS (FEMA, 2003). The CSM is based on the comparison between the capacity curve and the demand curve in the acceleration-displacement plane. The intersection between the two curves is the performance point, i.e. the maximum expected displacement corresponding to an assigned seismic event. In HAZUS (FEMA, 2003) the capacity curves are obtained from the pushover curves, derived from non-linear static analyses on typical American prototype structures. The main limitation of this method is that the variability of the curves is given through a combination of performance data, earthquake field data, expert opinion and judgment.	In this Manual many typologies of structures are taken into account.
Bernardini et al. (1990)	The VULNUS method allows estimating the seismic vulnerability of a single building using the fuzzy-set theory and the definition of collapse multipliers. This method was recently modified according to the Italian Seismic Code and written in Visual Basic programming language. The approach is based on building survey, in order to collect geometrical and structural information, handled through qualitative judgment. VULNUS estimates the global vulnerability of regular (both in plan and in height) masonry structures with a limited number of storeys. It applies either to single buildings or building aggregates. The major limitation of this method is the static treatment of the dynamic seismic action.	Masonry building
Erberik (2008)	They focused on the seismic safety evaluation of masonry buildings in Turkey for in-plane failure modes using fragility curves. Masonry buildings are classified and a set of fragility curves are generated for each class. The fragility curves are generated by using time history (for demand) and pushover (for capacity) analyses. From the generated sets of fragility curves, it is observed that the damage state probabilities are significantly influenced from the number of stories and wall material strength.	Masonry building
Borzi et al. (2008a)	A simplified pushover-based earthquake loss assessment (SP-BELA) method, which was originally developed to study the vulnerability of RC buildings, has been adapted to produce vulnerability curves for unreinforced masonry buildings. The curves have been calibrated using data related to the structural characteristics of Italian buildings.	Masonry building
Oropeza et al. (2010)	They describe the results obtained with an analytical displacement-based methodology to assess the seismic risk in existing unreinforced masonry buildings through fragility functions. Since fundamental period, ultimate drift, damage levels and torsional behaviour have significantly influenced fragility curves, new formulations are proposed. A 15-storey unreinforced masonry existing building with plan-irregularities is analyzed. Impact and accuracy of main parameters are addressed in this shear-wall building. The seismic behaviour of this building is also estimated with ambient vibration measurements.	Masonry building
Rota et al. (2010)	They propose a new analytical approach for the derivation of fragility curves for masonry buildings. The methodology is based on nonlinear stochastic analyses of building prototypes. Since such structures are assumed to be representative of wider typologies, the mechanical properties of the prototypes are considered as random variables, assumed to vary within appropriate ranges of values. Monte Carlo simulations are then used to generate input variables from the probability density functions of mechanical parameters. The model is defined and nonlinear analyses are performed. In particular, nonlinear static (pushover) analyses are used to define the probability distributions of each damage state whilst nonlinear dynamic analyses allow to determine the probability density function of the displacement demand corresponding to different levels of ground motion. Convolution of the complementary cumulative distribution of demand and the probability density function of each damage state allows to derive fragility curves.	Masonry building

This project has received funding from the European Union's Horizon 2020 research and innovation programme under grant agreement No 821046

Ceran and Erberik (2013)	This study focuses on the evaluation of seismic safety of unreinforced masonry buildings in Turkey by using fragility curves generated for two behavior modes of load bearing walls: in-plane and out-of-plane. During generation of fragility curves, a force-based approach has been used. There are two limit states in terms of base shear strength for in-plane behavior mode and flexural strength for out-of-plane behavior mode. Fragility curves generated for in-plane behavior were verified by the observed damage during the 1995 Dinar earthquake and fragility curves generated for out-of-plane behavior were verified by the observed damage during the 2010 Elazığ earthquake.	Masonry building
D'Ayala (2013)	In the past, seismic vulnerability assessment of masonry structures has been conducted using empirical methods, based on post-event collection of damage data. This approach does not allow easy correlation of structural behaviour with observed damage and quantification of the effect of seismic strengthening on seismic resistance. They present the rationale and algorithm of a procedure based on limit state analysis and collapse mechanisms (FaMIVE), to derive capacity curves for masonry structures. It is shown how the procedure can be used to derive vulnerability and fragility functions following the methodology of the capacity spectrum method and the performance-based assessment method.	Masonry building
Lagomarsino and Cattari (2014)	They propose a method for the vulnerability assessment of ordinary masonry buildings at territorial scale, to be used in the framework of a probabilistic seismic risk analysis. The general definition of fragility functions is recalled, using static non-linear analysis for the evaluation of the capacity spectrum and the calculation of the maximum displacement by the demand spectrum. The selection of proper IMs for masonry buildings is treated, as well as the definition of damage and performance limit states. A detailed procedure for the propagation of uncertainties is proposed. Finally, fragility functions are derived for ten different classes of masonry buildings, defined by a list of tags from the taxonomy, in order to show the capabilities of the proposed methods and their cross-validation.	Masonry building
Karantoni et al. (2014)	In order to account for out-of-plane failure modes, linear static Finite Element analysis in 3D of prototype regular buildings is performed using a nonlinear biaxial failure criterion for masonry. More than 1100 analyses are carried out, so as to cover the practical range of the most important parameters, namely the number of storeys, percentage of side length in exterior walls taken up by openings, wall thickness, plan dimensions and number of interior walls, type of floor and pier height-to-length ratio. Results are presented in the form of damage and fragility curves.	Masonry building
Simões et al. (2015)	They have implemented curves for unreinforced masonry buildings in Portugal using nonlinear static analyses in order to describe the building performance.	Masonry building
Kappos et al. (1996)	They have proposed a hybrid approach for the vulnerability assessment of RC structures in Greece. It combines statistical data from earthquake-damaged Greek buildings with appropriately processed results from non-linear dynamic or static analyses.	RC building

This project has received funding from the European Union's Horizon 2020 research and innovation programme under grant agreement No 821046

Dumova-Jovanoska (2000)	They propose a method for the development of earthquake intensity–damage relations, given as fragility curves and DPMs. The proposed method is applied on reinforced-concrete frame-wall structures. Two sets of fragility curves and DPMs are developed. The first one is for RC frame structures lower than 10 stories. For this purpose, a six-story frame structure is used. The other set is defined for RC frame-wall structures higher than 10 stories. A 16-story frame-wall structure was chosen as a sample. The sample structures were designed according to Macedonian design code. Response of the sample structures under earthquake excitation was defined performing nonlinear dynamic analysis. Five damage states were defined to express the condition of damage. As a result of the analytical research, the values of the global damage index corresponding to each damage state were determined. Using the dates from the nonlinear dynamic analysis of the sample structures under all 240 synthetic time histories, the two sets of fragility curves and DPMs were defined.	RC building
Crowley et al. (2004)	They have applied a direct displacement based method to RC buildings, giving rise to the Displacement-Based Earthquake Loss Assessment (DBELA) method. DBELA allows having the capacity curve of RC buildings by starting from the calculation of the displacement capacity of a single-degree-of-freedom system for three different damage limit states. Once the displacements are calculated for each damage limit state, the displacement demand is compared with the displacement capacity and the fragility curves are obtained through probabilistic approaches.	RC building
Rossetto and Elnashai (2005)	Adaptive pushover analysis is employed within a capacity spectrum framework of assessment, to determine the performance of a population of building models for increasing ground motion intensity. The building model population is generated from a single design through consideration of material parameter uncertainty. Uncertainty in ground motion is accounted for through the use of suites of accelerograms with characteristics that are representative of the hazard level associated with the performance level assessed in each vulnerability curve. The new homogeneous RC damage scale is used to determine the damage state of the building at the performance point. The results of the assessments are used to construct response surfaces from which the damage statistics forming the basis of the vulnerability curves are generated through re-sampling.	RC building
Cosenza et al. (2005)	In Italy, this was one of the first study on the assessment of building and it was based on the opening of plastic hinges leading to the structural collapse. In this case, the capacity curve is the outcome of non-linear static analyses performed on several 3D buildings, designed according to the regulations at the time of construction. These buildings belong to the same structural type and they are generated through Monte Carlo method by varying the geometrical characteristics, together with the mechanical properties of the materials.	RC building
Kircil and Polat (2006)	The aim of this study is to develop the fragility curves for mid-rise RC frame buildings in Istanbul, which have been designed according to the 1975 version of the Turkish seismic design code, based on numerical simulation with respect to the number of stories of the buildings. Sample 3, 5 and 7 story buildings were designed according to the Turkish seismic design code. Incremental dynamic analyses were performed for those sample buildings using twelve artificial ground motions to determine the yielding and collapse capacity of each sample building. Based on those capacities, fragility curves were developed in terms of elastic pseudo spectral acceleration, peak ground acceleration (PGA) and elastic spectral displacement for yielding and collapse damage levels with lognormal distribution assumption.	RC building

This project has received funding from the European Union's Horizon 2020 research and innovation programme under grant agreement No 821046

Borzi et al. (2008b)	The method presented defines the nonlinear behaviour of a random population of RC buildings through a simplified pushover and displacement-based procedure. Displacement capacity limits are identified on the pushover curve and these limits are compared with the displacement demand from a response spectrum for each building in the random population, thus leading to the generation of vulnerability curves.	RC building
Akansel et al. (2012)	In this study fragility curves of a shear wall building with torsional irregularity have been obtained. This building was subjected to synthetic earthquake motions on the AZALEE shaking table under the coordination of CEA (Commissariat à l'Energie Atomique) and Electricité de France (EDF) in Saclay, Paris under the scope of the SMART program. Maximum inter-story drift values have been used as the damage indicator to obtain the fragility curves and different seismic IMs such as PGA, PGV, PGD and CAV have been used. Thirty bi-directional horizontal ground motions have been applied for the time history analyses. Micro modeling approach has been used to obtain reasonably accurate and consistent results with experiments. ANSYS finite element software has been used for the response history analyses.	RC building
Silva et al. (2014)	They have developed fragility curves for RC buildings in Portugal. Synthetic portfolios of RC structures were generated through Monte Carlo simulations and analysed against a set of one hundred ground motion records using non-linear dynamic analysis.	RC building
Vona (2014)	After having selected and characterized a significant number of building types for the Italian RC building stock, their seismic behaviour have been analysed through accurate non-linear dynamic analysis. The fundamental step of this study is the correct definition of the relationship between damage level and damage status determined through accurate non-linear analyses. Although very reliable in terms of reproducing numerically the seismic performance, the methodologies based on non-linear dynamic analyses present the negative aspect of having high computational requirements, which is instead lower for methodologies based on non-linear static analysis.	RC building
Tsionis and Fardis (2014)	They have developed fragility curves for the RC buildings in the city of Thessaloniki through non-linear static analysis. Their methodology is based on the non-linear analysis of simplified models and accounts for uncertainties in the capacity and demand quantities due to the modelling and the variability of materials, geometry as well as to the seismic action.	RC building
Hancilar and Çaktr (2015)	They have developed fragility curves for RC buildings by means of non-linear dynamic analysis on RC moment-resisting frame buildings in Turkey.	RC building
Karapetrou et al. (2015)	They have investigated the influence of soil-structure interaction in modifying the seismic fragility analysis of RC structures in Greece. A two-step uncoupled approach is applied to examine the relevant contribution of SSI and site effects on the structural response and fragility. A 9-story RC moment resisting frame designed with low seismic code provisions is adopted as a reference structure. Two-dimensional incremental dynamic analysis is performed to assess the seismic performance of the fixed base and SSI structural systems. Fragility curves are derived as a function of outcropping PGA for the immediate occupancy and collapse prevention limit states.	RC building
Del Gaudio et al. (2015)	They have developed fragility curves for RC Italian buildings through simplified mechanics-based method, founded on the use of an equivalent single degree of freedom system.	RC building

This project has received funding from the European Union's Horizon 2020 research and innovation programme under grant agreement No 821046

Masi et al. (2015)	Fragility curves relevant to existing RC framed building types representative of the Italian building population designed only to vertical load and regular in-plan have been derived from an extensive campaign of non-linear dynamic analyses. In the generation of the fragility curves, damage states according to the EMS98 scale (Grüntal et al., 1998) have been considered while the IM has been defined by adopting an integral parameter, such as the Housner intensity. Fragility curves have been generated by varying different parameters, including building age, number of storeys, presence and position of infill panels, plan dimensions, external beams stiffness and concrete strength.	RC building
Borzi et al. (2016)	They have been investigated the application of SP-BELA (Simplified Pushover-Based Earthquake Loss Assessment) method to different structural building types. SP-BELA represents a simplified mechanics-based method to determine the structural capacity of a building using nonlinear static analysis. The methodology allows to modify the input parameters, such as geometry, loads and mechanics-based characteristics of materials. The paper explores the versatility of this method and illustrates its capacity to adequately reproduce the behaviour of buildings. In particular, the procedure has been applied to obtain fragility curves of RC frame buildings that can represent the building typologies of the city of Nablus in Palestine. To highlight the vulnerability of Nablus buildings, the resulting fragility curves have been compared with SP-BELA fragility curves for RC frame Italian buildings and HAZUS (1999) fragility curves for unreinforced masonry infill walls (Pre-Code).	RC building
Faravelli et al. (2019)	They present an analytical method for large-scale vulnerability assessment used in order to simulate damage scenarios corresponding to those observed during past earthquakes in Italy. The method, already published in the technical literature with the acronym SP-BELA (Simplified Pushover-Based Earthquake Loss Assessment), has been adopted to calculate fragility curves for Italian building stock classified as RC and masonry buildings. The method has been calibrated through the comparison of numerically calculated damage scenarios and data on observed damage collected during earthquakes occurred in Italy starting from the 1976 Friuli earthquake. The use of observed damage data allowed to validate the method and to add reliability to the calculation of damage scenarios, which gives an input to plan the emergency response immediately after an earthquake.	Masonry and RC building
Bolognini et al. (2008)	Vulnerability curves of traditional Italian RC precast structures are evaluated through the Simplified Pushover-Based Earthquake Loss Assessment method (SP-BELA) proposed in Borzi et al. (2008). The main characteristics of the RC precast structures are not always consistent with seismic criteria. In particular, the connections are one of the weak points in terms of local resistance capacity and global seismic response. Within the procedure adopted, four structural typologies are defined as representative of the majority of the current Italian production and used to randomly generate a population of buildings. The structural behaviour of this population is evaluated through simplified pushover analysis. The generation of vulnerability curves is based on displacement capacity limits of the structures and on the displacement demand. The input motion severity is described through the PGA.	RC precast building
Casotto et al. (2015)	They took advantage of pushover analysis to establish a number of damage limit states and then performed nonlinear dynamic analysis to compare the maximum demand with the limit state capacity to allocate the structure into a damage state.	RC precast building

This project has received funding from the European Union's Horizon 2020 research and innovation programme under grant agreement No 821046

Buratti et al. (2017)	They analyse the seismic fragility of precast RC buildings using observational damage data gathered after the 2012 Emilia earthquakes that struck Northern Italy. The damage level in 1890 buildings was collected, classified and examined. Damage matrices were then evaluated, and finally, empirical fragility curves were fitted using Bayesian regression. Building damage was classified using a six-level scale derived from EMS98 (Grüntal et al., 1998). The completeness of the database and the spatial distribution of the buildings investigated were analysed using cadastral data as a reference. The intensity of the ground motion was quantified by the maximum horizontal PGA, which was obtained from ShakeMaps.	RC precast building
Bessason et al. (2020)	In June 2000 two shallow, strike-slip, Mw6.5 earthquakes occurred in the middle of Iceland's largest agricultural region. The epicentres were close to small towns and villages, and almost 5000 residential buildings were affected. A complete loss database was established, including all residential buildings in the affected area. Due to the high proportion of no-loss buildings in the dataset (~84%) a new and novel vulnerability model was applied based on zero-inflated beta regression model. The model was calibrated for the three main building typologies in the affected region, i.e. low-rise, structural wall, RC, timber and masonry buildings. The proposed model can be used to predict the mean and desired prediction intervals of the losses for a given intensity level as well as to create fragility functions as presented in the paper.	Low-rise RC, timber & masonry buidings.
Ioannaou et al. (2018)	In June 2000, two Mw6.5 earthquakes occurred within a 4-day interval in the largest agricultural region of Iceland causing substantial damage but no loss of life. The distance between the earthquake epicentres and the fault rupture was approximately 15 km. Nearly 5000 low-rise residential buildings were affected, some of which were located between the faults and exposed to strong ground motion from both events. The construction of vulnerability curves from this database is hampered by the fact that the loss values represent the cumulative damage from two sequential earthquakes in some areas, and single earthquakes in others. A novel methodology based on beta regression is proposed to define the geographical limits on areas where buildings sustained cumulative damage and predict the seismic losses for future sequence of events in the area or other similar areas	Low-rise RC, timber & masonry buidings.
Bessason et al. (2016)	In June 2000 two Mw6.5 earthquakes occurred in South Iceland and in May 2008 an Mw6.3 quake struck the zone again. High PGAs were registered in all cases. Nearly 9500 residential buildings were affected by these events. In this paper, classical methods based on lognormal distribution assumption were used to construct fragility curves using the combined loss dataset from both the 2000 and the 2008 events. Loss ratios in predefined range define the damage stages.	Low-rise RC, timber & masonry buidings.
Bessason et al. (2014)	In May 2008 a shallow Mw6.3 earthquake struck South Iceland with an epicentre close to two small towns, Hveragerdi and Selfoss.Nearly 5000 low-rise residential buildings were affected. A great deal of damage occurred, there were no fatlities. In Iceland all buildings are registered in a detailed official database and insurance against natural disasters is obligatory. To fulfill insurance purposes the repair costs for every affected building was assessed and classified in a number of subcategories covering structural and non-structural damage. In this paper the statistics of the losses in different subcategories is given. The non-structural losses dominated the overall losses.The main losses were cosmetic damage of partition walls and flooring. The structural systems performed quite well and no buildings collapsed.	Low-rise RC, timber & masonry buidings.

This project has received funding from the European Union's Horizon 2020 research and innovation programme under grant agreement No 821046

Martins & Silva (2020)	They described the development of an analytical fragility and vulnerability model covering the most common building classes at the global scale. Nearly five hundred functions were developed to cover the majority of combinations of construction material, height, lateral load resisting system and seismic design level. The fragility and vulnerability were derived using nonlinear time-history analyses on equivalent single degree-of-freedom oscillators and a large set of ground motion records representing several tectonic environments. The resulting fragility and vulnerability functions were validated through a series of tests which include the calculation of the average annual loss ratio for a number of locations, the comparison of probabilities of collapse across all building classes, and the repetition of past seismic events. The set of vulnerability functions was used for the assessment of economic losses due to earthquakes as part of the global seismic risk model supported by the Global Earthquake Model (GEM) Foundation.	Masonry (unreinforced (MUR) reinforced (MR) or confined (MCF)), reinforced concrete (CR), adobe/earthen (MUR-ADO), timber/wood (W), steel (S) and composite (SCR) (i.e. combination of reinforced concrete with steel).

This project has received funding from the European Union's Horizon 2020 research and innovation programme under grant agreement No 821046

Table 2.2: Fragility models related to the building structural typology.

Reference	Methodology	IM Type	Damage Scale	Region	Construction Material	Building Structural Typology
Ahmad et al. (2010)	Analytical (NLS* without dispersion)	Sd(T_{LS}), PGA	Custom	Euro-Mediterranean Region	Masonry and RC	MUR+CLBRH/LWAL/HEX:2,4 MUR+ST99/LWAL/HEX:2,4 CR/LFM/HBET:2,8/IRRE/IRIR CR/LFM+DNO/HEX:2,5,8/IRIR+IRVP:SOS+IRVS:IRN CR/LFM+DNO/HEX:2,5,8/IRRE CR/LFM+DUC/HEX:2,5,8/IRIR+IRVP:SOS+IRVS:IRN CR/LFM+DUC/HEX:2,5,8/IRRE
Farsangi et al. (2016a)	Analytical (NLD**)	Sa(T)	Custom	Worldwide	RC	15 Story High Ductile and 7 story medium ductile RC-MRFs (Horizontal Excitation+Vertical Excitation)
Farsangi et al. (2016b)	Analytical (NLD)	Sa(T)	Custom	Worldwide	RC	2,5 and 9 Storey Non-Ductile RC-MRFs Horizontal+Vertical Excitation)
Akkar et al. (2005)	Analytical (NLS with dispersion)	PGV	-	Turkey	RC	CR/LFINF/HEX:2,3,4,5
Bessason et al. (2020)	Emperical	PGA	EMS98	Iceland	Masonry, RCand Wood	MUR+CB99/LWAL+DNO/HBET:1,3 CR/LWAL+DUL/HBET:1,3 and CR/LWAL+DUM/HBET:1,3 W/LWAL+DUM/HBET:1,2
Barbat et al. (2006)	Analytical (NLS)	Sd(T)	HAZUS	Spain	Massonry and RC	CR/LFLS/HEX:2,5,8 MUR/LWAL/HEX:2,4,6
Borzi et al. (2007)	Analytical (NLS without dispersion)	PGA	Custom	Italy	RC	CR/LFM+DNO/HEX:2,4,8/IRIR+IRVP:SOS+IRVS:IRN CR/LFM+DUC/HEX:2,4,8
Borzi et al. (2008a)	Analytical (NLS with dispersion)	PGA	Custom	Italy	RC	CR/LFM+DNO/HEX:4 CR/LFM+DUC/HEX:4 CR/LFINF+DNO/HEX:4 CR/LFINF+DUC/HEX:4 CR/LFINF+DNO/HEX:4/IRIR+IRVP:SOS+IRVS:IRN CR/LFINF+DUC/HEX:4/IRIR+IRVP:SOS+IRVS:IRN
Borzi et al. (2008b)	Analytical (SMM***-NLS)	PGA	Custom	Italy	RC	CR/LFM+DNO/HEX:2,3,4,5,6,8
Borzi et al. (2008c)	Analytical (NLS with dispersion)	PGA	Custom	Italy	Massonry	MUR+CLBRH/LWAL/HEX:2,3,4,5 MUR+STDRE/LWAL/HEX:2,4

This project has received funding from the European Union's Horizon 2020 research and innovation programme under grant agreement No 821046

Martins & Silva (2020)	Analytical (NLD)	Sa(T)	-	Worldwide	RC	CR/LFINF+DUL/H:2
D'Ayala et al. (1997)	Empirical	I & PGA	EMS92	Portugal	Massonry	MUR+STDRE/LWAL/HBET:2,6
Erberik & Elnashai (2004)	Analytical (NLD)	Sd(T)	HAZUS	United States	RC	CR/LFLSINF+DUC/HEX:5+HFEX:14/COM/PLFSQ/IRRE/EWMA/RSH1+RWCP/FC+FC1+FWCP
Giovinazzi & Lagomarsino (2004)	Empirical	PGA	EMS98	Macedonia, Italy, Greece	Masonry	MUR+ST99 MUR+CLBRH
Kappos et al. (2003)	Hybrid	PGA	EMS98	Greece	RC	CR/LDUAL+DUC/HBET:1,3,4,7,8,19/IRRE CR/LDUAL+DNO/HBET:1,3,4,7,8,19/IRRE CR/LFINF+DUC/HBET:1,3,4,7,8,19/IRRE CR/LFINF+DNO/HBET:1,3,4,7,8,19/IRRE CR/LFINF+DUC/HBET:1,3,4,7,8,19/IRIR+IRVP:CHV+IRVS:IRN CR/LFINF+DNO/HBET:1,3,4,7,8,19/IRIR+IRVP:CHV+IRVS:IRN CR/LFM+DUC/HBET:1,3,4,7,8,19/IRRE CR/LFM+DNO/HBET:1,3,4,7,8,19/IRRE
Kappos et al. (2006)	Hybrid	PGA	EMS98	Greece	Masonry and RC	URM-brick-HBET:2 URM-stone-HBET:2 CR/LFM/HEX:9+HFEX:28.5 CR/LFINF/HEX:9+HFEX:28.5 CR/LFINF+DUC/HEX:4+HFEX:13.5 CR/LFINF/HEX:4+HFEX:13.5 CR/LFINF/HEX:9+HFEX:28.5/IRIR+IRVP:SOS+IRVS:IRN CR/LDUAL/HEX:9+HFEX:28.5 CR/LDUAL+DUC/HEX:4+HFEX:13.5 CR/LDUAL/HEX:4+HFEX:13.5 CR/LDUAL/HEX:9+HFEX:28.5/IRIR+IRVP:SOS+IRVS:IRN CR/LFINF
Kostov et al. (2004)	Expert Opinion	PGA	EMS98	Bulgaria	Masonry and RC	M99/HBET:1,4/YPRE:1919/FW+FWCN M99/HBET:1,4/YBET:1919,2004/FW+FWCN M99/HBET:1,5/YBET:1920,1945/FC M99/HBET:1,5/YBET:1945,2004/FC CR/LFINF/HBET:1,6/YPRE:1945/EWMA/FC+FWCP CR/LFINF/HBET:1,6/YBET:1945,2004/EWMA/FC+FWCP CR+PC/HBET:5,9/YBET:1964,1987/FC CR+PC/HBET:5,9/YBET:1987,2004/FC

This project has received funding from the European Union's Horizon 2020 research and innovation programme under grant agreement No 821046

Kwon & Elnashai (2006)	Analytical (NLD)	PGA	Custom	US & CNE	RC	CR+CIP/LFM+DNO/HEX:3
Kyriakides et al. (2015)	Analytical (NLD)	PGA	Custom	Cyprus	RC	RC1_ERD_low (Cyprus) RC1_ERD_mod (Cyprus) RC1_noERD_low (Cyprus) RC1_noERD_mod (Cyprus)
Vargas et al. (2012)	Analytical (NLS)	Sd(TLS)	Custom	Spain	RC	WS/C/RC/R/HR-8 (SYNER-G)
Moreno-Gonzalez & Bairan (2013)	Analytical (NLS)	Sd(T)	HAZUS & EMS98	Spain	RC	WS/C/RC/R/HR-MR-LR (SYNER-G)
Cattari et al. (2004)	Analytical (NLS)	Sd(TLS)	Custom	Italy	Masonry	W/M/NC (SYNER-G)
Colombi et al. (2008)	Empirical	Sd(TLS)		Italy	Masonry	BW/M/LR-2/NC (SYNER-G)
Jeong & Elnashai (2007)	Analytical (NLD)	PGA	Custom	Worldwide	RC	MRF/C/RC-HSC-HY/R/R/B-X/D/HR-12/HC
Liel & Lynch (2012)	Empirical	PGA	Custom	Italy	RC	MRF/C/RC/RI-X/ND/MR-X/LC
Nuti et al. (1998)	Empirical	Intensity expressed in th MCS scale		Italy	Masonry	BW/M/URM/ /LR-X/NC MRF/C/RC/X/RI-X/ND/MR-X/LC BW/C-M/MR-X/NC BW/C-M/LR-X/NC BW/M/URM/MR-X/NC
Ozmen et al. (2010)	Analytical (NLD)	PGA	Custom	Turkey	RC	MRF/C/RC-LSC-LY/B-X/ND/LR-2/MC MRF/C/RC-LSC-LY/B-X/ND/MR-4/MC MRF/C/RC-ASC-HY/B-X/D/MR-4/HC MRF/C/RC-LSC-LY/B-X/D/MR-7/MC
Polese et al. (2008)	Analytical (NLS)	Sd(TLS)	HAZUS99	Italy	RC	MRF/C/RC/B-X/ND/HR-X/NC MRF/C/RC/B-X/ND/LR-X/NC MRF/C/RC/B-X/ND/MR-X/NC
RISK-UE (2003)	Analytical	Sd(TLS)	-	Europe	Different	Different topologies are considered
Rossetto & Elnashai (2003)	Empirical	PGA, Sd(T), Sd(TLS)	Custom	Europe	RC	340000 existing RC structures

This project has received funding from the European Union's Horizon 2020 research and innovation programme under grant agreement No 821046

Sarabandi et al. (2004)	Empirical	I RMS Drift Ratio Sd(T)	ATC13 HAZUS99 Vision2000	Worldwide - USA	RC	MRF/C/RC/B-X MRF-W/C/RC/
Tsionis et al. (2011)	Analytical (NLD)	PGA	Custom	Euro-Mediterranean Regions	RC	Different topologies are considered
UPAT deliverable	Analytical (NLS)	PGA	EMS98	Europe	Masonry	BW/M/URM/F,R-X/LR,MR-2,4,6
UTCB (2006) / RISK-UE (2003)	Analytical (NLD)	Sd(TLS)	HAZUS99	Bucharest, Romania	RC	CR/LFM&LWAL/HBET:(1,3)&(4,7)&(8,16)/YBET:(1941,1962)&(1963-1969)&(1970-1977)&(1978-1989)&(1990-2002)
Pavel et al. (2018)	Analytical (NLD)	Sd(TLS)	HAZUS99	Bucharest, Romania	RC	CR/LFM+DUC/HBET:5,7/YBET:2006,2020/FC CR/LFM+DUC/HBET:10,13/YBET:2006,2020/FC CR/LWAL+DUC/HBET:5,7/YBET:2006,2020/FC CR/LWAL+DUC/HBET:10,13/YBET:2006,2020/FC S/LFBR+DUC/HEX:7/YBET:2006,2020/FC S/LFBR+DUC/HBET:10,13/YBET:2006,2020/FC
Pavel et al. (2020)	Analytical (NLD)	Sd(TLS)	HAZUS99	Bucharest, Romania	RC	CR/LWAL/HEX:11/YEX:1968 CR/LWAL/HEX:11/YEX:1968 CR/LFM/HEX:11/YEX:1972 CR/LFM/HEX:11/YEX:1974 CR/LFM/HEX:11/YEX:1974 CR/LWAL/HEX:8/YEX:1983 CR/LWAL/HEX:8/YEX:1983 CR/LWAL/HEX:9/YEX:1980 CR/LWAL/HEX:9/YEX:1980

*NLS = Nonlinear Static Analysis, **NLD = Nonlinear Dynamic Analysis, ***SMM = simplified mechanic method

This project has received funding from the European Union's Horizon 2020 research and innovation programme under grant agreement No 821046

2.1.2 Infrastructures

2.1.2.1 Bridges

Herein we present a literature review of studies carried out since 1985 to date to assess the seismic vulnerability of roadway and railway bridges through the fragility curves. These studies are classified in relation to the proposed methodology and the type of bridges to which it is applied as well as the geographical area where the bridges are located.
The approaches to define the fragility curves are different; they can be derived on the basis of expert opinions, by empirical approach, or by an analytical approach. In the latter case, a further distinction must be made in relation to the type of the performed analysis, which can be:

- Linear elastic analysis;
- Non-linear dynamic analysis. This analysis can be performed on a 3D bridge model (MDOF), only in the longitudinal direction of the bridge (SDOF nonlinear dynamic) or by reconducting the behavior of the whole bridge to the one of its piers (SDOF nonlinear dynamic);
- Non-linear static analysis;
- Non-linear kinematic analysis. This analysis is performed to assess the seismic behavior of masonry arch bridges through the definition of the capacity curves.

A selection of fragility curves for different bridge taxonomy will be made available in TURNkey platform. A description of the classification in taxonomy defined by EUC for railway roadway bridges is given in §2.1.2.1.3. The parameters of fragility curves assigned with reference to two testbeds: TB-2: Pyrenees Mountain Range, France and TB-6: Groningen Province, Netherlands are given in §3.2.1 and §3.6. respectively.

2.1.2.1.1 Highway bridges

Table 2.3 reports the existing fragility models for roadway bridges in the literature. It is evident that most of the studies in the literature (especially the less recent ones) are addressed to either single/multi-span continuous or simply supported steel/RC deck bridges. However, some studies to assess the seismic behavior of masonry arch bridges and self-anchored suspension bridges have been found and herein reported.

Table 2.3: Existing fragility models for highway bridges in the literature.

Reference	**Methodology**	**Bridge Typology**
ATC (1985)	Expert opinion	Bridges in California classified in: • Conventional (less than 500 ft span) - Multiple single spans - Continuous monolithic (includes simple span) • Major (greater than 500 ft span).
Basös et al. (1999)	Empirical	Continuous and simply-supported RC and steel bridges in USA.
FEMA (1999) and following updates	MDOF non-linear dynamic	American RC and steel bridges are divided in 28 classes, macroscopically groupable in: • Major bridges (length>150 m) • Single span bridges • Multi-span simply supported bridges • Multi-span continuous bridges.
Shinozuka et al. (2000a)	Non-linear dynamic	Multi-span continuous RC bridges in Japan (2 case-studies).
Shinozuka et al. (2000b)	Non-linear static	Multi-span continuous RC bridges in USA (1 case-study).
Tanaka et al. (2000)	Empirical	RC and steel highway bridges in Japan (bridges belonging to the Hanshin Expressway Network).
Yamazaki et al. (2000)	Empirical	Kobe Highway bridges.

This project has received funding from the European Union's Horizon 2020 research and innovation programme under grant agreement No 821046

Saxena et al. (2000)	MDOF non-linear dynamic	Multi-span continuous RC bridges.
Monti & Nisticò (2002)	Non-linear static	Simply-supported deck bridges in the road network of the city of Catania, Sicily, South Italy.
Karim & Yamazaki (2003)	SDOF non-linear dynamic	Multi-span continuous highway RC bridges in Japan (4 RC bridge piers designed according to the 1964,1980,1990, and 1995 Japanese seismic design code; 2 RC bridge structures, of which one is an isolated-system and the other one not).
Gardoni et al. (2003)	Non-linear static	RC bridges in California (2 case studies: 1 single bent overpass and 1 two-bent overpass. Both overpasses have single-column bents).
Elnashai et al. (2004)	Empirical and MDOF non-linear dynamic	RC Bridges. The empirical fragility curves are defined by using the dataset from both Northridge and Kobe earthquakes. The analytical fragility method is instead applied to 1 case/study, i.e. multi-span continuous RC bridge in Greece.
Lupoi et al. (2004)	MDOF non-linear dynamic	Multi-span continuous RC bridges (1 case-study, South Italy).
Choi et al. (2004)	MDOF non-linear dynamic	RC and steel bridges in Central and South Eastern United States classified in: • Multi-span simply supported pre-stressed concrete girder bridge • Multi-span continuous pre-stressed concrete girder bridge • Multi-span simply supported steel girder bridge • Multi-span continuous steel girder bridge.
Kim & Shinozuka (2004)	MDOF non-linear dynamic	Multi-span continuous RC bridges (2 case-studies: 2 retrofitted bridges in California).
Mackie K. et Stojadinovic (2004)	Non-linear static	Multi-span RC bridges (1 case-study: single-bent reinforced concrete highway overpass bridge).
Lupoi et al. (2005)	MDOF non-linear dynamic	Multi-span continuous RC bridges (a sample of 27 pre-stressed concrete girder bridges composed with 5 spans and cantilever piers).
Kurian et al. (2006)	MDOF/SDOF nonlinear dynamic	Simply-supported RC bridges (1 case-study in India).
Nielson & DesRoches (2007)	Analytical fragility curves Non-linear time history-analyses	RC and steel bridges in Central and South Eastern United States classified in: • Single span concrete girder • Single span steel girder • Multispan simply supported concrete girder • Multispan simply supported concrete box girder • Multispan simply supported slab • Multispan simply supported steel girder • Multispan continuous slab • Multispan continuous concrete girder • Multispan continuous steel girder.
Zhang et al. (2008)	Non-linear static (for liquefaction) MDOF nonlinear dynamic	6 classes of typical bridges in California: • continuous bridge with monolithic abutments • continuous bridge with seat-type abutments • continuous bridge with seat-type abutments and an expansion joint at the center of mid-span • bridge isolated at the pier tops with continuous deck; • continuous bridges with expansion joint at mid-span in addition to the isolation • Simply supported bridge with seat-type abutments.
Kwon & Elnashai (2009)	MDOF non-linear dynamic by considering the soil-structure interaction	Multi-span continuous steel girder bridge in Illinois (1 case study).
Kwon et al. (2009)	MDOF non-linear dynamic by considering the effect of soil liquefaction	Multi-span continuous pre-stressed concrete bridge (1 case-study, USA).

This project has received funding from the European Union's Horizon 2020 research and innovation programme under grant agreement No 821046

Padgett & Des Roches (2009)	MDOF non-linear dynamic	Retrofitted RC and steel bridges in Central and Southeastern United States classified in: • Multi-span continuous steel girder • Multi-span simply supported steel girder • Multi-span continuous concrete girder • Multi-span simply supported concrete girder.
Pelà et al. (2009)	Non-linear static	Multi-span masonry arch bridges (2 case studies in Italy).
De Felice & Giannini (2010)	Non-linear static	Multi-span simply-supported RC bridges (2 case- studies from Italian highway network, with simply supported deck and either single stem or frame piers).
Cardone et al (2011)	Analytical-Inverse Adaptive Capacity Spectrum Method	Multi-span simply supported bridges (9 case studies from South-Italian highway network with simply supported deck and single frame, single shaft or single wall as piers)
Crowley et al. (2011) Fardis et al. (2011)	Linear elastic	Multi-span continuous bridges with single-box prestressed concrete girder classified in: • Roadway bridges with bearings and monolithic central pier • Roadway bridges with monolithic deck-pier connection • Roadway bridges with bearings. These fragility curves can be applied to the bridges located in all over Europe.
Shirazian et al (2011)	SDOF non-linear dynamic	Multi-span simply-supported RC bridges (1 case-study, Iran).
Li et al. (2012)	MDOF non-linear dynamic	Multi-span continuous RC girder (1 case-study in California).
Qi'ang et al. (2012)	MDOF non-linear dynamic	Multi-span continuous concrete girder bridges (1 case-study).
Gehl et al. (2014)	MDOF non-linear dynamic	Multi-Span simply supported concrete girder bridge (1 case-study).
Borzi et al. (2015)	MDOF non-linear dynamic	Italian bridges classified in: • Multi-span simply supported concrete girder • Multi-span simply supported concrete box girder • Multi-span simply supported slab • Multi-span simply supported steel girder • Multi-span continuous concrete girder • Multi-span continuous concrete box girder • Multi-span continuous slab • Multi-span continuous steel girder.
Zampieri et al. (2016)	Non-linear kinematic	Italian single-span masonry arch bridges.
Kamath (2017)	MDOF non-linear dynamic	American single-span masonry arch bridges.
Kibboua (2017)	SDOF non-linear dynamic	Multi-span simply-supported RC bridges (1 case-study that represents the most of Algerian bridges).
Pang and Wu (2018)	MDOF non-linear dynamic	Multi-span continuous RC girder bridges (the bridges are grouped in 8 classes on the basis of statistical analysis of existing RC bridges in China).
Cheng et al (2019)	MDOF non-linear dynamic	Self-anchored suspension bridge (1 case study in China).

2.1.2.1.2 Railway bridges

The research on fragility methods specific for railway bridges is not well-supplied as the one addressed to roadway bridges. Table 2.4 reports the approaches that we have been able to collect on this topic: they mainly concern single/multi-span continuous or simply-supported steel/RC deck bridges and single-span and multi-span masonry arch bridges.

Table 2.4: Existing fragility models for railway bridges in the literature.

Reference	**Methodology**	**Bridge Typology**
FEMA (1999) and following updates	MDOF non-linear dynamic	American bridges are divided in 10 classes, macroscopically groupable in: • Multi-span simply supported steel bridges • Multi-span continuous steel bridges • Steel and RC major bridges (bridge length<20m)

		• Single span steel and RC bridges (bridge length<20m and not in California) • Multi-span simply supported RC bridges (bridge length<20m and in California).
Crowley et al. (2011) Fardis et al. (2011)	Linear elastic	Continuous bridges classified in: • Railway bridges with bearings and monolithic central pier; • Railway bridges with monolithic deck-pier connection; • Railway bridges with bearings. These fragility curves can be applied to the bridges located in all over Europe.
Park & Choi (2011)	MDOF non-linear dynamic	Steel-plate-girder railway bridges in Korea (1 case-study).
Tecchio et al. (2016)	Non-linear kinematic	Italian single-span masonry arch bridges.
Zampieri et al. (2016)	Non-linear kinematic	Italian single-span masonry arch bridges.
Barbieri (2019)	Non-linear static	Masonry arch bridges (1 case-study: an arch double spans masonry bridge in Italy).
Bellotti et al. (2019a)	MDOF non-linear dynamic	Italian bridges classified in: • Multi-span simply supported concrete girder • Multi-span simply supported concrete box girder • Multi-span simply supported slab • Multi-span simply supported steel girder • Multi-span continuous concrete girder • Multi-span continuous concrete box girder • Multi-span continuous slab • Multi-span continuous steel girder.
Bellotti et al. (2019b)	MDOF non-linear/Non-linear static	Italian bridges classified in: • Multi-span simply supported concrete girder • Multi-span simply supported concrete box girder • Multi-span simply supported slab • Multi-span simply supported steel girder • Multi-span continuous concrete girder • Multi-span continuous concrete box girder • Multi-span continuous slab • Multi-span continuous steel girder.
Morandi et al. (2019)	Non-linear kinematic	Italian single-span and multi-span masonry arch bridges.

2.1.2.1.3 Taxonomies by EUC for single-span and multi-span roadway/railway bridges

This paragraph summarizes the criteria adopted by EUC to define and assign a taxonomy to single-span and multi-span girder and arch bridges. The aim is to estimate the seismic vulnerability using fragility functions, defined by cumulative probability of distribution that allow to evaluate the probability of exceeding a given level of damage for a given severity of the ground shaking. This procedure can be adopted when a low level of knowledge is available.

The approach can be used for single-span and multi-span girder bridges with substructures in RC and masonry and for masonry or unreinforced or lightly RC arch bridges.

Starting with a set of parameters related to the features of the bridge that affect the seismic response of the structures, a taxonomy and therefore a set of fragility functions can be associated.

Two levels of capacity are considered in the approach: one regarding the functionality (Damage Limit State, DLS) and the other regarding the bridge safety (Collapse Limit State, CLS).

- For girder bridges, these limit states concern the piers' deformation and resistance capacity (ductile and brittle failures) and the girders' loss of support. DLS refers to yield of piers or achievement of the maximum capacity in terms of resistance of supports, whereas CLS refers to two mechanisms. The first one refers to the loss-of-support mechanism of the deck, intended as the fall of the deck from the pier that implies partial collapse of the bridge. The second one refers to the collapse mechanism for the piers (deformation or brittle failures).
- For arch bridges, the seismic capacity was assessed by non-linear kinematic analysis. Both local and global collapse mechanisms were identified involving piers, abutments, arches and spandrel walls.

This project has received funding from the European Union's Horizon 2020 research and innovation programme under grant agreement No 821046

The mechanisms considered are different for single-span and multi-span bridges. Then for each collapse mechanism, capacity curves were defined and thresholds in terms of displacement capacity on the capacity curve were defined with reference to the DLS and CLS.

2.1.2.1.3.1 Girder bridge

The fragility models for girder bridges were based on analytical approach presented by Bellotti et al (2019a, 2019b), referred on MDOF non-linear dynamic analysis. Here, a large number of taxonomies (i.e. 24) were defined, in particular sixteen for multi-span girder bridges and eight for single-span girder bridges.
In detail, for girder bridges the minimum data requested are:

1. number of spans
2. material of substructure element (abutments and piers)
3. mean value of length of spans
4. height of abutments and piers
5. presence of seismic isolation devices to prevent the fall of the deck from piers.

The following tables reported the set of taxonomies developed from EUC for single-span and multi-span girder bridges. Table 2.5 summarizes the taxonomies related to multi-span girder bridges with substructure elements (abutments and piers) in masonry or concrete without reinforcement. Similarly, Table 2.6 summarizes the taxonomies related to multi-span girder bridges with substructure elements (abutments and piers) in RC. In Table 2.7 and Table 2.8 are indicated the taxonomies defined for single-span girder bridges with abutments in masonry or concrete without reinforcement and RC, respectively. It is important to highlight that different range of span length were used with reference to different deck material.

Table 2.5: Taxonomies to classify girder bridges: Multi-span bridges with abutments and piers in masonry/concrete without reinforcement

	Multispan girder bridges with abutments and piers in masonry or no RC		
Seismic isolation devices (SID)	Range H\L	• Steel I-beam fully covered with concrete slab deck: **3m < L1 < 20m** • Metal material deck: **3m < L1 < 60m** • Prestressed/simple RC deck: **3m < L1 < 18m**	• Prestressed/simple RC deck: **18 m < L2 < 40m**
With SID	H1 < 4m	T_PMH1L1_R	T_PMH1L2_R
	H2 > 4m	T_PMH2L1_R	T_PMH2L2_R
Without SID	H1 < 4m	T_PMH1L1	T_PMH1L2
	H2 > 4m	T_PMH2L1	T_PMH2L2

Table 2.6: Taxonomies to classify girder bridges: Multi-span bridges with abutments and piers in reinforced concrete

	Multispan girder bridges with abutments and piers in RC		
Seismic isolation devices (SID)	Range H\L	• Steel I-beam in concrete slab deck: **3m < L1 < 20m** • Metal material deck **3m < L1 < 60m** • Prestressed/simple RC deck: **3m < L1 < 18m**	• Prestressed/simple RC deck: **18 m < L2 < 40m**
With SID	H1 < 10m	T_PCH1L1_R	T_PCH1L2_R
	H2 > 10m	T_PCH2L1_R	T_PCH2L2_R
Without SID	H1 < 10m	T_PCH1L1	T_PCH1L2
	H2 > 10m	T_PCH2L1	T_PCH2L2

This project has received funding from the European Union's Horizon 2020 research and innovation programme under grant agreement No 821046

Table 2.7: Taxonomies to classify girder bridges: Single-span bridges with abutments and piers in masonry/concrete without reinforcement

	Single-span girder bridge with abutments and piers in masonry/no RC		
Seismic isolation devices (SID)	Range H\L	• Steel I-beam in concrete slab deck: **3m < L1 < 7m** • Metal material deck: **3m < L1 < 30m** • Prestressed/simple reinforced concrete deck: **3m < L1 < 8m**	• Steel I-beam in concrete slab deck: **7m < L2 < 20m** • Metal material deck: **30m < L2 < 80m** • Prestressed/simple RC deck: **8m < L2 < 25m**
With SID	H1<10 m	T_MMH1L1_R	T_MMH1L2_R
Without SID	H1<10 m	T_MMH1L1	T_MMH1L2

Table 2.8: Taxonomies to classify girder bridges: Single-span bridges with abutments and piers in reinforced concrete

	Single-span girder bridges with abutments and piers in RC		
Seismic isolation devices (SID)	Range H\L	• Steel I-beam in concrete slab deck: **3m < L1 < 7m** • Metal material deck: **3m < L1 < 30m** • Prestressed/simple RC deck: **3m < L1 < 8m**	• Steel I-beam in concrete slab deck: **7m < L2 < 20m** • Metal material deck: **30m < L2 < 80m** • Prestressed/simple RC deck: **8m < L2 < 25m**
With SID	H1<10 m	T_MCH1L1_R	T_MCH1L2_R
Without SID	H1<10 m	T_MCH1L1	T_MCH1L2

2.1.2.1.3.2 Arch bridge

The fragility models for arch bridges were based on analytical approach presented by Morandi et al. (2019), referred on nonlinear kinematic analysis. Here, a large number of taxonomies (i.e. 24) related to masonry and unreinforced (or lightly reinforced) concrete arch bridges were defined, in particular twelve for multi-span arch bridges and twelve for single-span arch bridges
Each taxonomy related to arch bridge is based on several parameters:

1. number of spans
2. bridge material (masonry or concrete)
3. arch geometry (circular of depressed arch)
4. span length
5. height of substructures (abutments and piers).

As in the previous paragraph, the following tables reported the set of taxonomies developed from EUC for arch bridge. Table 2.9 summarizes the taxonomies related to single-span and multi-span circular arch bridges, here only masonry bridges were considered. Table 2.10 summarizes the taxonomies related to single-span and multi-span depressed arch bridges. In this case both masonry and concrete bridges were considered. Generally, it is important to note that different range of span length were used with reference to different deck material.

Table 2.9: Taxonomies to classify single-span and multi-span circular arch bridges

	Single-span circular arch bridge				
	Masonry		-	-	
Range H\L	3 < L1 ≤ 5	30 > L2 > 5	-	-	-
H1 ≤ 4	A_MMH1L1_TS	A_MMH1L2_TS	-	-	-
15 > H2 > 4	A_MMH2L1_TS	A_MMH2L2_TS	-	-	-
	Multi-span circular arch bridge				
	Masonry		-	-	
Range H\L	3 < L1 ≤ 10	30 > L2 > 10	-	-	-
H1 ≤ 6	A_PMH1L1_TS	A_PMH1L2_TS	-	-	-
20 > H2 > 6	A_PMH2L1_TS	A_PMH2L2_TS	-	-	-

Table 2.10: Taxonomies to classify depressed arch bridges

	Single-span depressed arch bridge				
	Masonry			*Concrete or weakly RC*	
Range H\L	3 < L1 ≤ 5	30 > L2 > 5	Range H\L	3 < L1 ≤ 5	30 > L2 > 5
H1 ≤ 4	A_MMH1L1_SR	A_MMH1L2_SR	H1 ≤ 4	A_MCH1L1_SR	A_MCH1L2_SR
15 > H2 > 4	A_MMH2L1_SR	A_MMH2L2_SR	14 > H2 > 4	A_MCH2L1_SR	A_MCH2L2_SR
	Multi-span depressed arch bridge				
	Masonry			*Concrete or weakly RC*	
Range H\L	3 < L1 ≤ 10	30 > L2 > 10	Range H\L	3 < L1 ≤ 10	30 > L2 > 10
H1 ≤ 4	A_PMH1L1_SR	A_PMH1L2_SR	H1 ≤ 5	A_PCH1L1_SR	A_PCH1L2_SR
20 > H2 > 4	A_PMH2L1_SR	A_PMH2L2_SR	20 > H2 > 5	A_PCH2L1_SR	A_PCH2L2_SR

2.1.2.2 Port facilities

Ports represent complex systems of elements with different features and vulnerability. Thus, under earthquake loading, various facilities can be damaged, from wharves with their supporting systems to superstructures and utilities. Port facilities can be classified into three main categories: waterfront structures (i.e. wharves, seawalls); cranes, cargo handling and storage facilities; and port infrastructures, such as transportation and utility systems. Existing fragility models for the main port components available in the literature are summarized in Table 2.11. Concerning buildings (e.g. warehouses, port authority headquarters), railway (e.g. tracks) and roadway, the reader can refer to specific previously presented sections and/or to the general procedure provided by HAZUS (NIBS, 2004), according to the reccommendations provided on this issue by the European project SYNER-G.

Table 2.11: Existing fragility models for port components in the literature.

Reference	**Methodology**	**Port Component**
	Waterfront structures	
Ichii (2003, 2004)	Analytical fragility curves for gravity type quay walls. Simplified dynamic finite element analysis, considering also occurrence of liquefaction phenomena.	Gravity-type (caisson) quay wall
HAZUS - NIBS (2004)	Empirical fragility curves for waterfront structures. No distinction between different typologies. No specification of type and source of ground deformation (deformation due to ground shaking or ground failure).	Waterfront structures
Na et al. (2009)	Analytical fragility curves for pile-supported wharves. Liquefaction and lateral spreading in backfill and sand layers is taken into consideration.	Pile-supported wharves
Na & Shinozuka (2009), Na et al. (2008)	Analytical fragility curves for gravity-type (caisson) quay wall, considering also occurrence of liquefaction phenomena (effective stress analysis).	Gravity-type (caisson) quay wall
Ko et al. (2010)	Analytical fragility curves for sheet pile wharves of Hualien Harbor in Taiwan.	Sheet pile wharves
Kakderi & Pitilakis (2010)	Analytical fragility curves for ordinary gravity quay walls/retaining structures' typologies commonly used in Europe, exclusively for ground shaking (no liquefaction and ground failure).	Monolithic gravity quay walls
Shafieezadeh (2011)	Seismic performance of pile-supported wharf structures considering soil-structure interaction in liquefied soil. The wharf structure configuration is typical of wharves in seaports along the West Coast of the United States.	Pile-supported wharves
Thomopoulos & Lai (2012)	Preliminary definition of analitycal fragility curves for pile-supported wharves.	Pile-supported wharves
Calabrese and Lai (2013)	Analytical fragility functions for blockwork wharves using artificial neural networks, taking into account different geometries, liquefaction occurrence and type of failure mechanism.	Blockwork wharves
Mirfattah (2013); Bozzoni et al. (2014); Mirfattah & Lai (2015)	A methodlogy to compute deterministic and stochastic fragility curves for pile-supported wharves.	Pile-supported wharves

This project has received funding from the European Union's Horizon 2020 research and innovation programme under grant agreement No 821046

Ntritsos (2015); Ntritsos & Lai (2016)	A methodology enabling to take into account the effect of cumulated damage on pile-supported wharves due to a sequence by developing state-dependent fragility functions.	Pile-supported wharves
Ko & Yang (2019)	Analytical seismic fragility curves for sheet-pile wharves using finite element analysis for the sheet-pile wharves of a port in Taiwan.	Sheet-pile wharves
Mirzaeefard et al. (2021)	Time-dependent seismic fragility analysis of corroded pile-supported wharves with updating limit states.	Pile-supported wharves
Cranes and cargo handling equipment		
HAZUS - NIBS (2004)	Expert judgment. Description of damage states for cargo handling and storage components subject to ground shaking and ground failure	Cranes and cargo handling equipment
Kosbab (2010)	Kosbab (2010) proposed a fragility model to assess the seismic performance of container cranes.	Container cranes
Tran et al. (2019)	Analytical fragility curves for container cranes. A large number of nonlinear time-history analyses were applied for a three-dimensional finite element model to quantify the vulnerability of a Korean case-study container crane considering the uplift and derailment behavior. The uncertainty of the demand and capacity of the crane structures were also considered.	Container cranes
Fuel facilities		
HAZUS - NIBS (2004)	Empirical fragility curves that describe earthquake-induced damage to fuel facilities due to ground shaking and ground failure.	Fuel facilities
SRM-LIFE (2007)	Fragility curves for fuel facilities subject to ground shaking and to ground failure derived using a fault-tree analysis similar to HAZUS (NIBS 2004), modifying accordingly the fragility curves of the sub-components with respect to Greek typologies.	Fuel facilities
Components of the electric power unit		
HAZUS - NIBS (2004)	Fragility curves for electric power system components are defined with respect to classification and ground motion parameters. These curves are based on the probabilistic combination of subcomponent damage functions using Boolean expressions to describe the relationship of subcomponents.	Electric substations and distribution circuits

2.2 Loss estimation models

The effect of the earthquake on structures can be evaluated not only with fragility models but also in terms of expected losses through loss estimation models. Consequences may include population and economic losses. In the literature there are several proposals for the estimation of losses following an earthquake. The models present in the literature have been updated considering the data observed after significant earthquakes. In the following paragraphs, the loss estimation models found in the literature for buildings and infrastructures (bridges and port facilities) are illustrated.

2.2.1 Buildings

In Table 2.12, a collection of loss estimation models gained from the literature review with reference to buildings is reported.

Table 2.12: Existing loss estimation models for buildings in the literature.

Reference	**Methodology**	**Building Structural Typology**
Coburn & Spence (1992)	They define different earthquake loss costs: physical loss, economic loss, insured loss, shock loss, historical loss. The authors don't provide a measurement of the loss costs because it is extremely variable from case to case. For loss estimation studies to be useful for earthquake protection they need to include an assessment of the probable levels of human casualties, both deaths and injuries, which will be caused by the earthquake. Up to 25% of all deaths are from non-structural causes or follow-on hazards. For the large majority of earthquakes, deaths and injury are primarily related to building damage. Over 75% of deaths are caused by building collapse and, if secondary disasters are excluded, building collapse causes almost 90% of earthquake-related deaths. The authors provide a series of tables about (e.g.): estimated average percentage of occupants trapped by collapse, estimated injury distributions at collapse	Masonry and RC building

This project has received funding from the European Union's Horizon 2020 research and innovation programme under grant agreement No 821046

	(% of trapped occupants), percentage of trapped survivors in collapsed buildings that subsequently die.	
Spence et al. (2011)	Assessment of human casualties in earthquakes has become a topic of vital importance for national and urban authorities responsible for emergency provision, for the development of mitigation strategies and for the development of adequate insurance schemes. Based on the local context and considering the data observed after significant earthquakes throughout the world, the authors summarise current trends in the understanding of the factors influencing the numbers and types of casualties in earthquakes.	Masonry and RCbuilding
Zuccaro & Cacace (2011)	A possible model for evaluating seismic casualties in Italy is presented. The factors influencing the evaluation are discussed and the results of the first investigations concerning their quantification are presented. The model, derived from the idea of Coburn and Spence (1992), has been adapted to the Italian context thanks to the data collected in the field regarding either the percentage of the victims per structural type or the lifestyle of the population obtained from the National Institute of Statistics (ISTAT). An application of the model to the earthquake of L'Aquila 2009 is presented.	Masonry and RCbuilding
Di Ludovico et al. (2017a)	After the L'Aquila 2009 earthquake, for each damaged building, practitioners engaged by property owners designed repair and strengthening interventions and then computed the corresponding costs. These projects were the technical basis for funding applications that owners submitted to the government. Technical and financial information collected during the approval procedure of such applications allowed compilation of a database regarding 5775 residential buildings damaged. This study examines the restoration policy and the procedures regulating the reconstruction process of residential property outside city centres, in particular the data related to the first phase of the reconstruction process (the so-called "light damage" reconstruction) to recover the usability of slightly damaged buildings.	Masonry and RC building
Di Ludovico et al. (2017b)	The reconstruction process of residential buildings severely damaged by the L'Aquila 2009 earthquake, the so called "heavy damage" reconstruction, started after the "light damage" reconstruction process. The "heavy damage" reconstruction involved buildings outside the historical centres assessed as unusable due to high structural and/or non-structural risk. The procedures to deal with funding applications made by private owners were similar to those related to the "light damage" reconstruction, but specific regulations were issued to regulate the public contributions of severely damaged buildings.	Masonry and RCbuilding
Kappos et al. (2007)	Reliable loss assessment (in monetary terms) for buildings struck by an earthquake is an essential factor in the development of seismic risk scenarios for a given urban area. This study consists of predicting the loss to selected groups of buildings struck by the 1999 Athens earthquake using an analytical methodology and comparison with statistical repair costs collected after the earthquake. An in-situ survey of about 10% of the total building stock was performed, and data regarding the structural type, actual earthquake damage, and corresponding repair costs were collected. The statistically derived repair cost for the area was compared with the economic loss estimation obtained using the analytical procedure and various estimates of the seismic action in the area considered, and was found to agree with it reasonably for some of the seismic hazard scenarios.	Masonry and RCbuilding
Franchin (2013)	The casualty model is derived from an original idea developed by Coburn and Spence (1992). The model computes casualties directly caused by building damage for each class of buildings using a "Lethality Ratio" (LR). LR is defined as the ratio of the number of people killed to the number of occupants present in collapsed buildings of that class. Multiplying LR by the number of collapsed buildings of each class, the number of deaths for that building type can be estimated. The LR from Zuccaro and Cacace (2011) which are based on an application to the L'Aquila event are used but adapting it because here there are only three damage level (none, yield and collapse) instead of five. Besides of LR, tha paper provides usability percentages (Fully Usable, Partially Usable, Non Usable) by damage level.	Masonry and RCbuilding

This project has received funding from the European Union's Horizon 2020 research and innovation programme under grant agreement No 821046

Polese et al. (2015)	Tools for assessing building reparability via the estimation of expected Performance Loss (PL) and associated Costs for Repair (Cr) of existing RC building classes damaged by an earthquake are presented. The assessment approach rely on the availability of a number of suitably developed: i) Capacity Curves (CC) for representative building classes ii) curves relating global ductility demand to the expected PL for the same classes and iii) PL-Cr relationship calibrated on database collecting cost data of more than 2300 buildings damaged after 2009 L'Aquila earthquake.	RC building
Dolce et al. (2019)	In 2018 the Italian Civil Protection Department produced a National Risk Assessment, with the important support of the scientific community. Among the several risks considered, this document deals with the development of the seismic risk map of the Italian territory, relevant to the ordinary building stock. In order to provide useful risk quantities that describe the impact of earthquakes potentially occurring in the national territory in the future, the attention has been focused on the consequences for the population and for the building stock. The following impact quantities have been considered: No. of dead, No. of injured, No. of homeless, Direct economic losses (i.e. cost of repair or reconstruction of damaged/collapsed buildings) in euro, No. of unusable buildings and unusable dwellings in the short term, No. of unusable buildings/ dwellings in the long term, No. of collapsed buildings/dwellings. The evaluation of the above quantities is based on the values of the expected numbers of buildings affected by the different damage levels. The translation of the building/dwelling damage levels into the above said impact quantities is carried out by assuming the relationships described in the paper.	Masonry and RC building
HAZUS (FEMA 2003)	The Manual guides the users in the development of loss functions to calculate building losses as a function of damage-state probability. It provides the default values of direct economic loss for structural and nonstructural systems and the casualty rates.	Masonry and RC building

2.2.2 Infrastructures

In the next paragraphs we have reported the loss estimation models found in literature for the infrastructures considered in the platform: bridges and port facilities.

2.2.2.1 Bridges

Catastrophic events, such as the earthquakes in Loma Prietra (California, 1989), Northridge (California, 1994) and Kobe (Japan, 1995), have highlighted how fundamental it is to maintain the functionality of the transport networks, especially to allow the immediate rescue.
In order for the roadway and railway networks to be viable, it is necessary that also the elements constituting them are not damaged or, at least, quickly repairable. Among these elements, bridges are one of the roadway/railway infrastructures to which particular attention must be paid: in fact, their damage or even collapse can cause both loss of life and considerable repair and/or reconstruction costs (direct costs). In addition to the direct costs, indirect costs must also be considered: they quantify the social inconveniences experienced by user, e.g. driver delay, loss of opportunity, due to the closure of the roadway/railway section where the bridge is. In order to estimate all these costs, either total or singular ones, some researchers developed loss estimation models which provide the extent of likely damage and the socio-economic consequences caused by the bridge damage or collapse due to seismic events. Table 2.13 reports the loss estimation models for roadway bridges. Concerning the railway bridges, not much research has been found, except for the one proposed by HAZUS (see Table 2.14).

2.2.2.1.1 Highway bridges

In Table 2.13, a collection of loss estimation models retrieved from the literature review with reference to roadway bridges is presented.

This project has received funding from the European Union's Horizon 2020 research and innovation programme under grant agreement No 821046

Table 2.13: Existing loss estimation models for highway bridges in the literature.

Reference	Methodology	Bridge Typology
FEMA (1999) and following updates	HAZUS Methodology.	American RC and steel Highway bridges that are divided in 28 classes, macroscopically groupable in: • Major bridges (length>150 m) • Single span bridges • Multi-span simply supported bridges • Multi-span continuous bridges.
Shinozuka et al. (2003)	Probabilistic approach to estimate the losses due to driver's delay in case of repair of bridges damaged by an earthquake. Losses due to driver's delay in case of repair of bridges with and without retrofit also are also compared as well as the losses due to liquefaction. The latter are estimated with the aid of HAZUS.	2727 bridges in the freeway network in Los Angeles and Orange County, in the metropolitan area of Los Angeles. For the liquefaction, a cluster of 1307 bridges is considered.
Mackie et al (2005)	PEER PBEE methodology	Highway bridges in California.
Conte et al. (2007)	PEER PBEE methodology in which loss analysis – analytical step (4) – is performed using a multilayer Monte Carlo simulation approach.	Multi-span RC continuous bridges (1 case-study).
Tirasirichai & Enke (2007)	Regional Computable General Equilibrium (CGE) Model to estimate indirect economic losses.	Highway bridges the St. Louis metropolitan region.
Enke et al. (2008)	Procedure to estimate costs resulting from the increased time and distance used for transportation as a result of seismically damaged bridges lowering the capacity of the highway network.	Highway bridges the St. Louis metropolitan region.
Luna et al. (2008)	HAZUS-MH (FEMA, 2003) to estimate the direct losses.	Highway bridges the St. Louis metropolitan region.
Mackie et al (2008)	PEER PBEE methodology	RC bridges in California.
Mackie et al (2009)	Approach based on the linearization of the damage model (relationship between damage and repair quantity) in the PEER framework for the post-earthquake highway bridge loss modeling—particularly post-earthquake bridge repair costs and repair times.	RC Bridges in California (1 case-study).
Zhou et al. (2010)	Simulation-based study to estimate the social cost (i.e., driver delay and loss of opportunity) and to perform a socio-economic analysis due to the bridges retrofitting (i.e., bridge restoration cost, bridge retrofit cost, benefit from seismic, bridge retrofit and Cost-effectiveness of bridge seismic retrofitting).	3133 Bridges in Los Angeles and Orange Counties, California.
Miano et al. (2015)	Procedure to estimate the direct economic losses, i.e. repair cost.	Highway bridges in the Campania region, Italy.
Seo & Park (2015)	Approach to define restoration cost curves through the use of surface metamodels (RSMs) in conjunction with Monte Carlo Simulation (MCS).	99 curved steel I-girder bridges with no skewed supports located in the state of the states of Pennsylvania, Maryland, and New York.
Forcellini (2018)	Methodology to assess the indirect losses.	RC Californian highway bridges (1 case-study).

This project has received funding from the European Union's Horizon 2020 research and innovation programme under grant agreement No 821046

2.2.2.1.2 Railway bridges

Not much research on the existing loss estimation models for railway bridges has been found with the exception of the HAZUS methodology (FEMA, 2003) that allows to estimate the direct and indirect costs of American railway bridges, simply classified as conventionally and seismically designed.

In Table 2.14, a collection of loss estimation models gained from the literature review with reference to railway bridges is presented.

Table 2.14: Existing loss estimation models for railway bridges in the literature.

Reference	Methodology	Bridge Typology
FEMA (2003)	HAZUS Methodology	American railway bridges, simply classified as conventionally and seismically designed.

2.2.2.2 Port facilities

Main worldwide studies available in the literature on the estimation of seismic functional and systemic losses for ports are presented in Table 2.15. Further details on these approaches are provided in Deliverable 4.3.

Table 2.15: Existing loss estimation models for port systems in the literature.

Reference	Methodology	Component
Pachakis & Kiremidjian (2004)	A study that calculated operational losses occurring after scenario earthquakes in multi-terminal container ports. A queuing model with a maximum wait capacity was implemented for incoming container ships. Expected cargo throughput (based on all possible damage states) was calculated for the port in both the damaged and undamaged state and then compared.	Port system
Werner & Taylor (2004)	The study evaluates the systemwide seismic performance and upgrade options of several berths in the Port of Oakland. A simplified operational model is used to evaluate business interruption losses by comparing the average daily demands to the average daily post earthquake capacities.	Port waterfront
Na & Shinozuka (2009)	A simulation-based study to estimate losses in ports. It focuses on losses for ports containing quay walls. The study did estimate damage using fragility curves for quay wall damage developed specifically for their study (Na et al. 2009) and then input that information into a terminal operation program to calculate resulting throughput. Total loss is estimated through the use of fragility curves calculated from resulting throughputs. This study also features a retrofit to the quay wall and calculates system fragility curves for both conditions.	Port waterfront
Kakderi et al. (2012; 2013)	A first attempt to address the interdependencies among the elements of a port system has been performed with reference to the port of Thessaloniki in Greece.	Port system
Burden et al. (2016)	Development of a risk framework for forecasting earthquake losses in port systems. This work not only looks at the port as a system but also allows for the evaluation of performance based on metrics valuable to the stakeholders within the port.	Port system
Bozzoni et al. (2018); Conca et al. (2020)	A simulation-based methodology for the assessment of the seismic risk of ports as systems of interconnected structural and infrastructural elements has been developed and applied to a large commercial port in Italy. The results of the analyses are expressed as the loss of performance of an element that can be attributed to either direct damage or interdependencies (i.e., domino effects).	Port system

This project has received funding from the European Union's Horizon 2020 research and innovation programme under grant agreement No 821046

3 FRAGILITY MODELS AND LOSS ESTIMATION MODELS IN THE TURNKEY TESTBEDS

In the next paragraphs, the fragility models and loss estimation models selected for each testbed have been described. It is worth noting that for buildings the reference are the 5 damage levels of the EMS98 scale (Grünthal, 1998):

- D1: Light damage
- D2: Moderate damage
- D3: Extensive damage
- D4: Complete damage

3.1 D5: Collapse.TB-1: Bucharest, Romania

Bucharest is the capital of Romania, having about 2 million residents and more than 131.875 residential buildings out of which at least 43,8% can be considered pre-code (according to 2011 census data – a newer census will take place in 2021). The city is located in the southern part of the country, in the Wallachian Plain, in a region with a thick layer of sediments which tend to amplify seismic waves originating from the Vrancea intermediate-depth source located 140-170 km hypocentral depth away. Earthquakes with magnitudes greater than 7 from this source (such as the one on 4 March, 1977, which resulted in the death of 1578 persons out of which 90% in Bucharest) can induce long fundamental periods that need to be accounted correspondently by design codes and rapid loss estimation models.

3.1.1 Fragility models selected for Bucharest residential buildings

High quality exposure data is a critical component of damage estimation. The main official data regarding residential buildings and population in Bucharest were collected during the 2011 National Census. The datasets are collected, administered and shared by the National Institute of Statistics. However, the dataset needed some additional processing in order to be implemented within the SeisDaRo (System for Rapid Estimation of Seismic Damage in Romania) framework. This action was performed within the Ro-Risk Project, DACEA project or other collaborations. The existing exposure dataset for Romania (including Bucharest) was also used to compute the European Seismic Risk Model ESRM 2020 (Crowley et al., 2020). For Bucharest, the data are presented at the sector level (6 sectors).

By knowing the peculiarities of the Bucharest building stock, one of the most important factors that contribute to the specific fragility of the buildings is the construction period, mainly from the seismic design code point of view. According to the census data, more than 500 high-rise (more than 6 storeys) buildings were erected without specific earthquake resistance, due to the lack of official regulations. Specific fragility functions taking the socialist development of the urban built environment into account were derived and should be implemented into the loss estimations.

For residential buildings in Bucharest we consider as most suitable for the moment the fragility models described in Table 3.1. Some of the functions developed by the Technical University of Civil Engineering Bucharest (UTCB), also within the RISK-UE Project, are being used by the System for Rapid Estimation of Seismic Damage in Romania - Seisdaro (Toma-Danila et al., 2018) and contributed to seismic loss estimation studies for Bucharest such as Lang et al (2012), Toma-Danila et al. (2015) or Pavel and Vacareanu (2016). Newer fragility models for representative construction periods in Bucharest (also for High Design Code period – after 2006) are also included (Pavel et al., 2018; 2020); these are also for RC (as the RISK-UE functions), but also for concentrically braced steel structures. For adobe, masonry and wood buildings, no local fragility functions are available, therefore the use of regional and global functions is needed – following a detailed test to be performed in this project. As a mention, in Seisdaro the HAZUS fragility functions (FEMA, 1999) were used for the aforementioned typologies, providing satisfactory results. However, improvements in validation and refinements in exposure data is expected to provide insights into the suitability of the fragility models.

This project has received funding from the European Union's Horizon 2020 research and innovation programme under grant agreement No 821046

Table 3.1: Selected fragility models for buildings in Bucharest, where α is the median and β the standard deviation of the lognormal distribution. HAZUS99 (FEMA, 1999) damage scale to EMS98 damage scale (Grüntal et al., 1998) conversion parameters are presented in Table 3.2

			Slight Damage (HAZUS99)		Moderate Damage (HAZUS99)		Extended Damage (HAZUS99)		Complete Damage (HAZUS99)	
Blds structural type - GEM Taxonomy	**Reference**	**IM Type [unit]**	**α**	**β**	**α**	**β**	**α**	**β**	**α**	**β**
CR/LFM/HBET:1,3/YBET:1941, 1962	UTCB (2006)	SD [m]	0.0014	0.65	0.0029	0.75	0.0044	0.85	0.0103	0.95
CR/LFM/HBET:4,7/YBET:1941, 1962	UTCB (2006)	SD [m]	0.0038	0.65	0.0078	0.75	0.0118	0.85	0.0279	0.95
CR/LFM/HBET:8,16/YBET:1941 ,1962	UTCB (2006)	SD [m]	0.0087	0.65	0.018	0.75	0.0273	0.85	0.0646	0.95
CR/LWAL/HBET:1,3/YBET:194 1,1962	UTCB (2006)	SD [m]	0.0001	0.65	0.0003	0.75	0.0005	0.85	0.0011	0.95
CR/LWAL/HBET:4,7/YBET:194 1,1962	UTCB (2006)	SD [m]	0.0012	0.65	0.0024	0.75	0.0036	0.85	0.0086	0.95
CR/LWAL/HBET:8,16/YBET:19 41,1962	UTCB (2006)	SD [m]	0.004	0.65	0.0083	0.75	0.0126	0.85	0.0297	0.95
CR/LFM/HBET:1,3/YBET:1963, 1969	UTCB (2006)	SD [m]	0.002	0.65	0.0041	0.75	0.0062	0.85	0.0147	0.95
CR/LFM/HBET:4,7/YBET:1963, 1969	UTCB (2006)	SD [m]	0.0034	0.65	0.0071	0.75	0.0108	0.85	0.0255	0.95
CR/LFM/HBET:8,16/YBET:1963 ,1969	UTCB (2006)	SD [m]	0.0056	0.65	0.0115	0.75	0.0175	0.85	0.0414	0.95
CR/LWAL/HBET:1,3/YBET:196 3,1969	UTCB (2006)	SD [m]	0.0004	0.65	0.0008	0.75	0.0012	0.85	0.0028	0.95
CR/LWAL/HBET:4,7/YBET:196 3,1969	UTCB (2006)	SD [m]	0.0025	0.65	0.0053	0.75	0.008	0.85	0.0189	0.95
CR/LWAL/HBET:8,16/YBET:19 63,1969	UTCB (2006)	SD [m]	0.0047	0.65	0.0098	0.75	0.0148	0.85	0.0351	0.95
CR/LFM/HBET:1,3/YBET:1970, 1977	UTCB (2006)	SD [m]	0.0021	0.65	0.0043	0.75	0.0066	0.85	0.0156	0.95
CR/LFM/HBET:4,7/YBET:1970, 1977	UTCB (2006)	SD [m]	0.0036	0.65	0.0075	0.75	0.0114	0.85	0.027	0.95
CR/LFM/HBET:8,16/YBET:1970 ,1977	UTCB (2006)	SD [m]	0.0059	0.65	0.0123	0.75	0.0187	0.85	0.0442	0.95
CR/LWAL/HBET:1,3/YBET:197 0,1977	UTCB (2006)	SD [m]	0.0003	0.65	0.0006	0.75	0.0009	0.85	0.0022	0.95
CR/LWAL/HBET:4,7/YBET:197 0,1977	UTCB (2006)	SD [m]	0.0024	0.65	0.0049	0.75	0.0075	0.85	0.0177	0.95
CR/LWAL/HBET:8,16/YBET:19 70,1977	UTCB (2006)	SD [m]	0.005	0.65	0.0104	0.75	0.0157	0.85	0.0372	0.95
CR/LFM/HBET:1,3/YBET:1978, 1989	UTCB (2006)	SD [m]	0.005	0.65	0.0111	0.75	0.0172	0.85	0.0415	0.95
CR/LFM/HBET:4,7/YBET:1978, 1989	UTCB (2006)	SD [m]	0.0126	0.65	0.0279	0.75	0.0432	0.85	0.1043	0.95
CR/LFM/HBET:8,16/YBET:1978 ,1989	UTCB (2006)	SD [m]	0.0287	0.65	0.0635	0.75	0.0982	0.85	0.2372	0.95
CR/LWAL/HBET:1,3/YBET:197 8,1989	UTCB (2006)	SD [m]	0.0003	0.65	0.0007	0.75	0.001	0.85	0.0025	0.95
CR/LWAL/HBET:4,7/YBET:197 8,1989	UTCB (2006)	SD [m]	0.0043	0.65	0.0092	0.75	0.0141	0.85	0.0337	0.95
CR/LWAL/HBET:8,16/YBET:19 78,1989	UTCB (2006)	SD [m]	0.0141	0.65	0.0303	0.75	0.0465	0.85	0.1115	0.95
CR/LFM/HBET:1,3/YBET:1990, 2002	UTCB (2006)	SD [m]	0.0063	0.65	0.0132	0.75	0.0201	0.85	0.0478	0.95
CR/LFM/HBET:4,7/YBET:1990, 2002	UTCB (2006)	SD [m]	0.0158	0.65	0.0332	0.75	0.0506	0.85	0.1203	0.95
CR/LFM/HBET:8,16/YBET:1990 ,2002	UTCB (2006)	SD [m]	0.0359	0.65	0.0755	0.75	0.1151	0.85	0.2735	0.95
CR/LWAL/HBET:1,3/YBET:199 0,2002	UTCB (2006)	SD [m]	0.0004	0.65	0.0008	0.75	0.0012	0.85	0.0029	0.95
CR/LWAL/HBET:4,7/YBET:199 0,2002	UTCB (2006)	SD [m]	0.0054	0.65	0.011	0.75	0.0166	0.85	0.039	0.95
CR/LWAL/HBET:8,16/YBET:19 90,2002	UTCB (2006)	SD [m]	0.0179	0.65	0.0364	0.75	0.0549	0.85	0.1289	0.95

This project has received funding from the European Union's Horizon 2020 research and innovation programme under grant agreement No 821046

CR/LFM+DUC/HBET:5,7/YBET:2006,2020/FC	Pavel et al (2018)	PGA [m/s^2]	0.90	0.538	1.56	0.588	5.46	0.637	9.74	0.562
CR/LFM+DUC/HBET:10,13/YBET:2006,2020/FC	Pavel et al (2018)	PGA [m/s^2]	0.88	0.692	1.67	0.774	7.38	0.537	9.25	0.421
CR/LWAL+DUC/HBET:5,7/YBET:2006,2020/FC	Pavel et al (2018)	PGA [m/s^2]	1.57	0.661	2.63	0.566	8.28	0.504	11.04	0.415
CR/LWAL+DUC/HBET:10,13/YBET:2006,2020/FC	Pavel et al (2018)	PGA [m/s^2]	1.75	0.636	2.87	0.565	8.14	0.51	10.51	0.375
S/LFBR+DUC/HEX:7/YBET:2006,2020/FC	Pavel et al (2018)	PGA [m/s^2]	0.90	0.546	1.80	0.597	6.25	0.669	14.68	0.574
S/LFBR+DUC/HBET:10,13/YBET:2006,2020/FC	Pavel et al (2018)	PGA [m/s^2]	1.13	0.565	2.31	0.584	4.97	0.605	12.49	0.6
CR/LWAL/HEX:11/YEX:1968	Pavel et al (2020)	PGA [m/s^2]	1.67	0.47	3.14	0.52	4.61	0.53	6.86	0.56
CR/LWAL/HEX:11/YEX:1968	Pavel et al (2020)	PGA [m/s^2]	1.47	0.48	2.94	0.5	4.31	0.55	5.98	0.55
CR/LFM/HEX:11/YEX:1972	Pavel et al (2020)	PGA [m/s^2]	0.88	0.55	2.35	0.61	3.82	0.66	5.69	0.62
CR/LFM/HEX:11/YEX:1974	Pavel et al (2020)	PGA [m/s^2]	0.59	0.62	1.77	0.68	2.84	0.71	4.61	0.68
CR/LFM/HEX:11/YEX:1974	Pavel et al (2020)	PGA [m/s^2]	0.49	0.65	1.57	0.66	2.55	0.74	4.12	0.64
CR/LWAL/HEX:8/YEX:1983	Pavel et al (2020)	PGA [m/s^2]	2.35	0.49	4.22	0.47	5.59	0.57	8.04	0.6
CR/LWAL/HEX:8/YEX:1983	Pavel et al (2020)	PGA [m/s^2]	2.75	0.52	4.90	0.5	6.47	0.54	9.51	0.54
CR/LWAL/HEX:9/YEX:1980	Pavel et al (2020)	PGA [m/s^2]	1.08	0.61	2.65	0.58	4.41	0.64	6.37	0.61
CR/LWAL/HEX:9/YEX:1980	Pavel et al (2020)	PGA [m/s^2]	1.27	0.54	2.84	0.54	4.22	0.68	6.96	0.59
MUR/HBET:1,2/YPRE:1963	HAZUS	SD [m]	0.00813	1.15	0.01651	1.19	0.04115	1.2	0.09601	1.18
MUR/HBET:3,5/YPRE:1963	HAZUS	SD [m]	0.0127	0.99	0.0257	0.97	0.0640	0.9	0.1494	0.88
MUR/HBET:1,2/YBET:1963,1992	HAZUS	SD [m]	0.0104	0.99	0.0206	1.05	0.0516	1.1	0.1201	1.08
MUR/HBET:3,5/YBET:1963,1992	HAZUS	SD [m]	0.0160	0.91	0.0320	0.92	0.0800	0.87	0.1867	0.91
MR/LWAL/HBET:1,2/YBET:1993,2020	HAZUS	SD [m]	0.01829	0.8	0.03658	0.81	0.10973	0.91	0.32004	0.98
MR/LWAL/HBET:3,5/YBET:1993,2020	HAZUS	SD [m]	0.03048	0.71	0.06096	0.79	0.18288	0.7	0.5334	0.73
MR/LWAL/HBET:6,10/YBET:1993,2020	HAZUS	SD [m]	0.04394	0.66	0.08788	0.65	0.2634	0.66	0.7681	0.72
W/HBET:1,2/YPRE:1963	HAZUS	SD [m]	0.01016	1.01	0.0254	1.05	0.07849	1.07	0.19202	1.06
W/HBET:1,2/YBET:1964,1977	HAZUS	SD [m]	0.0127	0.93	0.03175	0.97	0.09804	1.03	0.24003	0.99
W/HBET:1,2/YBET:1978,1992	HAZUS	SD [m]	0.0127	0.84	0.03175	0.86	0.09804	0.89	0.24003	1.04
W/HBET:1,2/YBET:1993,2020	HAZUS	SD [m]	0.0127	0.8	0.03835	0.81	0.12802	0.85	0.32004	0.97

In order to convert the HAZUS99 damage levels (FEMA, 1999) in Table 3.1 to EMS98 damage levels (Grüntal et al., 1998), we propose the conversion scheme in Table 3.2, to be applied after computing the results. This scheme is based on the work of Hill and Rosetto (2008).

Table 3.2: Conversion scheme between HAZUS99 (FEMA, 1999) and EMS98 damage scales (Grüntal et al., 1998).

EMS98 damage scale	**Scheme of conversion for HAZUS99**
Level 1: negligible to slight	100% * Slight damage results
Level 2: moderate	100% * Moderate damage results
Level 3: substantial to heavy	50% * Extensive damage results
Level 4: very heavy	50% * Extensive damage results + 50% * Complete damage results
Level 5: destruction	50% * Complete damage results

This project has received funding from the European Union's Horizon 2020 research and innovation programme under grant agreement No 821046

3.1.2 Loss estimation models selected for Bucharest residential buildings

No monetary value estimation is currently planned: the main target indicator is the casualties (dead and injured). This can be calculated, for 4 injury levels, using the humanloss basic methodology implemented in version 6 of SELENA software (Molina et al., 2010). The number of casualties due to direct structural damage for any given structural type, level of building damage, and injury severity can be calculated as a products of casualty rates of severity, structural damage probability for a specific damage type and number of people in the building model type. Casualty rates, as also used in Seisdaro, generally have the values provided in Table 3.3, but further adjustments and modifications are expected – also if new building typologies are included for Bucharest.

Table 3.3: Default casualty rates (%) used by the SELENA casualty estimation module of Seisdaro.

Damage Levels	**Severity 1**	**Severity 2**	**Severity 3**	**Severity 4**
Slight Damage	0.05	0.005	0	0
Moderate Damage	0.2	0.02	0	0
Extensive Damage	1	0.5	0.01	0.01
Complete Damage	10	8	4	4
Complete Collapse (generally between 3 to 15% from overall Complete Damage, depending on buiding typology)	50	15	10	10

where:

- Severity 1: Injuries requiring basic medical aid; would require bandages or observation.
- Severity 2: Injuries requiring a greater degree of medical care and use of medical technology such as x-rays or surgery, but not expected to progress to a life threatening status.
- Severity 3: Injuries that pose an immediate life threatening condition if not treated adequately and expeditiously.
- Severity 4: instantaeously killed or mortally injured.

3.2 TB-2: Pyrenees Mountain Range, France

TB-2, located in the Pyrenees mountain range in France, concentrates on two specific areas, namely: *(i)* the Luchon valley containing a few dozen of rural settlements connected with 118 bridges, and *(ii)* the 44 km high-speed railway line between Perpignan (France) and Figueras (Spain) operated by LFP Perthus.

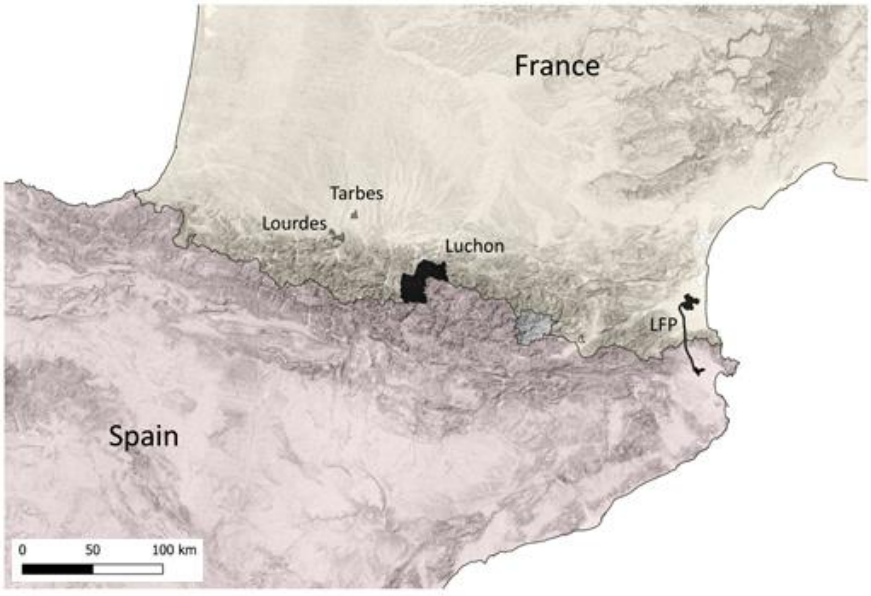

Figure 3.1: Focus areas within TB-2.

This project has received funding from the European Union's Horizon 2020 research and innovation programme under grant agreement No 821046

3.2.1 Fragility models selected for TB-2

3.2.1.1 Fragility models for residential buildings

For Luchon area, the exposure data of the buildings are available from three different approaches for data collection and inventory at level I and level II. The common descriptive characteristics of all three databases are essentially: buildings administrative location, number of floors above ground, age of buildings/ or design code, and demographic class. Here, we gather theses information from: (i) the SERA European Building Exposure Database that collects the data in France per municipality, which is a commonly used level of resolution in regional loss modeling (Level I), (ii) the National statistics data INSEE at municipality level and infra-municipality and (Level I) and (iii) the Field inventory at homogeneous census block level (Level II). The different sources give the information about the material of construction, the technique of construction, the number of the stories and the number of occupants, with the assumption that the building stock is lumped at a single coordinate (i.e., centroids of polygons representing built areas) with different resolution.The different exposure data are associated to vulnerability index following the building classification scheme proposed within the framework of the Risk-UE European project.

The typological classification of the exposure data is defined based on the EMS98 (Grünthal et al., 1998), for which we associate the corresponding RISK-UE typology classes and the associated vulnerability index *Vi* as defined by the RISK-UE approach (Milutinovic & Trendafilovski, 2003). This parameter is corrected if low consideration was given for the design code during the construction and it also takes into account the number of stories. A vulnerability index *V* is then computed to the 53 municipalities in Luchon area by averaging the *Vi* of the buildings in each of the commune. The specific values are shown in Table 6.1of the Annex.

Following the approach detailed by Giovinazzi & Lagomarsino (2005), the mean damage value μ_D is expressed as a function of the macroseismic intensity *I* which may be obtained from the distribution of IMs via ground-motion intensity conversion equations:

$$\mu_D = 2.5\left[1 + \tanh\left(\frac{I + 6.25V - 13.1}{2.3}\right)\right] \quad (3.1)$$

Ultimately, the proportion of damage states in each built area, based on the EMS98 scale (Grünthal, 1998) is obtained by applying a discrete beta distribution based on μ_D.
The damage probability distribution is function of the mean damage value:

$$p_B(x) = \frac{\Gamma(t)}{\Gamma(r) - \Gamma(t-r)} \frac{(x-a)^{r-1}\,(b-x)^{t-r-1}}{(b-a)^{t-1}} \quad (3.2)$$

Where a, b, and t are equal to 0,6, and 8, respectively. The variables x and r are instead defined as following:

$$a \leq x \leq b - 1 \quad (3.3)$$

$$r = \mathrm{t} * (0.007 * {\mu_D}^3 - 0.052 * {\mu_D}^2 + 0.2875 * \mu_D) \quad (3.4)$$

The fragility curves defining the probability of reaching or exceeding a certain damage level are obtained directly from the cumulative probability beta distribution:

$$P_B = \int_a^x p_B(x)\, dx \quad (3.5)$$

$$P(D \geq D_k) = 1 - P_B(k) \quad (3.6)$$

In Table 3.4 the fragility functions that can be used as an alternative to the Vi-based damage assessment previously described are reported.

This project has received funding from the European Union's Horizon 2020 research and innovation programme under grant agreement No 821046

Table 3.4: Selected fragility models for buildings in the Pyrénées (Luchon valley), where α is the median value and β is the standard-deviation. *SAavg* is defined as the geometrical mean of the spectral ordinates in a given interval of periods (defined as 0.2T < T<1.5T, with T the first-mode period of the building).

Blds structural type	Reference	IMType	D_1		D_2		D_3		$D_4 + D_5$	
			α [g]	β [-]	α [g]	β [-]	α [g]	β [-]	α [g]	β [-]
CR+PC/LWAL+CDN/HBET:3-5	Martins & Silva (2020)	SAavg	0.3972	0.4007	1.1723	0.4006	1.8491	0.3986	2.4446	0.3876
CR/LDUAL+CDM/HBET:6-/7.0	Martins & Silva (2020)	SAavg	0.5236	0.4151	1.4947	0.4145	2.3326	0.4025	3.1903	0.4201
CR/LDUAL+CDN/HBET:6-	Martins & Silva (2020)	SAavg	0.4037	0.4326	1.2639	0.4323	2.0172	0.4253	2.7613	0.436
CR+PC/LWAL+CDN/HBET:6-	Martins & Silva (2020)	SAavg	0.4102	0.4242	1.2616	0.424	2.0162	0.418	2.7527	0.4256
CR/LFINF+CDL/H:1/4.0	Martins & Silva (2020)	SAavg	0.4963	0.6444	1.1397	0.6338	1.6265	0.6597	2.0509	0.6455
CR/LFINF+CDM/H:2/7.0	Martins & Silva (2020)	SAavg	0.4306	0.4853	1.1966	0.4845	1.8072	0.4757	2.3922	0.4858
CR/LFINF+CDL/H:2/4.0	Martins & Silva (2020)	SAavg	0.2978	0.4292	0.9055	0.4292	1.3885	0.4287	1.8141	0.4256
W/LWAL+CDN/H:1	Martins & Silva (2020)	SAavg	0.2937	0.4515	0.7590	0.4515	1.1169	0.4513	1.4288	0.4503
CR/LFINF+CDN/HBET:3-5	Martins & Silva (2020)	SAavg	0.2993	0.4271	0.9940	0.427	1.6014	0.4256	2.1492	0.4175
CR/LFINF+CDM/H:1/7.0	Martins & Silva (2020)	SAavg	0.8316	0.7021	1.9329	0.7126	2.7938	0.7033	3.5353	0.7089
MUR+ST/LWAL+CDN/H:2	Martins & Silva (2020)	SAavg	0.2598	0.373	0.5306	0.373	0.7690	0.373	0.9898	0.373
CR/LDUAL+CDL/HBET:3-5/4.0	Martins & Silva (2020)	SAavg	0.3766	0.3887	1.1477	0.3887	1.8130	0.3874	2.4046	0.3792
MUR+CL/LWAL+CDN/H:2	Martins & Silva (2020)	SAavg	0.2518	0.3683	0.5637	0.3683	0.8371	0.3683	1.0904	0.3683
CR/LDUAL+CDM/HBET:3-5/7.0	Martins & Silva (2020)	SAavg	0.5103	0.4005	1.3875	0.4003	2.1391	0.3948	2.8939	0.3921
W/LWAL+CDN/H:2	Martins & Silva (2020)	SAavg	0.2219	0.3757	0.7486	0.3757	1.1878	0.3757	1.5882	0.3755
CR/LFLS+CDN/HBET:6-	Martins & Silva (2020)	SAavg	0.1931	0.4089	0.3022	0.4089	0.4123	0.4089	0.5232	0.4088
MUR+CL/LWAL+CDN/H:1	Martins & Silva (2020)	SAavg	0.3500	0.4836	0.6212	0.4836	0.8460	0.4836	1.0464	0.4833
CR/LDUAL+CDL/HBET:6-/4.0	Martins & Silva (2020)	SAavg	0.4037	0.4326	1.2639	0.4323	2.0172	0.4253	2.7613	0.436
MUR+ST/LWAL+CDN/H:1	Martins & Silva (2020)	SAavg	0.2833	0.5066	0.5790	0.5066	0.8127	0.5065	1.0169	0.5061
CR/LFLS+CDM/HBET:3-5/7.0	Martins & Silva (2020)	SAavg	0.5699	0.4162	1.3864	0.4158	2.1499	0.4064	2.9409	0.4079
CR/LFLS+CDL/HBET:3-5/4.0	Martins & Silva (2020)	SAavg	0.3438	0.3923	0.7929	0.3923	1.2264	0.392	1.6479	0.3899
MCF/LWAL+CDL/H:2	Martins & Silva (2020)	SAavg	0.4118	0.4648	0.9198	0.4647	1.3515	0.4636	1.7390	0.4592
CR+PC/LWAL+CDN/H:2	Martins & Silva (2020)	SAavg	0.3556	0.5342	1.1511	0.5322	1.7425	0.5181	2.3215	0.5325
MCF/LWAL+CDL/H:1	Martins & Silva (2020)	SAavg	0.8716	0.6754	1.7146	0.6856	2.4203	0.6841	3.0566	0.681
CR/LFLS+CDN/HBET:3-5	Martins & Silva (2020)	SAavg	0.3489	0.395	0.5263	0.395	0.7007	0.395	0.8728	0.395
CR/LDUAL+CDM/HBET:6-/4.0	Martins & Silva (2020)	SAavg	0.5236	0.4151	1.4947	0.4145	2.3326	0.4025	3.1903	0.4201
CR/LDUAL+CDM/HBET:3-5/4.0	Martins & Silva (2020)	SAavg	0.5103	0.4005	1.3875	0.4003	2.1391	0.3948	2.8939	0.3921
CR/LFINF+CDM/H:1/4.0	Martins & Silva (2020)	SAavg	0.8316	0.7021	1.9329	0.7126	2.7938	0.7033	3.5353	0.7089
CR/LFINF+CDM/H:2/4.0	Martins & Silva (2020)	SAavg	0.4306	0.4853	1.1966	0.4845	1.8072	0.4757	2.3922	0.4858
CR/LFINF+CDL/H:2/8.0	Martins & Silva (2020)	SAavg	0.2978	0.4292	0.9055	0.4292	1.3885	0.4287	1.8141	0.4256
CR/LDUAL+CDL/HBET:6-/8.0	Martins & Silva (2020)	SAavg	0.4037	0.4326	1.2639	0.4323	2.0172	0.4253	2.7613	0.436
CR/LFINF+CDM/H:1/11.0	Martins & Silva (2020)	SAavg	0.8316	0.7021	1.9329	0.7126	2.7938	0.7033	3.5353	0.7089
CR/LDUAL+CDM/HBET:6-/11.0	Martins & Silva (2020)	SAavg	0.5236	0.4151	1.4947	0.4145	2.3326	0.4025	3.1903	0.4201
CR/LFINF+CDM/H:2/11.0	Martins & Silva (2020)	SAavg	0.4306	0.4853	1.1966	0.4845	1.8072	0.4757	2.3922	0.4858
CR/LDUAL+CDM/HBET:3-5/11.0	Martins & Silva (2020)	SAavg	0.5103	0.4005	1.3875	0.4003	2.1391	0.3948	2.8939	0.3921
CR/LDUAL+CDL/HBET:3-5/8.0	Martins & Silva (2020)	SAavg	0.3766	0.3887	1.1477	0.3887	1.8130	0.3874	2.4046	0.3792
CR/LFINF+CDL/H:1/8.0	Martins & Silva (2020)	SAavg	0.4963	0.6444	1.1397	0.6338	1.6265	0.6597	2.0509	0.6455
CR/LFLS+CDL/HBET:3-5/0.0	Martins & Silva (2020)	SAavg	0.3438	0.3923	0.7929	0.3923	1.2264	0.392	1.6479	0.3899
MCF/LWAL+CDN/H:1	Martins & Silva (2020)	SAavg	0.8716	0.6754	1.7146	0.6856	2.4203	0.6841	3.0566	0.681
MCF/LWAL+CDN/H:2	Martins & Silva (2020)	SAavg	0.4118	0.4648	0.9198	0.4647	1.3515	0.4636	1.7390	0.4592
CR/LDUAL+CDL/HBET:3-5/0.0	Martins & Silva (2020)	SAavg	0.3766	0.3887	1.1477	0.3887	1.8130	0.3874	2.4046	0.3792
CR/LFINF+CDM/H:2/0.0	Martins & Silva (2020)	SAavg	0.4306	0.4853	1.1966	0.4845	1.8072	0.4757	2.3922	0.4858
CR/LFINF+CDL/H:2/0.0	Martins & Silva (2020)	SAavg	0.2978	0.4292	0.9055	0.4292	1.3885	0.4287	1.8141	0.4256

This project has received funding from the European Union's Horizon 2020 research and innovation programme under grant agreement No 821046

3.2.1.2 Fragility models for bridges in the transportation network

The generic typologies of the 118 bridges are identified based on photographs and aerial pictures and they are assigned to existing fragility functions taken from the SYNER-G database (Crowley et al., 2011), except in the case of arch bridges where a more recent reference is used (Zampieri, 2014). The most common bridge type consists of short single span bridges (length < 50 m), followed by masonry arch bridges (Table 3.5). In total, 18 different fragility curves have been assigned:

- 3 models for the 83 single span RC bridges (Shinozuka et al., 2003): Empirical functions using data from Japan and US earthquakes. Characteristics:length, abutment type, pier characteristics.
- 3 models for the 7 continuous multi-span RC bridges (Kaynia et al., 2013): Seismic analysis is performed for the EC8 design spectrum and different q-factors for bridges with limited ductile or ductile behaviour. Characteristics: length, type of pier, number of columns, pier height, seismic design code.
- 12 models for the 28 arch bridges (Zampieri, 2014): Fragility curves derived with non-linear kinematic analysis, simplified fragility asssessment (spectrum-based). Characteristics: span length, arch rise, arch thickness.

In Table 3.6 the fragility parameters for the bridges, obtained by typological assignment of existing functions, are reported.

Table 3.5: Identification of typology and associated fragility ID for the bridges.

Bridge ID	Latitude	Longitude	Type	Features	Fragility ID
2	42.91565	0.69188	Arch Bridge	Arch length 6-10m ; arch rise/length ratio 0.4-0.5 ; arch thickness/length ratio 0.075-0.1	***14***
110	42.82867	0.60115	Single Span	Span length 0-20m	***1***
242	42.96615	0.63977	Mutiple Span	Span length >60m	***23***
263	42.87290	0.73442	Arch Bridge	Arch length 10-20m ; arch rise/length ratio 0.4-0.5 ; arch thickness/length ratio 0.05-0.1	***18***
306	42.88548	0.61642	Arch Bridge	Arch length 10-20m ; arch rise/length ratio 0.4-0.5 ; arch thickness/length ratio 0.05-0.1	***18***
454	42.86725	0.74190	Single Span	Span length 20-60m	***2***
457	42.95304	0.64300	Mutiple Span	Span length 0-20m	***21***
459	42.95259	0.64282	Mutiple Span	Span length 0-20m	***21***
462	42.91214	0.64478	Arch Bridge	Arch length 3-6m ; arch rise/length ratio 0.4-0.5 ; arch thickness/length ratio 0.075-0.1	***8***
464	42.91264	0.64490	Single Span	Span length 0-20m	***1***
467	42.92760	0.65529	Mutiple Span	Span length 0-20m	***21***
470	42.82869	0.60188	Arch Bridge	Arch length 3-6m ; arch rise/length ratio 0.4-0.5 ; arch thickness/length ratio 0.075-0.1	***8***
473	42.86758	0.60941	Single Span	Span length 0-20m	***1***
476	42.99340	0.63065	Single Span	Span length 20-60m	***2***
478	42.99116	0.62759	Single Span	Span length 20-60m	***2***
480	42.98979	0.63235	Single Span	Span length 20-60m	***2***
482	42.98561	0.63620	Single Span	Span length 20-60m	***2***
484	42.98191	0.65964	Single Span	Span length 20-60m	***2***
486	42.97282	0.64737	Single Span	Span length 20-60m	***2***
488	42.95727	0.64467	Single Span	Span length 0-20m	***1***
491	42.93878	0.64731	Single Span	Span length >60m	***3***
493	42.93798	0.64913	Single Span	Span length 20-60m	***2***
495	42.93443	0.65123	Single Span	Span length 20-60m	***2***

This project has received funding from the European Union's Horizon 2020 research and innovation programme under grant agreement No 821046

497	42.92971	0.65402	Single Span	Span length 20-60m	***2***
499	42.92385	0.68226	Single Span	Span length 20-60m	***2***
501	42.91236	0.69221	Mutiple Span	Span length 20-60m	***22***
503	42.91158	0.69466	Single Span	Span length 20-60m	***2***
505	42.91023	0.69078	Single Span	Span length 0-20m	***1***
507	42.90918	0.69800	Single Span	Span length 20-60m	***2***
508	42.92101	0.80454	Arch Bridge	Arch length 20-30m ; arch rise/length ratio 0.3-0.4 ; arch thickness/length ratio 0.05-0.2	***19***
510	42.92164	0.80303	Single Span	Span length 20-60m	***2***
512	42.93266	0.80703	Single Span	Span length 0-20m	***1***
514	42.92435	0.64265	Single Span	Span length 20-60m	***2***
516	42.91737	0.64740	Single Span	Span length 20-60m	***2***
517	42.91495	0.63919	Single Span	Span length 20-60m	***2***
519	42.91362	0.65880	Single Span	Span length 0-20m	***1***
521	42.89597	0.71066	Single Span	Span length 20-60m	***2***
523	42.89247	0.72673	Single Span	Span length 20-60m	***2***
525	42.89600	0.69963	Single Span	Span length 20-60m	***2***
527	42.88381	0.71491	Single Span	Span length 20-60m	***2***
529	42.88171	0.71742	Single Span	Span length 20-60m	***2***
531	42.96820	0.66071	Single Span	Span length 0-20m	***1***
533	42.86635	0.74682	Single Span	Span length >60m	***3***
535	42.86655	0.75038	Arch Bridge	Arch length 10-20m ; arch rise/length ratio 0.2-0.3 ; arch thickness/length ratio 0.05-0.1	***16***
537	42.87452	0.78090	Arch Bridge	Arch length 10-20m ; arch rise/length ratio 0.4-0.5 ; arch thickness/length ratio 0.05-0.1	***18***
539	42.87493	0.78207	Arch Bridge	Arch length 10-20m ; arch rise/length ratio 0.4-0.5 ; arch thickness/length ratio 0.05-0.1	***18***
540	42.87148	0.78677	Arch Bridge	Arch length 10-20m ; arch rise/length ratio 0.4-0.5 ; arch thickness/length ratio 0.05-0.1	***18***
543	42.86533	0.79809	Single Span	Span length 0-20m	***1***
545	42.86237	0.74810	Single Span	Span length 20-60m	***2***
546	42.84921	0.73570	Single Span	Span length >60m	***3***
547	42.90500	0.62819	Single Span	Span length 20-60m	***2***
549	42.89929	0.63057	Arch Bridge	Arch length 10-20m ; arch rise/length ratio 0.4-0.5 ; arch thickness/length ratio 0.05-0.1	***18***
554	42.89520	0.62174	Single Span	Span length 20-60m	***2***
555	42.89696	0.61571	Single Span	Span length 20-60m	***2***
557	42.89007	0.62010	Arch Bridge	Arch length 10-20m ; arch rise/length ratio 0.4-0.5 ; arch thickness/length ratio 0.05-0.1	***18***
562	42.87791	0.61418	Mutiple Span	Span length >60m	***23***
565	42.87577	0.61296	Mutiple Span	Span length 20-60m	***22***
567	42.87629	0.60822	Single Span	Span length 20-60m	***2***
569	42.86651	0.61257	Arch Bridge	Arch length 20-30m ; arch rise/length ratio 0.3-0.4 ; arch thickness/length ratio 0.05-0.2	***19***
571	42.86817	0.60964	Single Span	Span length 20-60m	***2***
573	42.86876	0.60829	Single Span	Span length 0-20m	***1***
575	42.86612	0.60629	Single Span	Span length 20-60m	***2***
577	42.86559	0.60692	Single Span	Span length 20-60m	***2***

This project has received funding from the European Union's Horizon 2020 research and innovation programme under grant agreement No 821046

580	42.86460	0.60411	Arch Bridge	Arch length 20-30m ; arch rise/length ratio 0.3-0.4 ; arch thickness/length ratio 0.05-0.2	***19***
583	42.85285	0.60261	Single Span	Span length 20-60m	***2***
585	42.85267	0.62241	Arch Bridge	Arch length 10-20m ; arch rise/length ratio 0.3-0.4 ; arch thickness/length ratio 0.05-0.1	***17***
587	42.84509	0.61149	Single Span	Span length 0-20m	***1***
589	42.83826	0.60581	Arch Bridge	Arch length 20-30m ; arch rise/length ratio 0.3-0.4 ; arch thickness/length ratio 0.05-0.2	***19***
591	42.83778	0.60381	Single Span	Span length 20-60m	***2***
593	42.83559	0.60321	Single Span	Span length 20-60m	***2***
595	42.83189	0.60215	Single Span	Span length 20-60m	***2***
597	42.82876	0.60377	Single Span	Span length 20-60m	***2***
601	42.80590	0.60315	Single Span	Span length >60m	***3***
603	42.80295	0.60823	Single Span	Span length 0-20m	***1***
605	42.79596	0.60897	Single Span	Span length 20-60m	***2***
607	42.79434	0.59679	Single Span	Span length 0-20m	***1***
609	42.79383	0.59290	Single Span	Span length 20-60m	***2***
610	42.79135	0.59950	Single Span	Span length 20-60m	***2***
612	42.78277	0.59870	Single Span	Span length 20-60m	***2***
614	42.77285	0.60320	Single Span	Span length 20-60m	***2***
616	42.77216	0.60354	Single Span	Span length 20-60m	***2***
618	42.76964	0.62085	Single Span	Span length 0-20m	***1***
619	42.75361	0.60875	Single Span	Span length >60m	***3***
621	42.74168	0.61445	Single Span	Span length 0-20m	***1***
624	42.74037	0.61552	Single Span	Span length 0-20m	***1***
625	42.71952	0.65014	Single Span	Span length 0-20m	***1***
627	42.72132	0.65352	Single Span	Span length 0-20m	***1***
629	42.74492	0.61016	Arch Bridge	Arch length 20-30m ; arch rise/length ratio 0.3-0.4 ; arch thickness/length ratio 0.05-0.2	***19***
631	42.74474	0.60848	Arch Bridge	Arch length 20-30m ; arch rise/length ratio 0.3-0.4 ; arch thickness/length ratio 0.05-0.2	***19***
633	42.74867	0.58113	Single Span	Span length 20-60m	***2***
635	42.74854	0.57368	Single Span	Span length 20-60m	***2***
637	42.74956	0.57237	Single Span	Span length 20-60m	***2***
639	42.75034	0.57421	Single Span	Span length 20-60m	***2***
641	42.75079	0.58025	Single Span	Span length 0-20m	***1***
643	42.75056	0.58131	Single Span	Span length 20-60m	***2***
645	42.76063	0.58630	Arch Bridge	Arch length 10-20m ; arch rise/length ratio 0.3-0.4 ; arch thickness/length ratio 0.05-0.1	***17***
647	42.80108	0.56514	Single Span	Span length 20-60m	***2***
649	42.80281	0.56318	Single Span	Span length 20-60m	***2***
650	42.80649	0.56094	Arch Bridge	Arch length 10-20m ; arch rise/length ratio 0.3-0.4 ; arch thickness/length ratio 0.05-0.1	***17***
653	42.80584	0.53240	Single Span	Span length 20-60m	***2***
655	42.80326	0.52359	Single Span	Span length 20-60m	***2***
656	42.80469	0.52200	Single Span	Span length 20-60m	***2***
658	42.80843	0.51496	Single Span	Span length 20-60m	***2***

This project has received funding from the European Union's Horizon 2020 research and innovation programme under grant agreement No 821046

661	42.79531	0.50560	Arch Bridge	Arch length 20-30m ; arch rise/length ratio 0.3-0.4 ; arch thickness/length ratio 0.05-0.2	***19***
662	42.79282	0.48638	Single Span	Span length 20-60m	***2***
665	42.80991	0.50883	Single Span	Span length 20-60m	***2***
667	42.81420	0.48794	Arch Bridge	Arch length 20-30m ; arch rise/length ratio 0.3-0.4 ; arch thickness/length ratio 0.05-0.2	***19***
668	42.81098	0.47260	Arch Bridge	Arch length 20-30m ; arch rise/length ratio 0.3-0.4 ; arch thickness/length ratio 0.05-0.2	***19***
671	42.80755	0.47185	Arch Bridge	Arch length 6-10m ; arch rise/length ratio 0.3-0.4 ; arch thickness/length ratio 0.075-0.1	***12***
673	42.80193	0.46920	Single Span	Span length 20-60m	***2***
675	42.82547	0.54826	Arch Bridge	Arch length 20-30m ; arch rise/length ratio 0.3-0.4 ; arch thickness/length ratio 0.05-0.2	***19***
676	42.83001	0.55055	Single Span	Span length 20-60m	***2***
679	42.83454	0.55051	Single Span	Span length 20-60m	***2***
681	42.83600	0.55047	Single Span	Span length 20-60m	***2***
682	42.84371	0.53956	Single Span	Span length 20-60m	***2***
685	42.84669	0.52864	Arch Bridge	Arch length 10-20m ; arch rise/length ratio 0.4-0.5 ; arch thickness/length ratio 0.05-0.1	***18***
687	42.85081	0.52308	Arch Bridge	Arch length 10-20m ; arch rise/length ratio 0.4-0.5 ; arch thickness/length ratio 0.05-0.1	***18***
688	42.85249	0.51882	Arch Bridge	Arch length 20-30m ; arch rise/length ratio 0.3-0.4 ; arch thickness/length ratio 0.05-0.2	***19***

Table 3.6: Fragility parameters for the bridges, obtained by typological assignment of existing functions, with median value α and standard-deviation β. D1 refers to Minor Damage (bridge remains crossable), D2 refers to Moderate Damage, D3 refers to Major Damage.

		D1		**D2**		**D3**	
Fragiltiy ID	**Reference**	**α (g)**	**β**	**α (g)**	**β**	**α (g)**	**β**
1	Shinozuka et al. (2003)	1.447	0.897	1.753	1.086	2.694	1.669
2	Shinozuka et al. (2003)	0.669	0.271	0.755	0.306	1.057	0.429
3	Shinozuka et al. (2003)	0.79	0.787	1.524	1.518	2.879	2.867
8	Zampieri (2014)	0.11	0.02	0.18	0.04	0.3	0.07
12	Zampieri (2014)	0.19	0.05	0.3	0.07	0.53	0.17
14	Zampieri (2014)	0.11	0.02	0.2	0.05	0.3	0.08
16	Zampieri (2014)	0.28	0.13	0.45	0.23	0.82	0.31
17	Zampieri (2014)	0.16	0.03	0.27	0.07	0.45	0.23
18	Zampieri (2014)	0.09	0.02	0.2	0.05	0.25	0.07
19	Zampieri (2014)	0.15	0.03	0.32	0.08	0.45	0.23
21	Kaynia et al. (2013)	1.166	1.123	1.61	1.551	2.846	2.74
22	Kaynia et al. (2013)	0.99	1.019	1.263	1.3	2.354	2.423
23	Kaynia et al. (2013)	0.575	0.328	0.656	0.374	0.932	0.531

As an alternative, EUC has developed, for the single-span and multi-span girder and arch bridges fragility models for bridges located in Italy based on the different taxonomies defined and described in §2.1.2.1.3.
For the girder bridges the assignment of a taxonomy is based on several parameters: number of spans; material of substructure element (abutments and piers); mean value of length of spans; deck material; height of abutments and piers; presence of seismic isolation devices to prevent the fall of the deck from piers.While for arch bridges the parameters considered are: number of spans; bridge material (masonry or concrete); arch geometry (circular of depressed arch); span length; height of substructures (abutments and piers).

This project has received funding from the European Union's Horizon 2020 research and innovation programme under grant agreement No 821046

Figure 3.2 shows the location of bridges in Luchon area. The EUC approach has only been applied to some selected bridges, based on their importance in the road network. The fragility functions based on taxonomies described in §2.1.2.1.3 assigned to arch and girder bridges and the fragility parameters for Damage Limit State (DLS) and Collapse Limit State (CLS) are summarized in Table 3.7 and Table 3.8, respectively, where α is the median value and β is the standard deviation of lognormal distribution.

Table 3.7: Fragility functions assigned to arch bridges in Luchon area by EUC for Damage Limit State (DLS) and Collapse Limit State (CLS), where (α) is the median value and (β) the standard deviation of lognormal distribution.

									DLS		CLS	
id	Number of spans	Tot. length[m]	Span lenght[m]	Bridge material	Vertical element material	Height[m]	Bridge type	Taxonomy	α[g]	β[-]	α[g]	β[-]
2	1	20	20	Masonry	Masonry	3	Depressed arch	A_MMH1L2_SR	0.325	0.401	0.987	0.323
263	3	50	20	Masonry	Masonry	<4m	Depressed arch	A_PMH1L2_SR	0.199	0.394	0.536	0.236
580	1	34	34	masonry	Masonry	<4m	Circular arch	A_MMH1L2_TS	0.124	1.106	0.474	0.342

Table 3.8: Fragility functions assigned to girder bridges in Luchon area by EUC for Damage Limit State (DLS) and Collapse Limit State (CLS), where (α) is the median value and (β) the standard deviation of lognormal distribution.

								DLS		CLS	
id	Number of spans	Tot. length[m]	Span lenght[m]	Deck material	Vertical element material	Height[m]	Taxonomy	α[g]	β[-]	α[g]	β[-]
242	1	45	45	RC	RC	5	T_MCH1L2	0.179	0.873	1.405	0.425
459	3	56	18.6	RC	RC	3	T_PCH1L1	0.154	0.907	0.633	0.354
478	3	45	15	RC	masonry	3	T_PMH1L1	0.113	0.793	0.397	0.534
491	1	60	60	RC	RC	3	T_MCH1L2	0.179	0.873	1.405	0.425
501	1	36	36	RC	masonry	2	T_MMH1L2	0.109	0.560	0.503	0.738
516	1	38	38	RC	RC	H<10m	T_MCH1L2	0.179	0.873	1.405	0.425
533	3	125	40	metallic	RC	3	T_PCH1L2	0.113	1.00	0.471	0.310
546	1	50	50	RC	RC	3	T_MCH1L2	0.179	0.873	1.405	0.425
562	3	46	15	RC	RC	4	T_PCH1L2	0.113	1.000	0.471	0.310
597	1	22	22	RC	masonry	2	T_MMH1L2	0.109	0.560	0.503	0.738
609	1	15	15	RC	RC	3	T_MCH1L2	0.179	0.873	1.405	0.425

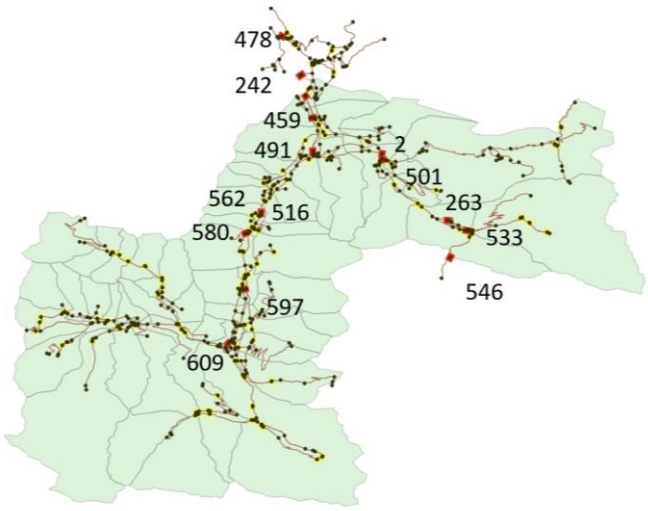

Figure 3.2: Map showing the 53 municipalities and the road network in Luchon area. The dots represent the intersection of 3 or more segments as well as the ending roads. Yellow dots define the bridges. Red dots indicate 14 bridges studied using two different approaches for fragility modelling.

This project has received funding from the European Union's Horizon 2020 research and innovation programme under grant agreement No 821046

The comparison of the fragility curves obtained with the two methods is shown in Figure 3.3, for 14 bridges. For comparison purposes, the first limit state is referred to as 'Damaged bridge'. The third limit state reflects the complete collapse of the bridge and is referred to as 'Collapsed bridge'.

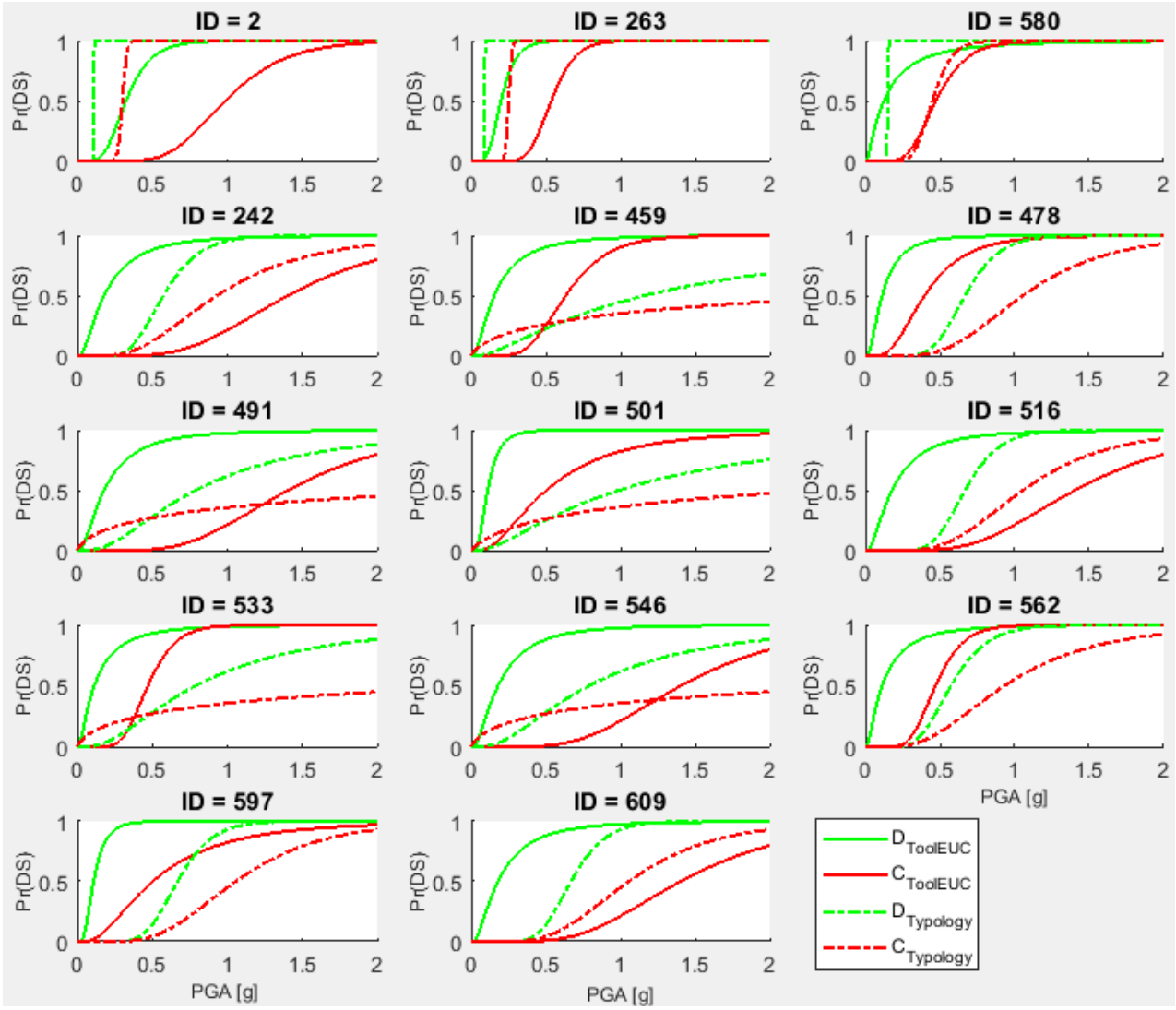

Figure 3.3: Fragility curves for 14 bridges out of 118 in the transportation network connected Luchon area. Green curves refer to damaged bridges (not functional) whereas the red curves refer to collapsed bridges. Dashed lines refer to fragility cruves extracted following the typological-identification approach, while filled lines refer to fragility curves following the EUC approach.

3.2.2 Loss estimation models selected for the Luchon area

No monetary value estimation is currently planned: the main target indicator is the casualties (dead and injured) and the number of homeless.

We estimate human losses using a casualties matrix, based on values proposed by Coburn and Spence (1992). This matrix relates the damage state of the structure to the percentage of human losses expressed in terms of P0: no injury, P1: light injury, P2: injury requiring hospitalization, P3: life threatening injury; and P4: death.

This project has received funding from the European Union's Horizon 2020 research and innovation programme under grant agreement No 821046

Table 3.9: Casualty estimation matrix, based on the EMS98 damage levels (Grüntal et al., 1998) of residential buildings.

Casualty severity	EMS98 Damage levels					
	D0	D1	D2	D3	D4	D5
P0	1	0.999807	0.99825	0.9725	0.765	0.18
P1	0	0.000165	0.0015	0.025	0.2	0.34
P2	0	0.000022	0.0002	0.002	0.03	0.13
P3	0	0	0	0	0	0.13
P4	0	0.0000055	0.00005	0.0005	0.005	0.22

3.3 TB-3: Hveragerði, South Iceland and Húsavík, North Iceland

3.3.1 Fragility models selected for Hveragerdi and Húsavik

For the town Hveragerði in South Iceland and the town Húsavík in North Iceland the fragility models for residential buildings and service buildings will be based on statistical vulnerability models presented by Bessason et. al. 2020. The common standard methodology in the literature is first to construct fragility curves and then use them to create and build loss estimation models also called vulnerability models. The fragility models for testbed 3 (TB-3) in Iceland, are determined in reversed order, first a statistical vulnerability model is constructed that can be used to predict losses and from this model fragility curves are computed. Due to this reversed order, the methodology for both the loss estimation models and the fragility models is described in the next section.

3.3.2 Loss estimation models selected for Hveragerdi and Húsavik

The statistical loss estimation model was evaluated from complete empirical loss data recorded after the two M_w6.5 South Iceland Earthquakes of June 2000 (Bessason et al. 2020). The loss data from these events is complete in the sense it covers all affected buildings in the affected area where estimated PGA was greater than 0.05g, it total almost 5000 buildings. Due to the high proportion of no-loss buildings in the loss database (~84%), a zero-inflated beta regression model (Ospina et al. 2012) was fitted to data and used to model the damage ratio or damage factor, DF, defined as:

$$DF = \frac{\text{Estimated loss}}{\text{Replacement value}} \tag{3.7}$$

The factor is bounded to be in the range [0,1], where 0 means no-loss and 1 means total-loss (100%). The model was fitted to the three main building typologies in the affected region, i.e. low-rise structural wall RC (54% of the residential building stock), timber buildings (36%), and masonry buildings. (9.3%). Only, 0.3% of the residential building stock does not belong to any of these three classes. Seismic codes were first implemented in Iceland in 1976. Concrete buildings constructed before had a limited amount of reinforcement, typically only steel bars around openings in structural walls (low code). Most of the RC buildings (old and new) are in-situ cast and only a few are using prefabricated elements. Prescribed wind loads in Iceland are among the highest in Europe. The fundamental base value of wind velocity is $v_{b,0}$=36 m/s (CEN, 2005; Icelandic standards, 2010). Consequently, to withstand high wind loads, the Icelandic timber houses are strongly built and well suited to withstand earthquake forces. The bottom floor slab and the foundations are usually made of RC, as in the concrete houses. The masonry buildings were built of unreinforced manufactured hollow pumice (*high porosity volcanic rock*) blocks in walls and tied together with rigid RC floors. The weight density of the pumice blocks is low, typically around 14 kN/m^3, and consequently the inertia forces are lower than in ordinary Southern Europe stone or clay brick masonry buildings. Masonry buildings were mainly built before 1980 and are no longer constructed. An important characteristic of the Icelandic building stock is how young it is in an international context. No building was built before 1870 and 92% of them were constructed after 1940.

This project has received funding from the European Union's Horizon 2020 research and innovation programme under grant agreement No 821046

The details of the statistical vulnerability models are given in Bessason et al. (2020), see also Ioannou et al. (2018). The main structure and equations behind the model as well as model parameters are given below. The vulnerability model is constructed by combining a logistical regression model and a conditional beta regression model, commonly called zero-inflated beta regression model (Ospina et al., 2012). The logistical regression model is used to predict the probability, p_j, of getting loss (DF>0) as a function of PGA:

$$\log\left(\frac{p_j}{1-p_j}\right) = \beta_{0,j} + \beta_{1,j} \cdot PGA \tag{3.8}$$

where $\beta_{0,j}$ and $\beta_{1,j}$ are the regression parameters; and j refers to building typology. A conditional probability model for the loss expressed by DF, given the occurrence of a loss (DF>0), is modelled by a beta distribution which is bounded in the unit interval (0, 1) (Ferrari et al. 2004). In the case of total loss (DF=1) of a building, which only occurred in a very few cases in the South Iceland earthquakes of June 2000, DF was replaced with a value less than a unit (Bessason et al. 2020). The probability density function (PDF), expected value and variance of the model, are respectively given as:

$$f\left(x|DF>0\right) = \frac{\Gamma(\varphi)}{\Gamma(\mu\varphi)\Gamma(1-\mu)\varphi} x^{\mu\varphi-1}(1-x)^{(1-\mu)\varphi-1} \qquad 0<x<1 \tag{3.9}$$

$$E\left[X\middle|DF>0\right] = \mu \qquad 0<\mu<1 \tag{3.10}$$

$$\mathrm{Var}\left[X\middle|DF>0\right] = \frac{\mu(1-\mu)}{1+\varphi} \qquad \varphi>0 \tag{3.11}$$

where, μ is the mean value and φ is the precision. The mean value, μ, is related to the explanatory variables through the link function, $g_1(\cdot)$:

$$\mu = g_1^{-1}(\eta_1) \tag{3.12}$$

where η_1 is a function of the explanatory variable, PGA. The logit link function was adopted for the model:

$$g_1(\mu) = \mathrm{logit}(\mu) = \log\left(\frac{\mu}{1-\mu}\right) \tag{3.13}$$

Similarly, the precision, φ, which was considered as a constant intercept, is related to η_2, through a link function, g_2:

$$\varphi = g_2^{-1}(\eta_2) \tag{3.14}$$

In the model, the link function of the precision was expressed in the form:

$$g_2(\varphi) = \log(\varphi) \tag{3.15}$$

Instead of fitting one model to all the building typologies using categorical variables, models were fitted independently for each typology (Bessason et al. 2020). The functions of explanatory variables were taken in this study as:

$$\eta_{1j} = \theta_{0,j} + \theta_{1,j} \times log(PGA) \tag{3.16}$$

$$\eta_{2j} = \theta'_{0,j} \tag{3.17}$$

This project has received funding from the European Union's Horizon 2020 research and innovation programme under grant agreement No 821046

where θ_{0j}, θ_{1j} and θ'_{0j} are the regression parameters of the conditional beta regression model and j={RC, timber, masonry} as before. The parameter set for each building typology, therefore, consists of five regression parameters namely $\beta_{0,j}$, $\beta_{1,j}$ $\theta_{0,j}$, $\theta_{1,j}$ and $\theta'_{0,j}$.
To determine the expected value of loss or desired prediction limit, the logistical regression model and the conditional beta model were combined. The expected value and the variance are given as (Ospina & Ferrari, 2012):

$$E\left[DF_j\right] = \mu_j \cdot p_j \tag{3.18}$$

$$VAR\left[DF_j\right] = p_j \frac{\mu_j \cdot \left(1-\mu_j\right)}{\varphi_j + 1} + \left(1-p_j\right) \cdot p_j \cdot \mu_j^2 \tag{3.19}$$

here μ_j is computed from Eq. (3.12), (3.13) and (3.16)and p_j from Eq. (3.8). Any desired predictions interval can be computed as (Bessason et al. 2020):

$$\mathrm{P}\left[X < x\right] = 1 + p_j\left(F_X(x, \mu_j, \varphi_j) - 1\right) \tag{3.20}$$

where $F_X(x,\mu_j,\varphi_j)$ is the conditional beta cumulative distribution function for a given building typology j. By, for instance, putting P[$X < x$]=0.90 and solving Eq. (3.20) it is possible to find the 90% upper bound for *DF*, i.e. 90% of the losses (*DF*) will be less than this value.

When running the regression analysis, several different classifications of building typologies were tested in Ioannou et al. (2018), for instance the effect of construction year where the aim was to observe the effect of low code and high code buildings for RC buildings and timber buildings. The loss data did not show a significant difference in model parameters, so the result was models for only three different building typologies, i.e. RC, timber and masonry. According to the SERA taxonomy the RC buildings are assumed to cover two classes, while one class is assumed for both timber and masonry buildings:

- RC buildings: CR/LWAL+DUL/HBET:1,3 and CR/LWAL+DUM/HBET:1,3.
- Timber buildings: W/LWAL+DUM/HBET:1,2
- Masonry buildings: MUR+CB99/LWAL+DNO/HBET:1,3.

One reason for this can be related to the fact that a high proportion of the losses were due to non-structural losses (Bessason et al. 2014; Bessason et al. 2016) which is included in the loss model. The final results were the model parameters estimated for the three main building typologies, given in Table 3.10, (Bessason et al. 2020).

Table 3.10: Estimated model parameters, Mean and Standard Error (SE) based on two-step regression.

	β_0		β_1		θ_0		θ_1		θ'_0	
J	Mean	SE	Mean	SE	Mean	SE	Mean	SE	Mean	SE
RC	–3.503	0.123	11.953	0.632	–1.774	0.031	0.305	0.023	1.645	0.024
Timber	–3.457	0.143	7.267	0.517	–2.315	0.025	0.103	0.025	1.894	0.027
Masonry	–3.025	0.259	11.370	1.357	–0.360	0.031	0.725	0.019	1.012	0.017

The loss estimation mean curve (vulnerability curve) for each building typology presented as damage ratio (DF) is shown in Figure 3.4. Computed prediction interval that corresponds to ± one standard deviation in the standard normal distribution, i.e. by solving Eq. (3.20) with P[$X < x$]=0.16 and P[$X < x$]=0.84, as well as the mean curve plus one standard deviation given by Eq. (3.19), are also shown. It should be noted that mean minus one standard deviation can provide negative damage ratio, especially at low PGA, which has no meaning (negative loss). This fact explains why beta-model is preferable to construct the statistical model.

This project has received funding from the European Union's Horizon 2020 research and innovation programme under grant agreement No 821046

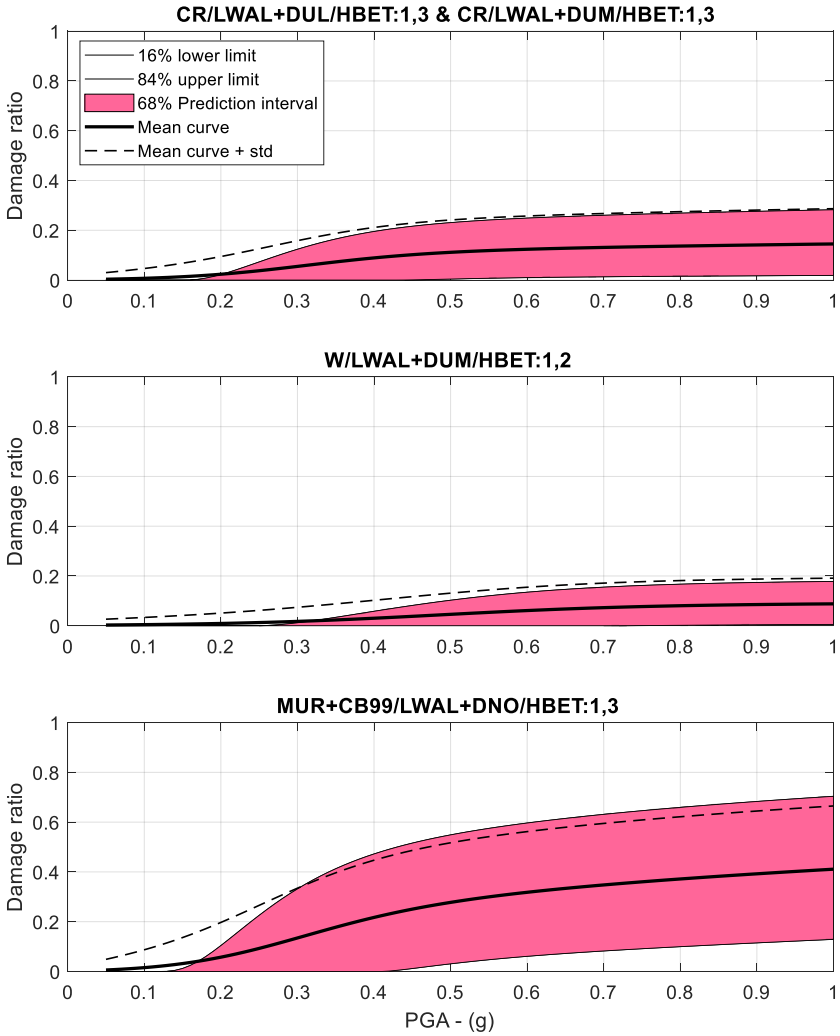

Figure 3.4: Comparison of mean curve (solid black line), prediction interval with 84% upper and 16% lower prediction bounds (pink area), and mean + plus one standard deviation curve (dotted line).

From the statistical model and Eq. (3.20), (P[X>x]=1-P[X<x]) it is also possible to construct fragility curves that can be used to compare with other studies. To do this, it is necessary to define damage levels in the form of loss bins. Five damage levels (D1-D5) are given below referring to the EMS98 scale (Grüntal et al., 1998). The link between damage levels and damage ratios is different between references but here it is based on Maiwald and Schwarz (2020). The damage lavels can be adjusted for any required damage ratio range without changing the parameters in Table 3.10:

- D0 – *No damage / No loss*
- D1 – *Negligible to slight damage*, loss in the range 0-1% of replacement value
- D2 – *Moderate damage*, loss in the range 1-7,5% of replacement value
- D3 – *Substantial to heavy damage*, loss in the range 7,5-20% of replacement value
- D4 – *Very heavy damage*, loss in the range 20-60% of replacement value
- D5 – *Destruction*, loss is more than 60% of replacement value, i.e in the range 60-100%.

In Figure 3.5 the probability of exceedence these damage levels are given, i.e. the fragility curves are shown and linked to the SERA taxonomy.

This project has received funding from the European Union's Horizon 2020 research and innovation programme under grant agreement No 821046

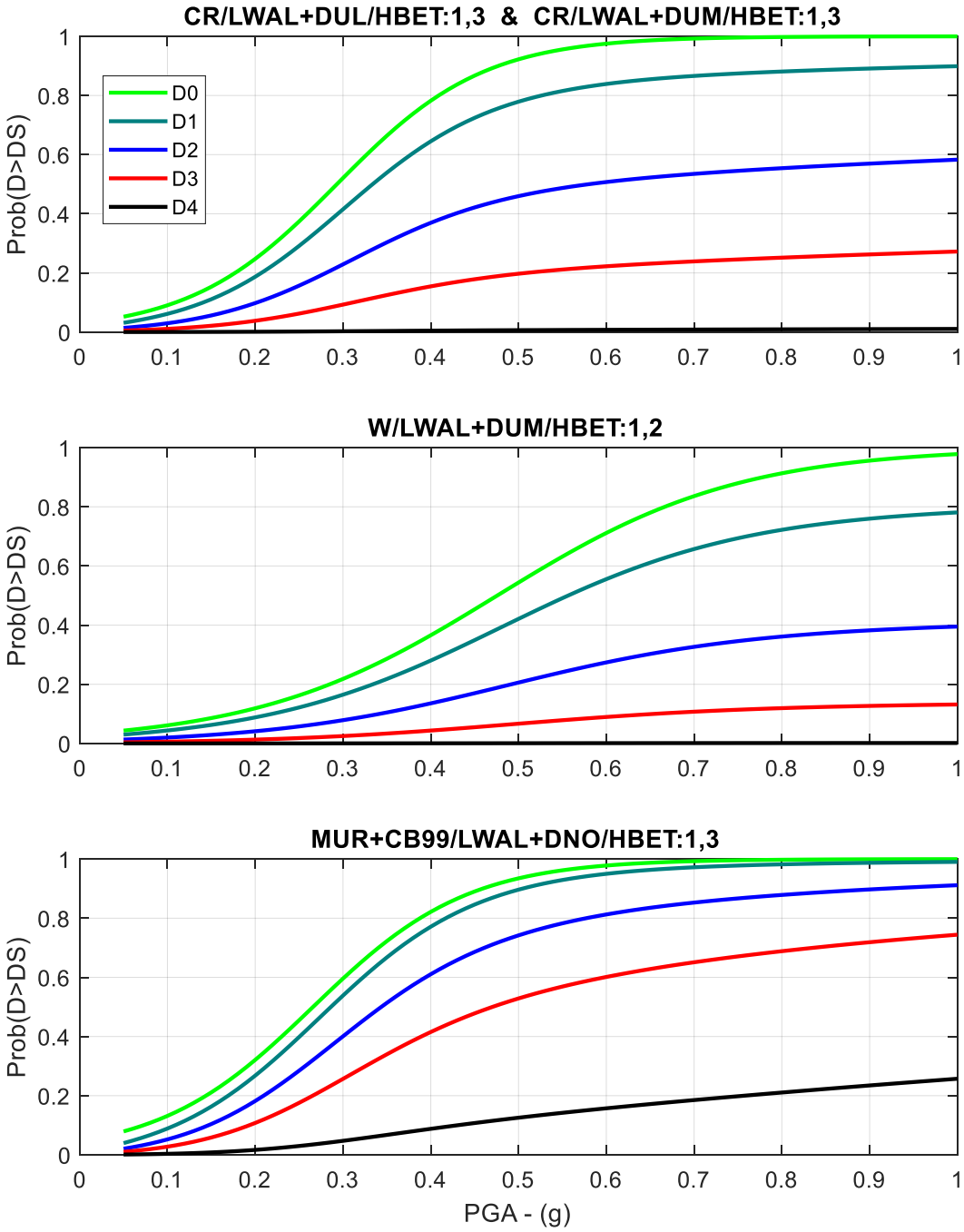

Figure 3.5: Fragility curves based on the statistical model for RC, timber and masonry buildings.

Finally, it should be underlined that the presented vulnerability model for TB3 is based on loss data from M_w6.5 earthquakes and it is belived to be representaive for seismic risk analysis in the magnitude range of 6.4 – 6.6. A caution is necessary when using the model outside these ranges as it may overpredict losses for lower magnitude earthquakes and underestimate losses for larger magnitude earthqukaes.

This project has received funding from the European Union's Horizon 2020 research and innovation programme under grant agreement No 821046

3.4 TB-4: Patras and Aegio, Greece

TB-4 covers the Achaia area and the western Corinth Gulf, central Greece, which includes the fastest deforming continental rift, presenting the highest seismic activity across Europe. The analysis for TB-4 regarding vulnerability, fragility and loss estimation models considers: (a) the city of Patras, the capital city of the Achaia Prefecture and the third largest city in population in Greece and, (b) the town of Aegion, which lies in a region of notable seismic hazard capable of producing strong earthquakes with short recurrence periods.

The city of Patras is a major centre of population and industry of the mainland Greece. It includes significant large infrastructure: facilities of public use, heritage monuments, one of the world's longest multi-span cable-stayed bridge (Rio-Antirrio), a harbor of principal commercial and tourist links with western Greece and Europe. Its urban planning, primarily is focused on socio-economic factors, with less attention to the intense geodynamic processes of engineering importance, such as the existence of an active fault (Agia Triada fault) spanning the city. More than 30,000 buildings, of both residential and public use, form the Patras city centre, and according to the analysis of the available census data (see following section): at least 67.48% are considered RC; 8.19% without Earthquake Resistance Design (ERD), 52.70% with moderate ERD and 6.58% with high ERD, while at least 28.06% are considered UnReinforced Masonry (URM); more specifically, 7.12% of simple stone, 16.97% of old bricks and 3.97% of old bricks with RC floors, as it is shown in Figure 3.6.

The town of Aegion displays a complex topography. The city has experienced significant structural damage caused by strong earthquakes in the past. The latest, on the 15th June 1995, an earthquake with magnitude Mw6.4, characterized as the most recent destructive earthquake in the region that generated almost 22.15% of heavy to very heavy structural damage and collapse in the town center. An exposure model produced in year 2016 for the Aegion town centre (after Giannaraki et al., 2018), consists of 3,216 buildings, both residential and commercial, with a proportion of 25.69% being URM; 4.13% adobe, 5.27% simple stone, 12.29% old bricks and 4% old bricks with RC floors, in addition to a proportion of 73.36% RC buildings, which more than 65% are considered to have moderate ERD and been erected with high ERD after the disastrous 1995 earthquake.

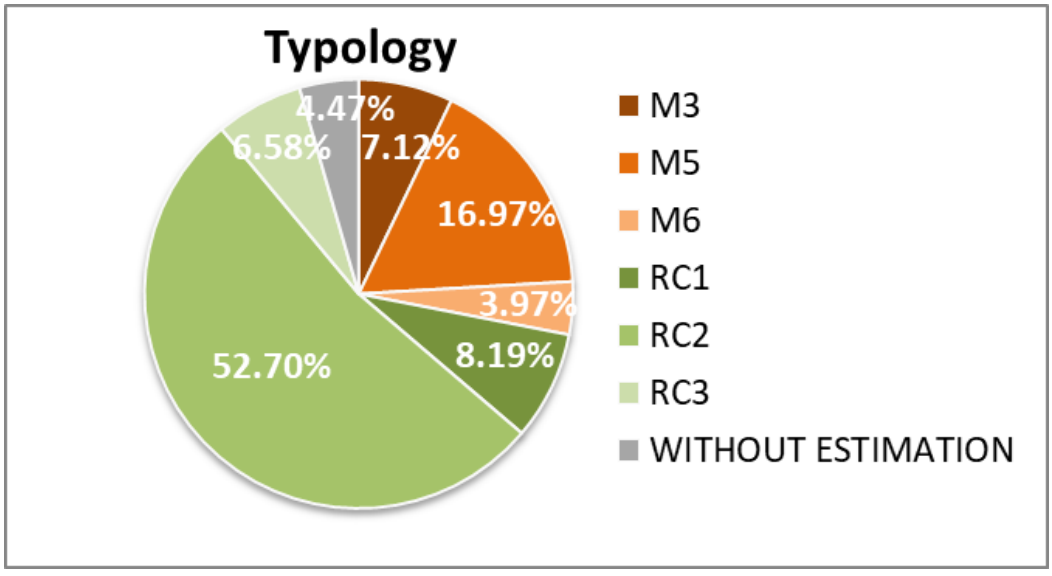

a)

This project has received funding from the European Union's Horizon 2020 research and innovation programme under grant agreement No 821046

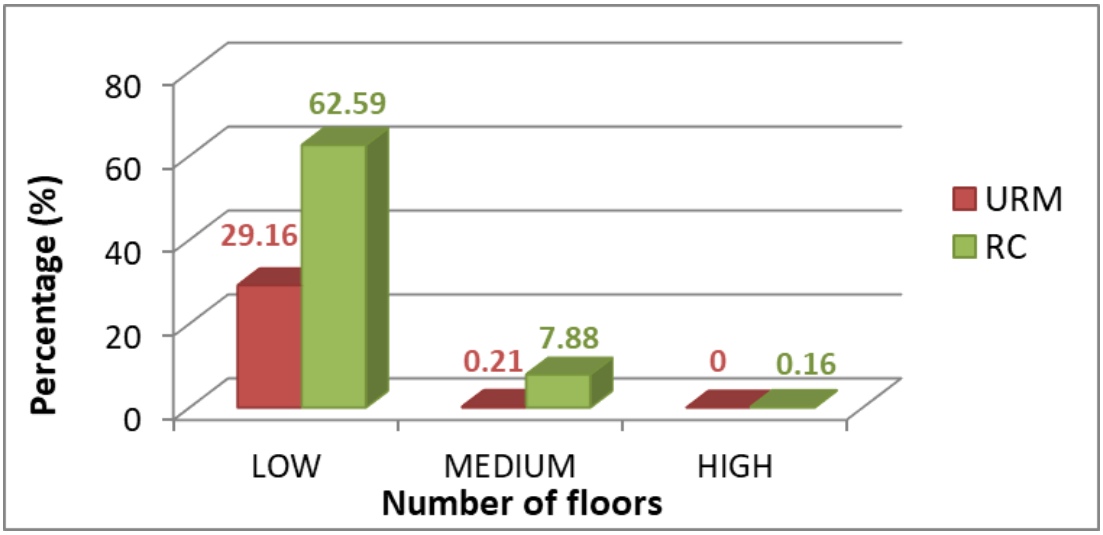

b)

Figure 3.6: a) The percentage of each URM and RC building typology classified in the city of Patras and b) their general percentage with respect to the number of floors.

3.4.1 TB4 available exposure data

The exposure model for TB4 is based on the available census data (EPANTYK, 2009) which contains the following information per inspected building:

- The census building block code which is common to the background of the available geospatial data and can be linked to the digitized building blocks.
- The existence of the building inside or outside the settlement; no records of buildings outside the study area are indicated in the available data.
- The existence of basement, ground floor, pilotis.
- The number of floors.
- The period of construction according to the numerical coding category, see in Table 3.11.
- Indication whether the respective building is detached or not to the adjacent neighboring buildings.
- The construction material: Concrete-béton, Steel, Timber, Bricks/Cement blocks, Stone, Other materials, Indefinite material.
- Roof coating form and roofing materials: Terrace/Slab, Tiled roof, Roof with overlapping sheets, Roof with other materials, Indefinite material.
- Exclusive use of the building: Mixed use, Residential, Church/Monastery, Hotel, Factory/Laboratory, School, Store/Professional office, Car station, Hospital/Health Clinic, Other use.
- Mixed/main and secondary use of the building with the previously mentioned subcategories.

It should be noted that in the specific data set, the exact position of the building inside its respective block is not specified, due to reasons of personal data retention and thus, the building stock of the city/town is represented after the analysis on a block-by-block level.

In the present analysis (first for the city of Patras), infrastructures that have not been recorded with a specific definition of construction material (probably mixed constructions in terms of material, RC/Concrete-béton and URM buildings of bricks/cement blocks for which the period of construction is not specified) are omitted, due to unavailable classification of the Typological Vulnerability Index. Steel and Timber typologies are additionally excluded from the elaboration of the dataset since the existence of these infrastructures cannot be confirmed nowadays. The latter was applied in the Patras city center analysis.

This project has received funding from the European Union's Horizon 2020 research and innovation programme under grant agreement No 821046

Hence, the final exposure sample consists of 30,175 buildings, both residential and public use, corresponding to 1,908 blocks, out of which 6 types are classified and considered for the vulnerability analysis in Patras according to the available census description of structural characteristics; 3 types of URM (28.06%) and 3 types of RC frames (67.48%) that have been classified in agreement with the evolution of the Greek Seismic Design Codes according to Table 3.11. URM buildings of bricks with RC floors (3.97%) have been considered herein to be corresponded after the year 1970 as newer constructions of masonry. Figure 3.6 shows the percentage of each building typology that is classified for Patras and the percentage of URM, RC building categories with respect to the number of floors according to the sample of the census dataset.

Table 3.11: Building Typologies in the city of Patras with the adopted Typological Vulnerability Index (V_I*) and scores for Behavior Modifier factors (V_{mk}) according to Giovinazzi and Lagomarsino, 2004. The most probable Vulnerability Class (VC) per EMS98 (Grüntal et al., 1998) is further attributed.

<table>
<tr><td rowspan="15">Behavior Modifiers</td><td rowspan="15">Attributes</td><td>Census coding of period of construction</td><td colspan="3">URM</td><td colspan="3">RC</td></tr>
<tr><td>1: < 1919</td><td rowspan="10">M3(3)</td><td rowspan="4">M5</td><td rowspan="4"></td><td rowspan="3">RC1</td><td rowspan="3"></td><td rowspan="9"></td></tr>
<tr><td>2: 1919 – 1945</td></tr>
<tr><td>3: 1946 – 1960</td></tr>
<tr><td>4: 1961 – 1970</td><td rowspan="7"></td><td rowspan="6">RC2</td></tr>
<tr><td>5: 1971 – 1980</td><td rowspan="6"></td><td rowspan="6">M6</td></tr>
<tr><td>6: 1981 – 1985</td></tr>
<tr><td>7: 1986 – 1990</td></tr>
<tr><td>8: 1991 – 1995</td></tr>
<tr><td>9: > 1996</td><td rowspan="2"></td><td rowspan="2">RC3</td></tr>
<tr><td>10: Under construction (> 2001)</td></tr>
<tr><td rowspan="14"></td><td colspan="5">V_I*</td></tr>
<tr><td colspan="2">0.74</td><td>0.616</td><td>0.644</td><td>0.484</td><td>0.324</td></tr>
<tr><td colspan="5">Most Probable VC per EMS98 (Grünthal, 1998)</td></tr>
<tr><td colspan="2">B</td><td colspan="2">C</td><td>D</td><td>E</td></tr>
<tr><td colspan="5">V_{mk}</td></tr>
<tr><td rowspan="3">Number of floors</td><td>Low: [0-2][a] ; [0-3][b]</td><td colspan="3">-0.04</td><td colspan="3">-0.02</td></tr>
<tr><td>Medium: [3-5][a] ; [4-7][b]</td><td colspan="5">0</td></tr>
<tr><td>High: ≥ 6[a] ; ≥ 8[b]</td><td colspan="2">0.04</td><td>0.08</td><td>0.06</td><td>0.04</td></tr>
<tr><td rowspan="3">Vertical Irregularity (Geometry/Mass distribution)</td><td>Existence of basement</td><td colspan="3" rowspan="2">0.04</td><td rowspan="2"></td><td rowspan="2"></td><td rowspan="2"></td></tr>
<tr><td>Mixed use(1)</td></tr>
<tr><td>Existence of pilotis</td><td colspan="3"></td><td>0.04</td><td>0.02</td><td>0</td></tr>
</table>

This project has received funding from the European Union's Horizon 2020 research and innovation programme under grant agreement No 821046

Roof (Weight, thrust & connections)	Existence of concrete roof		0.04	0	
Aggregate Building: position	Adjacent to neighboring buildings(2)		0.06		
	Adjacent/ Insufficient aseismic joints			0.04	0

(1) The designation of mixed use of buildings has been included for higher safety considering that this may indicate, e.g., the existence of department stores and therefore, the discontinuity of floors.
(2) The information of whether a building is adjacent to its neighbors buildings is available to the census dataset and not its exact position about how it is adjacent to them, therefore the aggregate position of header is considered in the case of URM buildings for higher safety.
(3) The code characterization of simple stone exists in the census dataset, therefore, the type M3 is considered in these cases of category description for higher safety.
[a] URM
[b] RC

3.4.2 Estimation of V_I in TB4 using empirical approach

Seismic vulnerability in the city of Patras has been assessed taking into consideration the empirical RiskUE-LM1 approach as proposed by Giovinazzi and Lagomarsino (2004).

Seismic Behavior Modifiers (ΔVm) and their corresponding empirical scores (Vmk) according to Giovinazzi and Lagomarsino (2004), have been additionally attributed to each certain building typology after the assignment of the most probable Typological Vulnerability Index (V_I*) accounting for structural and morphological peculiarities that can be deduced from the description of the available census dataset (Table 3.11).

A Vs30 distribution for the city of Patras (Figure 3.7) is also determined, in order to define Soil Modifiers by taking into consideration site effects for the dynamic characterization of both building categories and soil types. For this aim, available measurements of Vs30 from recording stations of the University of Patras Accelerographic Network (UPAN) have been taken into account (Batilas, 2015), after validating the accuracy of their location, through the referenced description and google earth, in addition to available Vs30 measurements of Stewart et al. (2014). In case of common locations from both aforementioned references, the highest value has been considered. The same approach was also considered for those measurements that were located quite close to each other. Consequently, the soil category in the city of Patras has been classified per building block according to EC-8 (CEN, 2004) and Table 3.12, after attributing to them a mean Vs30 value.

This project has received funding from the European Union's Horizon 2020 research and innovation programme under grant agreement No 821046

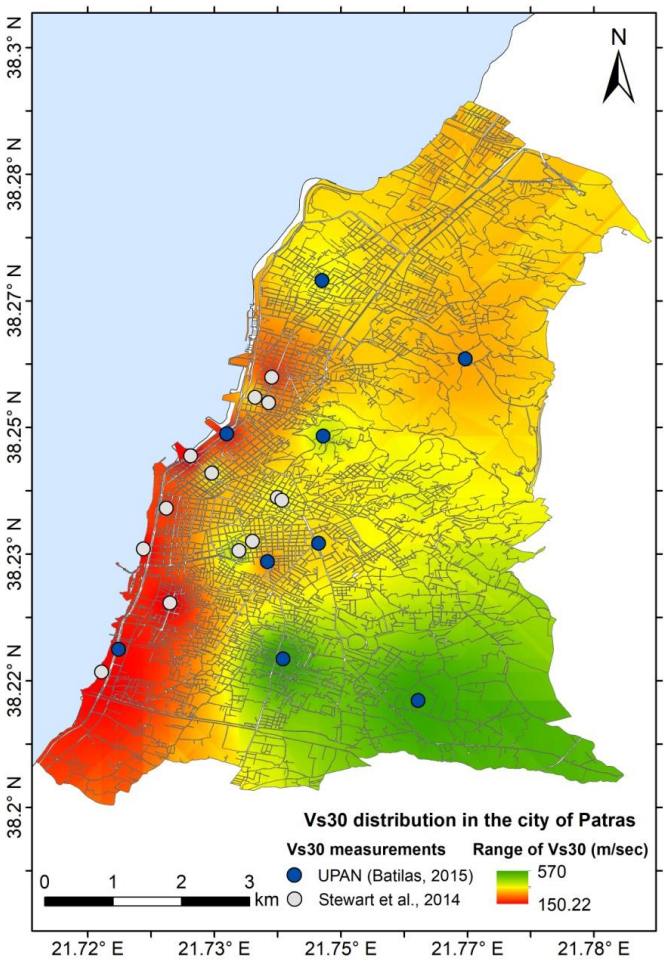

Figure 3.7: Export of a Vs_{30} distribution in the city of Patras baised on available Vs_{30} measurements.

Table 3.12: Soil classification based on EC-8; the estimation of the range of Vs_{30} is set in this way for higher safety.

Site Class	Vs_{30} (m/sec)
A	> 800
B	(360 - 800]
C	(180-360]
D	≤ 180

Intensity Increments (ΔI), coherent with the ones proposed in literature by Giovinazzi and Lagomarsino (2004), have been evaluated for the respective soil categories in the city of Patras and for the different range of height (Low, Medium, High) of URM and RC typologies as specified in Table 3.11. By assuming the proposed formula for macroseismic vulnerability curves as the link between Intensity and Vulnerability, the Vulnerability Increment (ΔV) corresponding to ΔI is attributed according to equation 3.21:

$$\Delta V = \frac{\Delta I}{6.25} \tag{3.21}$$

The Vulnerability Index (V_I) for Soil Modifiers as estimated for different building typologies, different ranges of height/number of floors and ground types in the city of Patras is shown in Table 3.13 and a total value of V_I for Soil Modifiers has been attributed per building block.

The Total V_I has then been computed according to equation 3.22 (Giovinazzi and Lagomarsino, 2014):

This project has received funding from the European Union's Horizon 2020 research and innovation programme under grant agreement No 821046

$$\bar{V}_I = V_I^* + \Delta V_m \rightarrow$$
$$\bar{V}_I = V_I^* + \sum_k r_k * V_{mk} \quad (3.22)$$

where rk is the ratio of building affected by the behavior modifier k characterized by a Vmk score; behavior and soil modifier factor. Hence, an average value of the Total V_I has been attributed per building block in the city of Patras. It should be noted that the Regional Vulnerability Factor is not considered in our analysis as an additional modification factor since no specific information through expert judgment is available on a regional level. Figure 3.8 shows the final distribution of the vulnerability analysis in the city of Patras from the general estimation of structural characteristics as well as with the inclusion of soil effect.

Table 3.13: Vulnerability Increments (ΔV) for EC-8 soil categories and building typologies with respect to their height range in the city of Patras. ΔV values are related to a fundamental period/multiplier factor of PGA for the different building typologies, which generates seismic action producing the same effect on specific building type built on specified soil category as if it was built on rock (Ground type A - rock).

ΔV	B/A		C/A		D/A	
	URM	RC	URM	RC	URM	RC
LOW	0.05	0.05	0.04	0.04	0.08	0.08
MEDIUM	0.05	0.11	0.04	0.15	0.08	0.24
HIGH	0.07	0.11	0.06	0.15	0.11	0.26

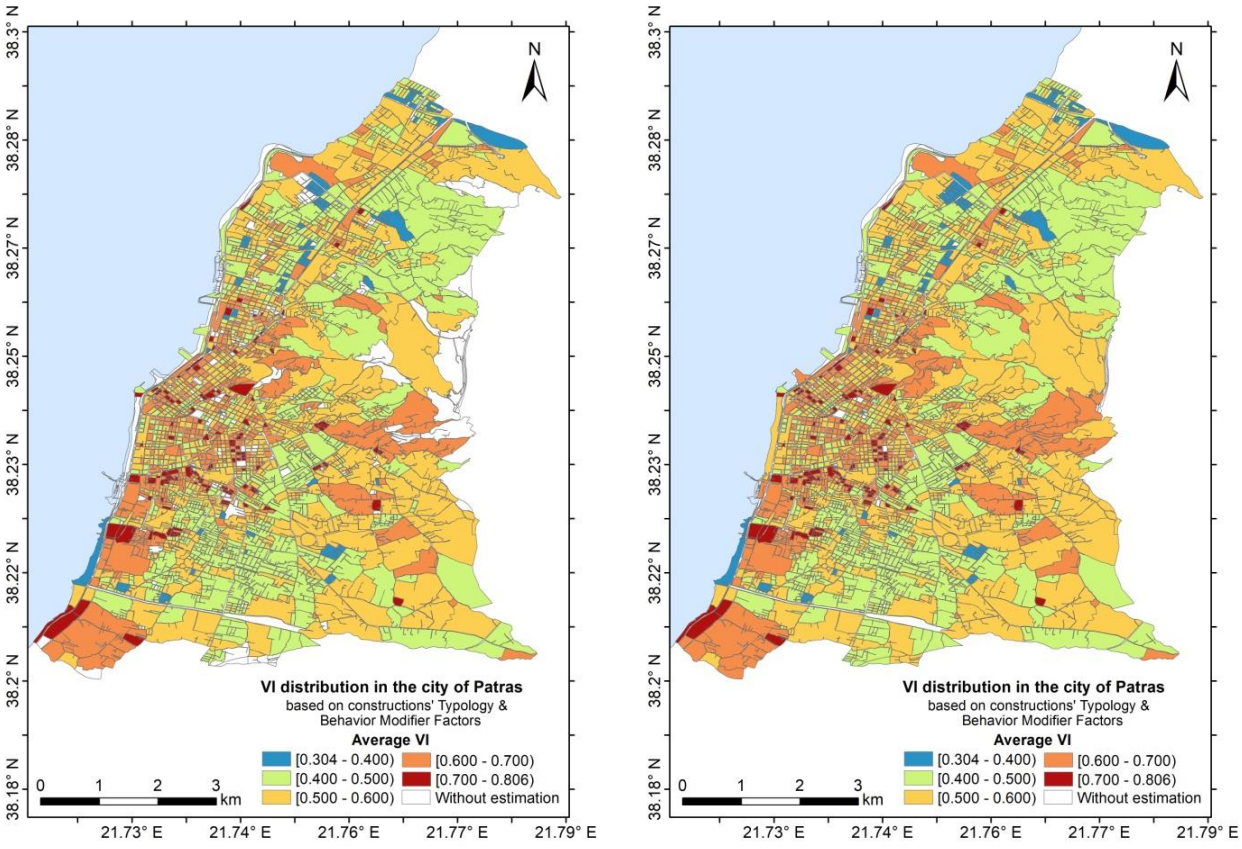

a) b)

This project has received funding from the European Union's Horizon 2020 research and innovation programme under grant agreement No 821046

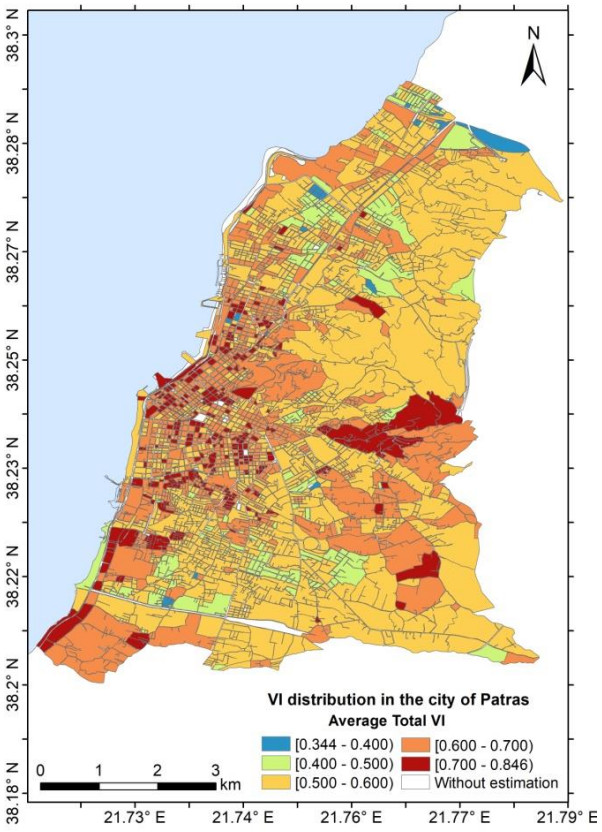

c)

Figure 3.8: Distribution of the estimated average total VI in the city of Patras based on constructions Typology and Behavior Modifier Factors: a) from the available census data, b) by including building blocks with missing data (via adoption of the Aerial geostatistical interpolation method) and c) by further attributing Soil Modifier.

3.4.3 Proposed fragility curves for TB4 area

For the city of Patras and the town of Aigion, fragility curves attributed to URM buildings are based on Rosti et al. (2020), as this can be identified by construction material, period of construction and number of floors according to Table 3.14. This study is fitted to observational damage data to derive typological fragility curves and it can be applicable to URM buildings of TB4 due to the similarity of the building stock sample.

According to Rosti et al. (2020), the fragility curve, i.e. the probability of reaching or exceeding a given damage state is described by the cumulative lognormal distribution as in equation 3.23:

$$P\left(ds \geq DS_i | PGA_j\right) = \boldsymbol{\Phi}\left[\frac{\log\left(PGA_j/\theta_i\right)}{\beta}\right] \tag{3.23}$$

Where Φ[.] is the cumulative standard normal distribution in terms of a PGA threshold defined for VCs/different URM building categories, θi is the median value of the fragility function corresponding to damage state DSi and β is the logarithmic standard deviation. The optimal parameters of the fragility model, i.e. θ and β, are derived by maximising the logarithm of the likelihood defined as in equation 3.24, while a unique constant value of dispersion (β) is assumed for all damage states of a given building typology to ensure the ordinal nature of damage and avoid crossing fragility functions.

This project has received funding from the European Union's Horizon 2020 research and innovation programme under grant agreement No 821046

$$(\theta, \beta) = \arg\max[\log(L(\theta, \beta)] = \arg\max\left[\log\left(\prod_{j=1}^{nPGA}\prod_{i=0}^{nDS}\frac{N_j!}{n_{ij}!}P(ds = DS_i|PGA_j)^{n_{ij}}\right)\right] \quad (3.24)$$

The building typologies of URM for TB4 are objectively merged into three VCs of decreasing vulnerability based on the similarity of the observed seismic fragility. The attribution is in accordance with the adopted clustering method for building typologies as it is implemented in Rosti et al. (2020).

More specifically, during the processing of census data in TB4, we consider any building of residential or public use with recorded construction material of stone and period of construction before the year of 1945 as the most vulnerable URM of M3 type and adobe-earth bricks/M2 type that is further included in the town of Aigion. The assumption of VC=B is considered to the census description of simple stone and attributed to the M3 type with period of construction after the year of 1945 for higher safety, since the possible existence of infrastructure with massive stone cannot be identified through the available census data. The same categorization is followed for brick URM as it is approached to the taxonomy criteria adopted in the empirical vulnerability assessment (Table 3.11).

Table 3.15 shows the parameters of the fragility curves developed by Rosti et al. (2020) and selected for URM buildings in TB4. For consistency with the rest of the deliberable, the median of the curves is indicated with the letter α instead of the letter θ used in the original paper and in equations 3.23 and 3.24.

Table 3.14: Correspondence between the URM classes and the 3 classes A, B, C considered in Rosti et al. (2020).

<table>
<tr><td>Census coding of period of construction</td><td colspan="4">URM</td></tr>
<tr><td>1: < 1919</td><td rowspan="2">M2/M3</td><td rowspan="2"></td><td rowspan="3">M5</td><td rowspan="2"></td></tr>
<tr><td>2: 1919 – 1945</td></tr>
<tr><td>3: 1946 – 1960</td><td rowspan="8"></td><td rowspan="9">M3</td><td rowspan="8"></td><td rowspan="9">M6</td></tr>
<tr><td>4: 1961 – 1970</td></tr>
<tr><td>5: 1971 – 1980</td></tr>
<tr><td>6: 1981 – 1985</td></tr>
<tr><td>7: 1986 – 1990</td></tr>
<tr><td>8: 1991 – 1995</td></tr>
<tr><td>9: > 1996</td></tr>
<tr><td>10: Under construction (> 2001)</td></tr>
<tr><td></td><td colspan="4">Attributed VC per EMS98 (Grönthal, 1998)</td></tr>
<tr><td></td><td>A</td><td colspan="2">B</td><td>C</td></tr>
</table>

Table 3.15: The median (α) and standard deviation (β) parameters of the lognormal fragility curves for the different damage levels (D_i) adopted in the case of TB4 for URM buildings according to Rosti et al. (2020).

Blds structural type	**Reference**	**IM Type**	**Parameters of fragility curves**									
			D_1		**D_2**		**D_3**		**D_4**		**D_5**	
			α[g]	**β[-]**	**α[g]**	**β[-]**	**α[g]**	**β[-]**	**α[g]**	**β[-]**	**α[g]**	**β[-]**
URM buildings, class A, low [0-2]	Rosti et al. (2020)	PGA	0.116	0.754	0.185	0.754	0.261	0.754	0.346	0.754	0.583	0.754
URM buildings, class B, low [0-2]			0.230	1.029	0.509	1.029	0.664	1.029	0.988	1.029	1.727	1.029

This project has received funding from the European Union's Horizon 2020 research and innovation programme under grant agreement No 821046

URM uildings, class C, low [0-2]			0.484	1.222	1.350	1.222	1.928	1.222	2.742	1.222	4.707	1.222
URM buildings, class A, Medium/ High [≥ 3]			0.113	0.821	0.176	0.821	0.226	0.821	0.314	0.821	0.584	0.821
URM buildings, class B, Medium/ High [≥ 3]			0.174	0.997	0.331	0.997	0.426	0.997	0.624	0.997	1.212	0.997
URM buildings, class C, Medium/ High [≥ 3]			0.418	1.199	1.073	1.199	1.444	1.199	2.118	1.199	3.818	1.199

Regarding fragility curves for RC buildings in case of TB4, we consider Pomonis et al. (2014), where damage-based vulnerability curves are derived from observed data that are fitted to structural types commonly found in Greece. The expected performance of RC frame buildings is based on four different periods of construction and the respective Greek ERDs in accordance with the available census coding; without ERD: before the year of 1960, Low ERD: between years 1960 and 1985, Moderate ERD: between years 1986 and 1995, High ERD: after the year of 1996. Moreover, the behavior modifiers of the number of floors and the existence or not of soft-storey at ground floor level are taken into account in cases for which Pomonis et al. (2014), provide available information. This analysis also fits best to the town of Aigion, since the compilation of the observed data sets includes the damage data of the June 15, 1995 Aigion earthquake, one of the most recent strong and destructive earthquakes that occurred in the broader TB4 area.

The derivation of fragility curves according to Pomonis et al. (2014), for RC buildings is based on the cumulative normal distribution; the probability that under a given macroseismic intensity (I) a building suffers damage as described by damage level Di or greater, and it is given by equation 3.25:

$$P[D \geq D_i / I] = \int_{-\infty}^{I} \frac{1}{\sigma\sqrt{2\pi}} \exp\left[\frac{-(I-\mu)^2}{2\sigma^2}\right] \quad (3.25)$$

where μ is the mean value of intensity I, which has been derived in this case from the observed damage distributions, under which 50% of the buildings suffer a damage level Di and σ is the standard deviation of a certain level of damage Di. Thus, each fragility curve depends on the two parameters of mean and standard deviation which are derived by fitting the curve to the cumulative damage distribution data corresponding to each damage level by minimizing the fit errors. There are cases where no curve fit exists for damage level grater than D4 and for some RC classes according to Table 3.16, because no buildings reached these damage levels in any of the surveyed areas.

The percentage of medium and high rise RC buildings in TB4 is relatively small with respect to the total sample of RC; e.g. 11.4 % in the case of Patras, and hence, these are further taken into account in the respective categorization of low rise RC, regardless the existence or not of soft storey as this is not specified by the adopted reference for all RC categories. The assumption of the existence of soft storey during the processing of census data is with respect to the attributes that are considered for RC buildings in Table 3.11 regarding vertical irregularity.

This project has received funding from the European Union's Horizon 2020 research and innovation programme under grant agreement No 821046

Table 3.16: The median (α) and standard deviation (β) parameters of the lognormal fragility curves for the different range of damage levels (Di) adopted in the case of TB4 for RC buildings as modified using Pomonis et al. (2014).

Blds structural type	**Behavior Modifiers**	**Reference**	**IM Type**	**Parameters of fragility curves**							
				≥D1		**≥D2**		**≥D3**		**≥D4**	
				α[I]	**β**	**α[I]**	**β**	**α[I]**	**β**	**α[I]**	**β**
RC1 (pre-1960)		Pomonis et al. (2014)	EMS98 Intensity	9.102	0.212	9.765	0.199	11.827	0.166	-	-
RC2_a (1961-1985)	Regular Low rise (0-3 floors)			8.752	0.246	10.001	0.217	14.197	0.156	-	-
	Low rise (0-3 floors) with Soft Storey			7.738	0.258	9.633	0.211	13.006	0.158	15.350	0.135
	Regular Medium & High rise (≥ 4 floors)			7.160	0.277	8.447	0.238	12.368	0.166	3.875	0.462
	Medium & High rise (≥ 4 floors) with Soft Storey			6.899	0.292	7.983	0.256	12.319	0.171	13.888	0.152
RC2_b (1986-1995)				8.826	0.268	12.186	0.199	-	-	-	-
RC3 (post 1996)				9.921	0.263	14.083	0.190	-	-	-	-

3.4.4 Proposed loss models for TB4 area

The expected economic loss in TB4 is based on the combination of the probabilities of occurrence of the different DGs and the respective damage ratio/Damage Function DF, with the latter representing a rough estimation of a building loss surface per damage level (Di). In TB4 it is proposed: (a) Kappos and Dimitrakopoulos (2008), for RC structures DFs, as it is considered for the Greek territory and the joint research of vulnerability assessment and damage scenarios using Italian and Greek methodologies, and (b) Dolce et al. (2006), for URM structures, presented in Table 3.17. Structural damage and direct economic loss can be taken into account by each building block area and the average number of floors and/or the existence of soft storey of the buildings typologies in each block by assuming a cost replacement unit.

Table 3.17: Statistical values/DFs of the relative repair cost relevant to DGs.

Buildings Type	Central Damage Index/Mean value (%)				
	D1	D2	D3	D4	D5
RC (Kappos and Dimitrakopoulos, 2008)	0.5	5	20	45	80
URM (Dolce et al., 2006)	3.5	14.5	30.5	80	95

3.5 TB-5: Port of Gioia Tauro, Italy

The port of Gioia Tauro is located in Southern Italy along the Tyrrhenian coast, within the Calabria region, which is the region in Italy characterized by the highest seismic hazard.

The seaport of Gioia Tauro is the largest terminal for container throughput in Italy. More than one-third of all national transhipment traffic in Italy takes place at the port of Gioia Tauro, which is classified by Italian law as a port of international economic relevance. It is also one of the most important transhipment hubs in the Mediterranean Sea by connecting the global and regional networks that cross the Mediterranean. The Gioia

This project has received funding from the European Union's Horizon 2020 research and innovation programme under grant agreement No 821046

Tauro port is close to the East-West route that stretches from the Strait of Gibraltar to the Suez Canal, which is one of the busiest maritime corridors in the world.
Furthermore, the port of Gioia Tauro plays a key role for Civil Protection purposes by serving, during the rescue operations, as priority entry point into a territory potentially affected by strong earthquakes (i.e. with magnitude greater than 7). In this framework, it is worth mentioning that the Italian Department of Civil Protection appointed EUC to develop a web-based GIS computational platform for Italian seaports, which is an interactive tool that allows users to assess the seismic risk of maritime ports (Bozzoni et al., 2018). The port of Gioia Tauro is included in this platform, as a critical infrastructure for the emergency management in case of a seismic event.
The Gioia Tauro port consists of an artificial channel, 200m (min) - 250m (max) wide and 3km long, running parallel to the coastline with a 300m wide entrance and an evolution basin of 750m in diameter. The port has eight docks with extensions of 5,125m and is composed of interconnected structural and infrastructural elements that constitute a framework supporting the functionality of the entire multicomponent system. Indeed, a variety of facilities exists within the seaport of Gioia Tauro, such as different typologies of wharf structures, infrastructure for cargo handling and storage, utility systems (e.g. electric power system), road and rail transportation lines, etc., as shown in Figure 3.9. The latter represents an excerpt of the GIS database built by EUC for the multicomponent seaport system of Gioia Tauro thanks to the data provided by the Port Authority.

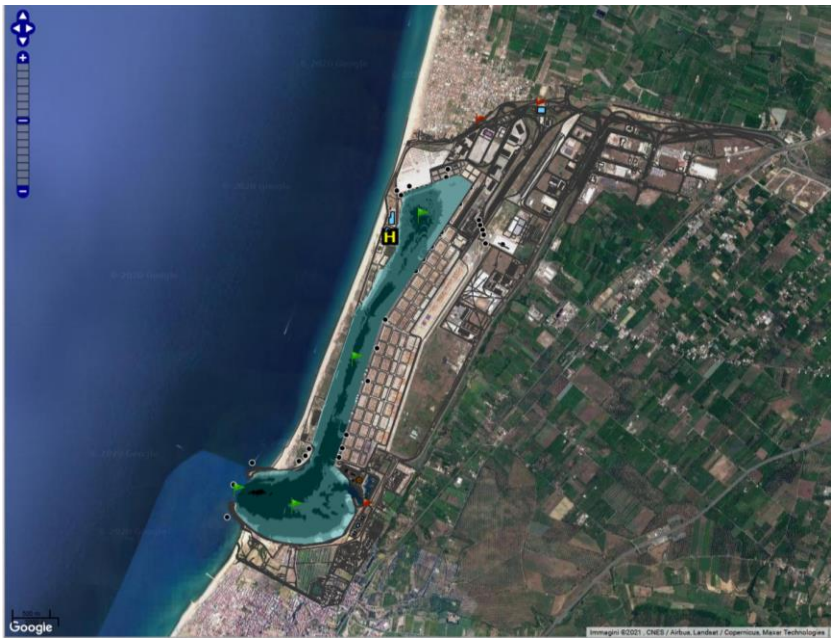

Figure 3.9: Excerpt of the GIS database set-up by EUC for the port of Gioia Tauro: general plan view of the port, infrastructure components, bathymetry, access points to the port area and geotechnical data. Google satellite image is displayed as base map (Base map data ©2021 Google).

The port of Gioia Tauro subjected to earthquake loading is modeled by EUC as a multicomponent system in which the vulnerability of every single element is estimated using an appropriate fragility function (Section 2.5.1). Assessment of the systemic vulnerability of the entire system is accomplished through a simulation-based method, that considers the interdependencies among the port elements at risk and estimates the induced losses of the whole system, as presented in Section 2.5.2.

3.5.1 Fragility models generated by EUC for the Port of Gioia Tauro

With specific reference to the TB5, EUC built a numerical model of a strategic infrastructure located at the port of Gioia Tauro with the aim of deriving analytical fragility functions. The computational platform adopted is OpenSees (*Open System for Earthquake Engineering Simulation*; https://opensees.berkeley.edu/index.php),

This project has received funding from the European Union's Horizon 2020 research and innovation programme under grant agreement No 821046

a software framework for simulating the seismic response of structural and geotechnical systems (McKenna et al., 2000).

A 2D numerical model takes into account the most strategic port facilities located in the Southern part of the port area, composed by a pile-supported wharf and a crane (Figure 3.10). Geometry of the model represents the drawings provided by the Port Authority. Soil elements are modelled with four node 6372 quadUP elements associated with well-known PressureDependentMultiYield02 (PDMY02) constitutive model developed by Yang et al. (2003), ideally permitting the consideration of the changes in the pore water pressure (pwp) distribution. It should be noted that the unlikelihood of soil liquefaction obtained through in-situ based soil liquefaction triggering analysis is found for deep layers, whereas superficial part may liquefy for strong seismic demands. Litostratigraphic layers and geotechnical properties are assigned according to the subsoil modelling carefully carried out by Bozzoni et al. (2014) starting from results obtained by in-situ ground investigation campaigns. Structural elements are modelled with linear (for deck and deck-pile connections) and nonlinear (for piles) formulations. Nonlinear formulation of the pile elements consists of connection of several fiber forced-based and displacement-based beam column elements. Per each pile, the latter group contains around 20 small segments with 3 integration sections for the embedded zone, while the former one constitutes a single element with 5 to 10 integration sections lying above the ground level. Constitutive models for the RC section consist of 1D uni-axial nonlinear models for concrete (Concrete01, Kent-Park-Scott), and steel (Steel02, Menegotto-Pinto) fibers. Taking into the account of potential deteriotion due to long exposure to an aggressive environment during its lifetime, the strength for the concrete has been considered as 30 MPa. Steel yield strength is assigned as 420 MPa. The interaction between soil and pile elements are modelled with t-z, and Q-z element formulations (TzSimple1, and QzSimple1) for circumferential, tangential and pile tip directions (Boulanger et al., 1999). For the horizontal direction, the soil and pile elements are connected together with rigid elastic elements. Since detailed data are not available on the cross-section properties of the crane, its idealized model is built by using linear elements. The fundamental period of the crane is considered as 1.5 s due to its close similarity with the well-known Californian (Kosbab, 2010) and Korean (Tran et al., 2019) jumbo cranes. Crane-wharf connection is pinned for both legs. Uplift condition is evaluated as reaching zero compressive force in the seaside leg. To ensure the 1D propagation at lateral sides, two bulky free-field columns are defined at sides and connected to the main mesh. Seismic motion is applied from the bottom horizontal boundary as force-time history calculated from the rock outcrop velocity time histories. At bottom boundary Lysmer-Kuhlemeyer type of viscous dashpots are defined to absorb the reflected wavefront. Overall geometry of the system is shown in Figure 3.10.

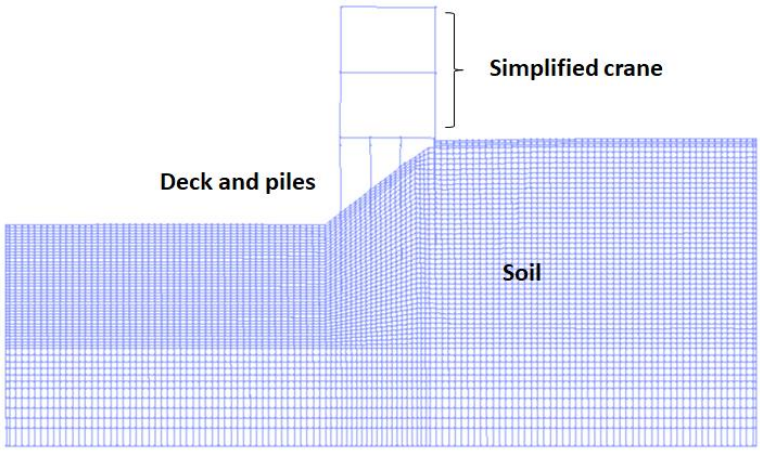

Figure 3.10: Numerical model built by EUC for a strategic infrastructure, composed by a pile-supported wharf and a crane, at the port of Gioia Tauro with the aim of deriving analytical fragility curves.

Numerical simulations have been carried out by EUC using a set of two component signals recorded at rock outcropping conditions in the Italian territory through their direct use and as well as with moderate linear scaling. Considering the both polarity of the signals of the both components, a total set consisting of 108

This project has received funding from the European Union's Horizon 2020 research and innovation programme under grant agreement No 821046

combinations has been analyzed. Fragility functions are generated based on material strains of the pile sections and relative vertical displacement between wharf-backfill at connection for wharf system; uplifting phenomenon and maximum portal drift for the overlying crane.

Fragility curves are usually described by a lognormal probability distribution function as follows:

$$P_f(\,ds \geq DS_i \mid S\,) = \Phi\left[\frac{1}{\beta}\cdot \ln\left(\frac{\mathrm{IM}}{\mathrm{IM}_{mi}}\right)\right] \tag{3.26}$$

where $P_f(\cdot)$ is the probability of exceeding a particular damage state, *DS*, for a given seismic intensity level defined by the earthquake IM; Φ is the standard cumulative probability function; IM_{mi} is the median threshold value of IM required to cause the i^{th} damage state; and β is the lognormal standard deviation.
Starting from the outcomes of the numerical results, analytical fragility curves were derived for port components. The level of the port infrastructure damage is described by a damage index expressing the exceedance of certain limit states and the fragility curves are estimated based on the evolution of damage index with increasing earthquake intensity. Damage limit states for wharf are obtained through the use of information provided in well-established international standards and guidelines (i.e. PIANC, 2001; POLA, 2010; POLB, 2012; ASCE 2014); however after modifications based on engineering judgment. Defined limit states correspond to elastic (minor damage-LS1), limited damage (moderate damage-LS2), and life safety (extensive damage-LS3) which should be satisfied for hazard levels with 50%, 10%, and 2% exceedance in 50 years; respectively. For the crane, two limit states are considered, i.e.: LS1 dictated by uplifting stading for the minor damage and LS3 dictated by 2% portal drift standing for the extensive damage. The damage states adopted are presented in Table 3.18.

Table 3.18: Definition of damage states for port infrastructure components.

Indicator	Component	Minor damage (LS1)	Moderate damage (LS2)	Extensive damage (LS3)
Steel strain (mm/mm) - above ground	Wharf	0.010	0.040	0.080
Steel strain (mm/mm) - below ground		0.005	0.010	0.020
Concrete strain (mm/mm)		0.004	0.008	0.012
Relative vertical displacement (cm)		10	-	-
Uplifting of sea side leg	Crane	Yes	-	-
Maximum portal drift (%)		-	-	2.0

An example of results obtained from numerical simulations are shown in Figure 3.11 in terms of PGV_{rock}-damage probability of crane (right) and wharf (left), respectively.

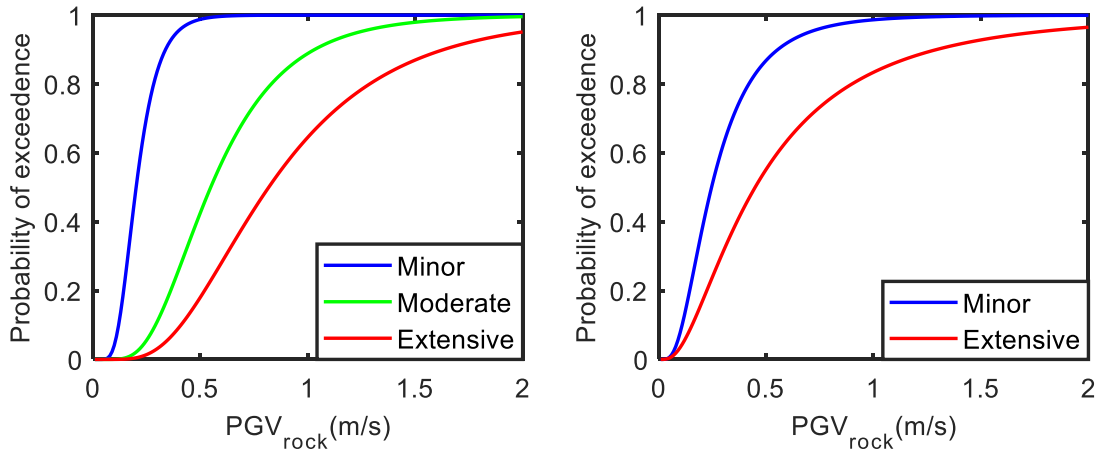

Figure 3.11: Analytical fragility curves developed by EUC for the assessment of seismic vulnerability of strategic port instrastructure components in Gioia Tauro: (left) for pile-supported wharf structure; (right) for cranes. The damage limit states are defined in Table 3.18.

This project has received funding from the European Union's Horizon 2020 research and innovation programme under grant agreement No 821046

Table 3.19: Lognormal parameters of the analytical fragility curves derived by EUC for the port instrastructure components in Gioia Tauro where α is the median and β the standard deviation of the lognormal distribution.

Damage states	IM Type	Parameters of fragility curves	
		α	β
Minor (crane)	PGV_{rock} (m/s)	0.247	0.633
Extensive/collapse (crane)		0.449	0.825
Minor (wharf)		0.201	0.403
Moderate (wharf)		0.549	0.492
Extensive (wharf)		0.818	0.539

The fragility curves derived herein by EUC can be adopted for a large number of infrastructure components within the port of Gioia Tauro. For the remaining ones, fragility curves from the literature will be considered. Indeed, fragility curves proposed by Ko and Yang (2019) could be adopted, in first approximation, for the sheet-pile wharves located in the port of Gioia Tauro. For the electric power network elements, the procedure by HAZUS (NIBS, 2004) will be used, based on the findings in previous European research projects (e.g. Kakderi et al., 2013).
Finally, the structural vulnerability of a strategic building aimed at controlling the port traffic is assessed though the fragility curves obtained from SP-BELA (Simplified Pushover-Based Earthquake Loss Assessment, Borzi et al. 2008b), a methodology developed in EUC, and available in literature. The considered structure is a 4-storeys RC pilotis buiding, placed in the Northern part of the port of Gioia Tauro. The reference for the damage level definition is the EMS98 scale (Grünthal et al., 1998).
The parameters of these curves are shown in Table 3.20.

Table 3.20: Selected fragility models for sheet-pile wharves, electric power network elements and for a strategic building aimed at controlling the traffic located in the port of Gioia Tauro, where α is the median and β the standard deviation of the lognormal distribution.

Element	Reference	IM Type	Parameters of fragility curves									
sheet-pile wharves	Ko and Yang 2019	PGA_{rock} (g)	Moderate				Extensive				Complete	
			α		β		α		β		α	β
			0.57		0.62		1.39		0.76		2.76	0.86
4-storeys r.c. pilotis buiding	Borzi et al. 2008b	PGA_{ampl} (g)	D_1		D_2		D_3		D_4		D_5	
			α	β	α	β	α	β	α	β	α	β
			0.378	0.518	0.573	0.518	0.699	0.518	0.816	0.529	1.633	0.529
electric power substation	HAZUS NIBS 2004	PGA_{ampl} (g)	Slight		Moderate		Extensive				Complete	
			α	β	α	β	α		β		α	β
			0.15	0.7	0.29	0.55	0.45		0.45		0.9	0.45

3.5.2 Loss estimation by EUC for the Port of Gioia Tauro

Recently, at EUC a novel procedure was developed within a simulation-based framework to account for cascading effects when assessing the seismic risk of seaport systems. The procedure is herein briefly described, while further details can be found in Conca et al. (2020) and in Deliverable D5.2 of TURNkey project.
The port system of Gioia Tauro is composed of a certain number of terminals. Each terminal represents a subsystem of the port and is composed of waterfront structures, operating cranes, and electric power systems. To be noted is that modelling the interdependencies among port elements represents one of the critical phases in assessing the seismic vulnerability of a multi-component system.
In each simulation (or scenario), a Monte Carlo analysis is used to sample the value of the seismic parameters from the associated probabilistic distributions to be used as IMs for the fragility functions. The physical damage of all of the components is then sampled from the fragility functions. Based on the sampled damage state of the single components in each scenario, the functionality of the port elements is evaluated. The functionality relies on not only the direct damage to the elements but also the damage suffered by the elements as a result of the interconnected components. At the end of the simulation, the results are calculated in terms of system performance and amount of loss.

This project has received funding from the European Union's Horizon 2020 research and innovation programme under grant agreement No 821046

Furthermore, for each component, a non-functionality level is calculated as the probability that the element is out of service. Once the functionality of each element is evaluated, the system performance of each scenario is measured by a metric that is called performance indicator (PI). The methodology has been implemented in the MATLAB (https://it.mathworks.com/) computing environment by the Object-Oriented Programming (OOP) paradigm. This procedure is repeated several times until the process converges toward stable results (achieved when the moving average of the PI converges to a constant) to fully characterize the uncertainty represented by the probability distributions of the input parameters and of the fragility models adopted for the port elements.

3.6 TB-6: Groningen Province, Netherlands

In the gas field of Groningen, a province in the North of the Netherlands, the earthquake activity has increased in the last years as a result of gas extraction. TB-6 focuses on the impact of induced seismicity on the existing buildings and infrastructures. In particular, the elements exposed to the seismic risk that have been considered are bridges, viaducts, underpasses and buildings. Existing fragility curves are selected for each element at risk, and fatality curves - as consequence of building collapse - are summarezed in the following paraghraphs.

3.6.1 Fragility models selected for the Groningen province

3.6.1.1 Bridges, viaducts and underpasses

For the single-span and multi-span girder bridges in the Groningen province the fragility functions were based on taxonomies defined by EUC and described in §2.1.2.1.3. The assignment of a taxonomy is based on several parameters: number of spans; material of substructure element (abutments and piers); mean value of length of spans; deck material; height of abutments and piers; presence of seismic isolation devices to prevent the fall of the deck from piers.
Figure 3.12, Figure 3.13 and Figure 3.14 show respectively the location of bridges, viaducts and underpasses in Groningen province.
The parameters of the fragility curves based on taxonomies described in §2.1.2.1.3 assigned to girder bridges for Damage Limit State (DLS) and Collapse Limit State (CLS) are summarized in Table 3.21 (girder bridges), Table 3.22 (viaducts) and Table 3.23 (underpasses). The values are expressed as median value (α) and standard deviation (β) of lognormal distribution.

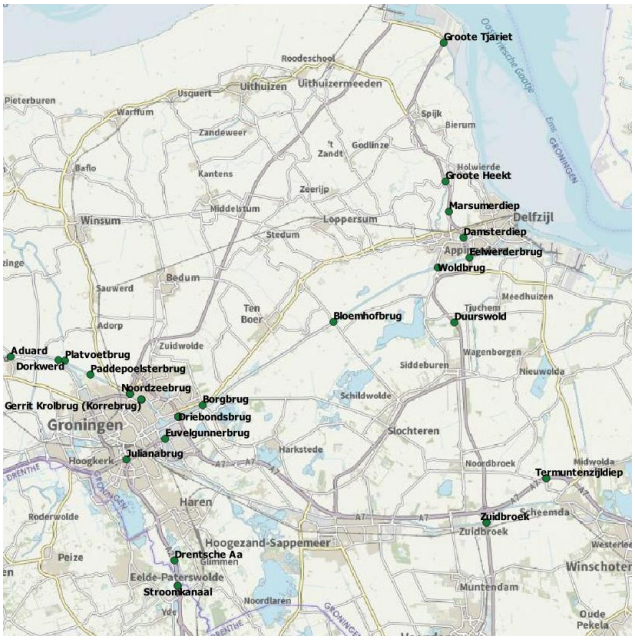

Figure 3.12: Locations of bridges in the Groningen province.

This project has received funding from the European Union's Horizon 2020 research and innovation programme under grant agreement No 821046

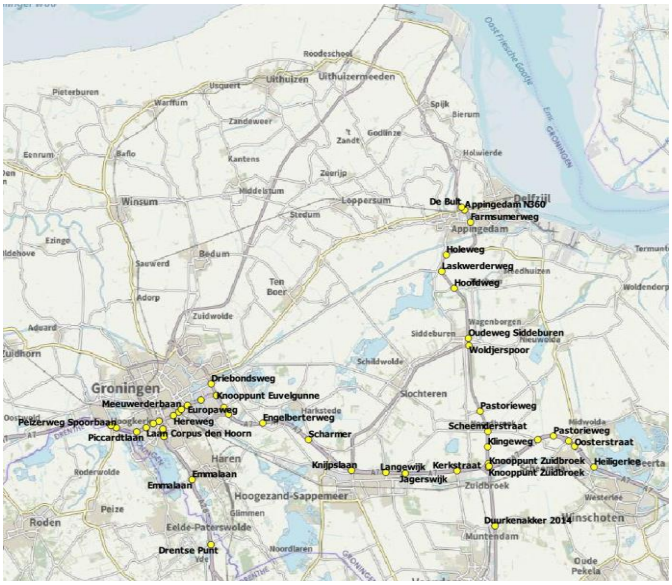

Figure 3.13: Location of viaducts in the Groningen province.

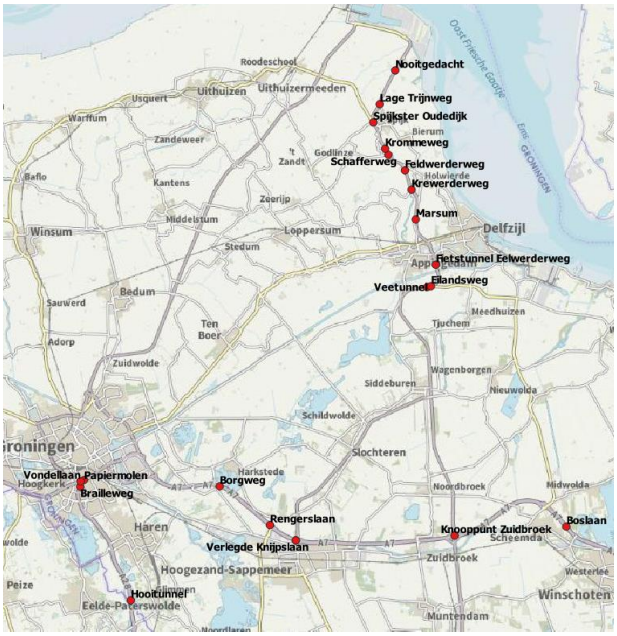

Figure 3.14: Location of underpasses in the Groningen province.

Table 3.21: Fragility functions for bridges in Groningen for Damage Limit State (DLS) and Collapse Limit State (CLS), where (α) is the median value and (β) the standard deviation of lognormal distribution. Locations are illustrated in Figure 3.12.

location	id	N°of spans	Span length [m]	Vertical element material	Height [m]	SID	Taxonomy	DLS α[g]	DLS β[-]	CLS α[g]	CLS β[-]
Groote Tjariet	03G-315	1	15	RC	4	NO	T_MCH1L1	0.173	0.837	0.764	0.497
Aduard	07C-114	1	28	MASONRY	4	YES	T_MMH1L2_R	0.108	0.548	0.312	0.515
Dorkwerd	07C-115	1	75	MASONRY	6	YES	T_MMH1L2_R	0.108	0.548	0.312	0.515
Platvoetbrug	07C-117	5	12	RC	6	NO	T_PCH1L1	0.154	0.907	0.633	0.354
Paddepoelsterbrug	07D-128	1	30	RC	2	YES	T_MCH1L2_R	0.165	0.848	1.975	0.344

Noordzeebrug	07D-130	1	60	MASONRY	8	YES	T_MMH1L2_R	0.108	0.548	0.312	0.515
Noordzeebrug	07D-130	1	60	MASONRY	8	YES	T_MMH1L2_R	0.108	0.548	0.312	0.515
Noordzeebrug	07D-130	1	60	MASONRY	8	YES	T_MMH1L2_R	0.108	0.548	0.312	0.515
Gerrit Krolbrug (Korrebrug)	07D-131	1	35	MASONRY	2	YES	T_MMH1L2_R	0.108	0.548	0.312	0.515
Borgbrug	07D-133	3	20	RC	4	NO	T_PCH1L2	0.113	1.000	0.471	0.310
Julianabrug	07D-319	4	16	MASONRY	6	YES	T_PMH1L1_R	0.144	0.537	0.324	0.517
Euvelgunnerbrug	07D-323	5	23	RC	8	NO	T_PCH1L2	0.113	1.000	0.471	0.310
Driebondsbrug	07D-326	4	25	RC	5	YES	T_PCH1L2_R	0.141	0.704	0.530	0.354
Driebondsbrug	07D-326	4	25	RC	5	YES	T_PCH1L2_R	0.141	0.704	0.530	0.354
Driebondsbrug	07D-326	4	25	RC	5	YES	T_PCH1L2_R	0.141	0.704	0.530	0.354
Bloemhofbrug	07E-105	3	20	RC	4	NO	T_PCH1L2	0.113	1.000	0.471	0.310
Eelwerderbrug	07F-108	3	30	RC	5	YES	T_PCH1L2_R	0.141	0.704	0.530	0.354
Damsterdiep	07F-111	3	35	RC	4	YES	T_PCH1L2_R	0.141	0.704	0.530	0.354
Groote Heekt	07F-115	1	15	RC	4	NO	T_MCH1L1	0.173	0.837	0.764	0.497
Woldbrug	07F-126	3	20	RC	4	NO	T_PCH1L2	0.113	1.000	0.471	0.310
Duurswold	07F-313	1	65	RC	4	NO	T_MCH1L2	0.179	0.873	1.405	0.425
Marsumerdiep	07F-315	1	18	RC	2	NO	T_MCH1L2	0.179	0.873	1.405	0.425
Termuntenzijldiep	07H-106	1	30	RC	5	NO	T_MCH1L2	0.179	0.873	1.405	0.425
Termuntenzijldiep	07H-106	1	30	RC	5	NO	T_MCH1L2	0.179	0.873	1.405	0.425
Drentsche Aa	12B-301	1	5	RC	3	NO	T_MCH1L1	0.173	0.837	0.764	0.497
Stroomkanaal	12B-303	1	8	RC	2	YES	T_MCH1L1_R	0.177	1.006	1.582	0.382
Stroomkanaal	12B-303	1	8	RC	2	YES	T_MCH1L1_R	0.177	1.006	1.582	0.382

Table 3.22: Fragility functions for the viaducts in Groningen for Damage Limit State (DLS) and Collapse Limit State (CLS), where (α) is the median value and (β) the standard deviation of lognormal distribution. Locations are illustrated in Figure 3.13.

location	id	N°of spans	Span length [m]	Vertical element material	Height [m]	SID	Taxonomy	DLS α[g]	DLS β[-]	CLS α[g]	CLS β[-]
Piccardtlaan	07D-001	1	5.5	RC	4	NO	T_MCH1L1	0.173	0.837	0.764	0.497
Helperzoom	07D-105	4	12	RC	5	NO	T_PCH1L1	0.154	0.907	0.633	0.354
Hereweg	07D-105	4	12	RC	5	NO	T_PCH1L1	0.154	0.907	0.633	0.354
Paterswoldseweg	07D-106	3	20	RC	4	NO	T_PCH1L2	0.113	1.000	0.471	0.310
Meeuwerderbaan	07D-107	3	11	RC	4	YES	T_PCH1L1_R	0.254	0.520	0.708	0.366
Vrijheidsplein	07D-111	6	30	RC	4	YES	T_PCH1L2_R	0.141	0.704	0.530	0.354
Peizerweg Spoorbaan	07D-112	1	7	RC	4	YES	T_MCH1L1_R	0.177	1.006	1.582	0.382
Zuiderweg	07D-113	2	15	RC	5	NO	T_PCH1L2	0.113	1.000	0.471	0.310
Laan Corpus den Hoorn	07D-118	2	20	RC	5	YES	T_PCH1L2_R	0.141	0.704	0.530	0.354
Knooppunt Euvelgunne	07D-121	2	35	RC	6	YES	T_PCH1L2_R	0.141	0.704	0.530	0.354
Olgerweg	07D-122	1	12	RC	3	YES	T_MCH1L2_R	0.165	0.848	1.975	0.344
Aansluiting Westerbroek	07D-123	2	28	RC	5	YES	T_PCH1L2_R	0.141	0.704	0.530	0.354
Iddekingeweg	07D-302	3	6	RC	4	YES	T_PCH1L1_R	0.254	0.520	0.708	0.366
Van Ketwich Verschuurlaan	07D-303	3	12	RC	4	YES	T_PCH1L1_R	0.254	0.520	0.708	0.366
Emmalaan	07D-304	3	11	RC	4	YES	T_PCH1L1_R	0.254	0.520	0.708	0.366
Emmalaan	07D-304	3	11	RC	4	YES	T_PCH1L1_R	0.254	0.520	0.708	0.366
Europaweg	07D-322	4	15	RC	4	NO	T_PCH1L1	0.154	0.907	0.633	0.354
Euvelgunnerweg	07D-324	2	16	RC	4	NO	T_PCH1L1	0.154	0.907	0.633	0.354

This project has received funding from the European Union's Horizon 2020 research and innovation programme under grant agreement No 821046

Driebondsweg	07D-325	3	17	RC	5	NO	T_PCH1L1	0.154	0.907	0.633	0.354
Laskwerderweg	07F-104	1	30	RC	6	YES	T_MCH1L2_R	0.165	0.848	1.975	0.344
Holeweg	07F-105	1	25	RC	6	YES	T_MCH1L2_R	0.165	0.848	1.975	0.344
Farmsumerweg	07F-110	3	8	RC	5	YES	T_PCH1L1_R	0.254	0.520	0.708	0.366
Appingedam N360	07F-112	3	22	RC	4	YES	T_PCH1L2_R	0.141	0.704	0.530	0.354
De Bult	07F-113	1	6	RC	4	NO	T_MCH1L1	0.173	0.837	0.764	0.497
Hoofdweg	07F-314	1	12	RC	4	YES	T_MCH1L2_R	0.165	0.848	1.975	0.344
Knijpslaan	07G-001	2	25	RC	4	NO	T_PCH1L2	0.113	1.000	0.471	0.310
Scharmer	07G-102	2	28	RC	6	NO	T_PCH1L2	0.113	1.000	0.471	0.310
Engelberterweg	07G-103	6	20	RC	5	YES	T_PCH1L2_R	0.141	0.704	0.530	0.354
Langewijk	07G-110	1	30	RC	4	NO	T_MCH1L2	0.179	0.873	1.405	0.425
Jagerswijk	07H-102	3	18	RC	5	NO	T_PCH1L2	0.113	1.000	0.471	0.310
Kerkstraat	07H-103	2	18	RC	5	NO	T_PCH1L2	0.113	1.000	0.471	0.310
Knooppunt Zuidbroek	07H-104	2	20	RC	4	YES	T_PCH1L2_R	0.141	0.704	0.530	0.354
Knooppunt Zuidbroek	07H-104	2	20	RC	5	YES	T_PCH1L2_R	0.141	0.704	0.530	0.354
Knooppunt Zuidbroek	07H-104	2	20	RC	5	YES	T_PCH1L2_R	0.141	0.704	0.530	0.354
Knooppunt Zuidbroek	07H-104	2	20	RC	5	YES	T_PCH1L2_R	0.141	0.704	0.530	0.354
Knooppunt Zuidbroek	07H-104	2	25	RC	5	YES	T_PCH1L2_R	0.141	0.704	0.530	0.354
Scheemderzwaag	07H-105	2	28	RC	5	NO	T_PCH1L2	0.113	1.000	0.471	0.310
Klingeweg	07H-306	2	20	RC	5	NO	T_PCH1L2	0.113	1.000	0.471	0.310
Scheemderstraat	07H-307	2	13	RC	5	NO	T_PCH1L1	0.154	0.907	0.633	0.354
Pastorieweg	07H-308	2	13	RC	5	NO	T_PCH1L1	0.154	0.907	0.633	0.354
Woldjerspoor	07H-310	2	10	RC	5	NO	T_PCH1L1	0.154	0.907	0.633	0.354
Oudeweg Siddeburen	07H-311	2	10	RC	5	NO	T_PCH1L1	0.154	0.907	0.633	0.354
Pastorieweg	08C-105	2	19	RC	5	NO	T_PCH1L2	0.113	1.000	0.471	0.310
Viaduct S18	08C-106	3	37	RC	5	YES	T_PCH1L2_R	0.141	0.704	0.530	0.354
Oosterstraat	08C-107	3	27	RC	5	YES	T_PCH1L2_R	0.141	0.704	0.530	0.354
Heiligerlee	08C-109	3	27	RC	5	YES	T_PCH1L2_R	0.141	0.704	0.530	0.354
Drentse Punt	12B-106	3	18	RC	5	YES	T_PCH1L2_R	0.141	0.704	0.530	0.354
Duurkenakker 2014	12B-106	1	13	RC	5	YES	T_MCH1L2_R	0.165	0.848	1.975	0.344
Piccardtlaan	12F-104	1	5.5	RC	4	NO	T_MCH1L1	0.173	0.837	0.764	0.497
Helperzoom	07D-001	4	12	RC	5	NO	T_PCH1L1	0.154	0.907	0.633	0.354
Hereweg	07D-105	4	12	RC	5	NO	T_PCH1L1	0.154	0.907	0.633	0.354

Table 3.23: Fragility functions for underpasses in Groningen for Damage Limit State (DLS) and Collapse Limit State (CLS), where (α) is the median value and (β) the standard deviation of lognormal distribution. Locations are listed in Figure 3.14.

location	id	N°of spans	Span length [m]	Vertical element material	Height [m]	SID	Taxonomy	DLS α[g]	DLS β[-]	CLS α[g]	CLS β[-]
Spijkster Oudedijk	03G-102	1	5.5	RC	4	NO	T_MCH1L1	0.173	0.837	0.764	0.497
Lage Trijnweg	03G-104	1	9.5	RC	4	NO	T_MCH1L1	0.173	0.837	0.764	0.497
Nooitgedacht	03G-105	1	5	RC	3	NO	T_MCH1L1	0.173	0.837	0.764	0.497
Brailleweg	07D-301	1	9.5	RC	4	NO	T_MCH1L1	0.173	0.837	0.764	0.497
Papiermolen	07D-320	1	9.5	RC	3	NO	T_MCH1L1	0.173	0.837	0.764	0.497
Vondellaan	07D-321	2	6	RC	4	NO	T_PCH1L1	0.154	0.907	0.633	0.354
Veetunnel	07F-106	1	2.5	RC	3	NO	T_MCH1L1	0.173	0.837	0.764	0.497
Eilandsweg	07F-107	1	10	RC	4	NO	T_MCH1L1	0.173	0.837	0.764	0.497
Fietstunnel Eelwerderweg	07F-109	1	3	RC	3	NO	T_MCH1L1	0.173	0.837	0.764	0.497
Krewerderweg	07F-116	1	8.7	RC	3	NO	T_MCH1L1	0.173	0.837	0.764	0.497
Feldwerderweg	07F-117	1	6.5	RC	3	NO	T_MCH1L1	0.173	0.837	0.764	0.497
Schafferweg	07F-118	1	7.5	RC	3	NO	T_MCH1L1	0.173	0.837	0.764	0.497
Krommeweg	07F-120	1	3.5	RC	2.5	NO	T_MCH1L1	0.173	0.837	0.764	0.497
Marsum	07F-316	1	11.5	RC	4	NO	T_MCH1L1	0.173	0.837	0.764	0.497
Verlegde Knijpslaan	07G-001	1	10.5	RC	4	NO	T_MCH1L1	0.173	0.837	0.764	0.497
Rengerslaan	07G-101	1	18	RC	4	NO	T_MCH1L2	0.179	0.873	1.405	0.425
Borgweg	07G-105	1	6.5	RC	3	NO	T_MCH1L1	0.173	0.837	0.764	0.497
Knooppunt Zuidbroek	07H-104	2	20	RC	5	YES	T_PCH1L2	0.113	1.000	0.471	0.310
Boslaan	08C-108	1	4.7	RC	3	NO	T_MCH1L1	0.173	0.837	0.764	0.497
Hooitunnel	12B-302	1	3.5	RC	3	NO	T_MCH1L1	0.173	0.837	0.764	0.497

3.6.1.2 Buildings

The v7 fragility models developed by Crowley and Pinho (2020), used in NAM's Hazard and Risk Assessment (HRA) 2020, are used for the buildings in Groningen.

The classification was performed to group buildings with similar structural and architectural characteristics. Each building was described using structural systems that combine 9 different attributes of the building, with the first related to the geometric layout (S-shed, U-unit, B-block, W-barn/warehouse, T-tower) and the following 8 attributes defined according to the GEM Building Taxonomy: material and type of lateral load-resisting system in each direction of the building, presence of external walls, floor system, number of floors and irregularities. In total, 35 vulnerability classes were considered.

One real representative building from each class was selected, and a MDOF was modelled. Due to the large computational effort, the fragility curves were computed based on an equivalent SDOF to the MDOF, via nonlinear dynamic analyses.

A large suite of hazard-consistent records was then utilized in the nonlinear dynamic analyses of these SDOF systems to model the record-to-record variability, and regression analysis is used to relate the average spectral acceleration (AvgSa) of each record to the nonlinear response in order to produce the fragility functions.

The probability of exceeding the limit displacement to each structural damage (SD) or collapse state (CS) *i* under a given level of ground shaking is calculated as follows:

$$P_{DL_{SDi}} = 1 - \Phi\left(\frac{ln(DL_{SDi}) - ln\eta_{S_d|\,ln(AvgSa)}}{\sigma_s}\right) \quad (3.27)$$

This project has received funding from the European Union's Horizon 2020 research and innovation programme under grant agreement No 821046

$$P_{DL_{CSi}} = 1 - \Phi\left(\frac{\ln\left(DL_{CSi}\right) - \ln\eta_{S_d|\ln(AvgSa)}}{\sigma_s}\right) \quad (3.28)$$

$$\ln\eta_{S_d|\ln(AvgSa)} = b_0 + b_1\ln\left(AvgSa\right) \quad (3.29)$$

where, ϕ() is the cumulative distribution function of the standard normal distribution, b_0 and b_1 are coefficients obtained from the linear regression, DL is the displacement limit of each damage or collapse state (provided in metres), ln(AvgSa) is the average spectral acceleration (in g), defined as the geometric mean of the spectral ordinates of the GMPE from 0.01 to 1.0 s, as provided by the hazard calculations of the risk engine, and σs is the logarithmic standard deviation due to record-to record variability. Input values are available in Crowley and Pinho (2020) for each vulnerability class and damage state.
The fragility curves are then explicitly computed for two structural damages (i.e., SD2 and SD3, respectively for slight structural damage and moderate structural damage) and for three structural collapses (CS1 and CS2 are partial structural collapses, whereas CS3 is the complete collapse). The damage levels are then converted to the ESM98 scale (Grüntal et al., 1998), where SD2 is treated as D2, SD3 to D3, CS1 to D4 and CS3 to D5.

The curves are summarized in Table 3.24, where α is the median and β the standard deviation of the lognormal distribution, for each of the 4 damage levels (D2 to D5) of the EMS98 scale (Grüntal et l., 1998). The curves are the middle branch of the logic tree proposed in the original study of Crowley and Pinho (2020).

For some structural systems defined in the taxonomy, a weighted average fragility curve has been calculated from the list in Table 3.24, and the values are summarized in Table 3.25. The weighting factors are listed in Table 3.26, computed based on the number of buildings of each taxonomy considered by Crowley and Pinho (2020).

Table 3.27, Table 3.28, Table 3.29 connect each taxonomy classification present in SERA with Crowley and Pinho (2020), considering residential, industrial and commercial buildings respectively.

Table 3.24: Selected fragility models for buildings in Groningen province, where α is the median and β the standard deviation of the lognormal distribution.

Crowley and Pinho (2020) taxonomy	IM Type	Parameters of fragility curves									
		D1		D2		D3		D4		D5	
		α[g]	β[-]	α[g]	β[-]	α[g]	β[-]	α[g]	β[-]	α[g]	β[-]
RC1L	PGA	N.A.	N.A.	0.23	0.41	0.34	0.41	1.59	0.41	1.59	0.41
RC1M	PGA	N.A.	N.A.	0.27	0.56	0.44	0.56	3.12	0.56	3.12	0.56
RC1H	PGA	N.A.	N.A.	0.35	0.80	0.62	0.80	6.13	0.80	6.13	0.80
RC2	PGA	N.A.	N.A.	0.22	0.66	0.37	0.66	2.34	0.66	2.34	0.66
PC2	PGA	N.A.	N.A.	0.20	0.69	0.35	0.69	2.42	0.69	2.42	0.69
RC3L	PGA	N.A.	N.A.	0.38	0.38	0.54	0.38	0.99	0.38	1.59	0.38
RC3M	PGA	N.A.	N.A.	0.40	0.54	0.64	0.54	1.63	0.54	2.84	0.54
RC3H	PGA	N.A.	N.A.	0.53	0.74	0.89	0.74	3.33	0.74	4.28	0.74
PC3L	PGA	N.A.	N.A.	0.35	0.21	0.61	0.21	1.03	0.21	1.33	0.21
PC3M	PGA	N.A.	N.A.	0.27	0.23	0.52	0.23	1.01	0.23	1.31	0.23
PC3H	PGA	N.A.	N.A.	0.15	0.25	0.39	0.25	1.29	0.25	1.53	0.25
W2	PGA	N.A.	N.A.	0.24	0.37	0.49	0.37	2.43	0.37	2.43	0.37
W3	PGA	N.A.	N.A.	0.40	0.31	0.69	0.31	1.88	0.31	1.88	0.31
S1L	PGA	N.A.	N.A.	0.19	0.64	0.31	0.64	3.37	0.64	3.37	0.64
S1H	PGA	N.A.	N.A.	0.23	0.94	0.40	0.93	6.07	0.94	6.07	0.94
S1M	PGA	N.A.	N.A.	0.43	0.88	0.71	0.88	8.32	0.88	8.32	0.88
S2L	PGA	N.A.	N.A.	0.29	0.37	0.42	0.37	1.76	0.37	1.76	0.37
S2H	PGA	N.A.	N.A.	0.29	0.59	0.50	0.59	4.12	0.59	4.12	0.59
S2M	PGA	N.A.	N.A.	0.41	0.87	0.74	0.87	7.79	0.87	7.79	0.87
S3	PGA	N.A.	N.A.	1.91	0.53	2.93	0.53	36.32	0.53	36.32	0.53

This project has received funding from the European Union's Horizon 2020 research and innovation programme under grant agreement No 821046

URM1F_B	PGA	N.A.	N.A.	0.23	0.34	0.37	0.34	0.62	0.34	0.62	0.34
URM1F_HA	PGA	N.A.	N.A.	0.35	0.56	0.83	0.56	2.93	0.56	2.93	0.56
URM1F_HC	PGA	N.A.	N.A.	0.28	0.46	0.51	0.46	1.17	0.46	1.17	0.46
URM2L	PGA	N.A.	N.A.	0.21	0.30	0.38	0.30	0.67	0.30	1.49	0.30
URM3L	PGA	N.A.	N.A.	0.34	0.41	0.54	0.41	0.99	0.41	0.99	0.41
URM3M_U	PGA	N.A.	N.A.	0.24	0.44	0.44	0.44	0.56	0.44	1.21	0.44
URM3M_D	PGA	N.A.	N.A.	0.24	0.34	0.37	0.34	0.89	0.34	0.96	0.34
URM3M_B	PGA	N.A.	N.A.	0.38	0.46	0.62	0.46	0.97	0.46	1.21	0.46
URM4L	PGA	N.A.	N.A.	0.10	0.41	0.22	0.41	0.93	0.41	0.93	0.41
URM5L	PGA	N.A.	N.A.	0.61	0.34	0.92	0.34	1.03	0.34	1.26	0.34
URM6L	PGA	N.A.	N.A.	0.66	0.35	0.95	0.35	2.00	0.35	2.00	0.35
URM7L	PGA	N.A.	N.A.	0.71	0.36	1.01	0.36	1.01	0.36	2.29	0.36
URM8L	PGA	N.A.	N.A.	0.35	0.34	0.35	0.34	0.35	0.34	1.09	0.34
URM9L	PGA	N.A.	N.A.	0.20	0.30	0.35	0.30	0.57	0.30	1.37	0.30
URM10	PGA	N.A.	N.A.	0.66	0.35	0.95	0.35	2.00	0.35	2.00	0.35

Table 3.25: Weighted averaged fragility curves for URM classes.

Crowley and Pinho (2020) taxonomy	IM Type	Parameters of fragility curves									
		D_1		D_2		D_3		D_4		D_5	
		α[g]	β[-]	α[g]	β[-]	α[g]	β[-]	α[g]	β[-]	α[g]	β[-]
avgURML:2to10	PGA	N.A.	N.A.	0.55	0.34	0.77	0.34	1.07	0.34	1.77	0.34
avgURML:3&4	PGA	N.A.	N.A.	0.30	0.41	0.48	0.41	0.98	0.41	0.98	0.41
avgURM3M	PGA	N.A.	N.A.	0.27	0.44	0.47	0.44	0.68	0.44	1.19	0.44
avgURM1F	PGA	N.A.	N.A.	0.27	0.42	0.52	0.42	1.33	0.42	1.33	0.42

Table 3.26: Weighting factors used to compute averaged fragility curves for URM classes.

Crowley and Pinho (2020) taxonomy	avgURML:2to10	avgURML:3&4	avgURM3M	avgURM1F
URM1F_B	-	-	-	0.53
URM1F_HA	-	-	-	0.26
URM1F_HC	-	-	-	0.21
URM2L	0.11	-	-	-
URM3L	-	0.83	-	-
URM3M_U	-	-	0.70	-
URM3M_D	-	-	0.08	-
URM3M_B	-	-	0.22	-
URM4L	-	0.17	-	-
URM5L	0.1	-	-	-
URM6L	0.237	-	-	-
URM7L	0.325	-	-	-
URM8L	0.186	-	-	-
URM9L	0.038	-	-	-
URM10	0.005			

Table 3.27: Mapping table from SERA taxonomy to Crowley and Pinho (2020) taxonomy for residential buildings.

SERA Taxonomy	Crowley and Pinho (2020) taxonomy
CR/LWAL+CDN/H:2	RC1L
CR/LWAL+CDN/HBET:3-5	RC1M
CR/LWAL+CDN/HBET:6-	RC1H
CR+PC/LWAL+CDN/HBET:3-5	PC3M
CR+PC/LWAL+CDN/HBET:6-	PC3H
MUR/LWAL+CDN/H:1	avgURML:2to10
MUR/LWAL+CDN/H:2	avgURML:3&4
MUR/LWAL+CDN/HBET:3-5	avgURM3M
W/LWAL+CDN/H:1	W3
W/LWAL+CDN/H:2	W3

This project has received funding from the European Union's Horizon 2020 research and innovation programme under grant agreement No 821046

Table 3.28: Mapping table from SERA taxonomy to taxonomy in Crowley and Pinho (2020) for industrial buildings

SERA Taxonomy	Crowley and Pinho (2020) taxonomy
CR/LFM+CDN/H:2	RC1M
CR+PC/LPB+CDN/H:1	PC2
CR+PC/LWAL+CDN/H:1	PC3L
S/LFBR+CDN/H:1	S2L
W+S/LPB+CDN/H:1	URM1F_B

Table 3.29: Mapping table from SERA taxonomy to Crowley and Pinho (2020) taxonomy for commercial buildings.

SERA Taxonomy	Crowley and Pinho (2020) taxonomy
CR/LFM+CDN/H:1	RC1L
CR/LFM+CDN/H:2	RC1L
CR/LFM+CDN/HBET:3-5	RC1M
CR/LFM+CDN/HBET:6-	RC1H
CR/LWAL+CDN/H:1	RC3L
CR/LWAL+CDN/H:2	RC3L
CR/LWAL+CDN/HBET:3-5	RC3M
CR/LWAL+CDN/HBET:6-	RC3H
CR+PC/LWAL+CDN/H:1	PC3L
CR+PC/LWAL+CDN/H:2	PC3L
CR+PC/LWAL+CDN/HBET:3-5	PC3M
CR+PC/LWAL+CDN/HBET:6-	PC3H
MUR/LWAL+CDN/H:1	avgURM1F
MUR/LWAL+CDN/H:1/FW	avgURM1F
MUR/LWAL+CDN/H:2	avgURM1F
MUR/LWAL+CDN/H:2/FW	avgURM1F
S/LFBR+CDN/H:1	S2L
S/LFBR+CDN/H:2	S2L
S/LFBR+CDN/HBET:3-5	S2M
S/LFBR+CDN/HBET:6-	S2H
S/LFM+CDN/H:1	S1L
S/LFM+CDN/H:2	S1L
S/LFM+CDN/HBET:3-5	S1M
S/LFM+CDN/HBET:6-	S1H

3.6.2 Loss estimation models selected for Groningen

A consequence model for buildings has been developed by Crowley and Pinho (2020) to estimate the fatality risk. The probability of dying inside the building, under a given level of ground shaking is calculated as follows:

$$P_{d,inside} = \left(P_{DL_{CS1}} - P_{DL_{CS2}}\right) \cdot P_{d,inside|CS1} + \left(P_{DL_{CS2}} - P_{DL_{CS3}}\right) \cdot P_{d,inside|CS2} + \\ + P_{DL_{CS3}} \cdot P_{d,inside|CS3} \quad (3.30)$$

where $P_{d,inside|CSi}$ refers to the probability of dying inside given structural collapse state.

The probability of dying outside the building, under a given level of ground shaking, is calculated as follows:

$$P_{d,outside} = P_{d,outside_{NoChC}} + P_{d,outside_{ChC}} \quad (3.31)$$

where:

$$P_{d,outside_{NoChC}} = \left(P_{DL_{CS1}} - P_{DL_{CS2}}\right) \cdot P_{d,outside|CS1} + \\ + \left(P_{DL_{CS2}} - P_{DL_{CS3}}\right) \cdot P_{d,outside|CS2} + P_{DL_{CS3}} \cdot P_{d,outside|CS3} \quad (3.32)$$

This project has received funding from the European Union's Horizon 2020 research and innovation programme under grant agreement No 821046

where $P_{d,outside|CSi}$ refers to the probability of dying outside given structural collapse state, and $P_{d,outside_{ChC}}$ is the effect of the chimney collapse. The probability of loss of life inside and outside of collapsed buildings, for a given collapse state (CSi) (i.e. $P_{d,inside|CSi}$ and $P_{d,outside|CSi}$), are summarized in Crowley and Pinho (2020).

The probability of loss of life inside and outside of collapsed buildings ($P_{d,inside}$ and $P_{d,outside_{NoChC}}$) is calculated using the original definitions of collapse states (CSi in Crowley and Pinho, 2020) and expressed directly in terms of PGA as a cumulative standard normal distribution as follows:

$$P_d = P_{d,\max}\Phi\left(\frac{\ln\left[PGA\right]-\ln\left(\alpha\right)}{\beta}\right) \tag{3.33}$$

where $P_{d,\max}$ is the maximum probability of loss of life for very large PGA, α and β are the median and standard deviation. The input values are summarized in Table 3.30.

The probability of dying outside due to chimney collapse, is computed as follows:

$$P_{d,outside_{ChC}} = \left(1-P_{D4}\right)\cdot\overline{P_{d,outside_{ChC}}} \tag{3.34}$$

where P_{D4} is the probability of a damage D4 (according to ESM98) for a given PGA, and $\overline{P_{d,outside_{ChC}}}$ is calculated directly as follows:

$$\overline{P_{d,outside_{ChC}}} = \Phi\left(\frac{\ln\left[min\left(PGA,0.75g\right)\right]-\ln\left(\overline{PGA_{chd}}\right)}{\beta_{chd}}\right) \tag{3.35}$$

where Φ is the cumulative distibution function of the standard normal distribution, PGA is the level of peak ground acceleration (or spectral acceleration at 0.01 seconds) in terms of g, $\overline{PGA_{chd}}$ is the median PGA of the chimney collapse vulnerability function (in terms of g) and β_{chd} is the standard deviation. Input parameters are listed in Table 3.32.

Table 3.30: Selected fatality models for buildings in Groningen province, where α is the median, β the standard deviation of the lognormal distribution, $P_{d,inside,max}$ is the max probability of dying inside the building and $P_{d,outsideNoChC,max}$ is the max probability of dying outside the building with no effect of the chimney collapse.

Vulnerability class	IM Type	Parameters of fatality curves					
		$P_{d,inside}$			$P_{d,outsideNoChC}$		
		α[g]	β[-]	$P_{d,inside,max}$	α[g]	β[-]	$P_{d,outsideNoChC,max}$
RC1L	PGA	1.59	0.41	0.06	1.59	0.41	0.026
RC1M	PGA	3.12	0.56	0.04612	3.12	0.56	0.02
RC1H	PGA	6.13	0.80	0.0231	6.13	0.80	0.01
RC2	PGA	2.34	0.66	0.06	2.34	0.66	0.026
PC2	PGA	2.42	0.69	0.06	2.42	0.69	0.026
RC3L	PGA	1.45	0.44	0.46125	1.45	0.44	0.2
RC3M	PGA	2.54	0.60	0.23062	2.54	0.60	0.1
RC3H	PGA	4.06	0.75	0.11535	4.06	0.75	0.05
PC3L	PGA	1.27	0.25	0.46125	1.27	0.25	0.2
PC3M	PGA	1.24	0.27	0.23062	1.24	0.27	0.1
PC3H	PGA	1.47	0.26	0.11535	1.47	0.26	0.05
W2	PGA	2.43	0.37	0.00473	2.43	0.37	0.006

W3	PGA	1.88	0.31	0.00473	1.88	0.31	0.006
S1L	PGA	3.37	0.64	0.0369	3.37	0.64	0.016
S1H	PGA	6.07	0.94	0.0231	6.07	0.94	0.01
S1M	PGA	8.32	0.88	0.01387	8.32	0.88	0.006
S2L	PGA	1.76	0.37	0.0369	1.76	0.37	0.016
S2H	PGA	4.12	0.59	0.0231	4.12	0.59	0.01
S2M	PGA	7.79	0.87	0.01387	7.79	0.87	0.006
S3	PGA	36.30	0.53	0.01387	36.30	0.53	0.006
URM1F_B	PGA	0.62	0.34	0.189	0.62	0.34	0.16
URM1F_HA	PGA	2.93	0.56	0.252	2.93	0.56	0.2
URM1F_HC	PGA	1.17	0.46	0.252	1.17	0.46	0.2
URM2L	PGA	1.49	0.30	0.315	1.44	0.42	0.5
URM3L	PGA	0.99	0.41	0.252	0.99	0.41	0.4
URM3M_U	PGA	1.16	0.49	0.252	1.16	0.49	0.536
URM3M_D	PGA	0.96	0.34	0.315	0.96	0.34	0.6667
URM3M_B	PGA	1.21	0.46	0.252	1.21	0.46	0.16
URM4L	PGA	0.93	0.41	0.252	0.93	0.41	0.4
URM5L	PGA	1.14	0.36	0.315	1.14	0.36	0.5
URM6L	PGA	2.00	0.35	0.315	2.00	0.35	0.25
URM7L	PGA	2.28	0.37	0.315	2.25	0.42	0.25
URM8L	PGA	1.09	0.34	0.315	0.79	1.05	0.25
URM9L	PGA	1.35	0.36	0.315	1.36	0.34	0.5
URM10	PGA	2.00	0.35	0.315	2.00	0.35	0.25

Table 3.31: Weighted average fatality curves for URM buildings, where α is the median, β the standard deviation of the lognormal distribution, $P_{d,inside,max}$ is the max probability of dying inside the building and $P_{d,outsideNoChC,max}$ is the max probability of dying outside the building with no effect of the chimney collapse. Weighting factors are listed in Table 3.26.

Vulnerability class	**IM Type**	**Parameters of fatality curves**					
		$P_{d,inside}$			**$P_{d,outsideNoChC}$**		
		α[g]	**β[-]**	**$P_{d,inside,max}$**	**α[g]**	**β[-]**	**$P_{d,outsideNoChC,max}$**
avgURML:2to10	PGA	1.76	0.35	0.32	1.68	0.51	0.31
avgURML:3&4	PGA	0.98	0.41	0.25	0.98	0.41	0.40
avgURM3M	PGA	1.16	0.47	0.26	1.16	0.47	0.46
avgURM1F	PGA	1.33	0.42	0.22	1.33	0.42	0.18

Table 3.32: Input parameters of chimney vulnerability functions (from Crowley and Pinho, 2019).

Vulnerability class	$\overline{PGA_{chd}}$ [g]	β_{chd} [-]
RC1L	0	0
RC1M	0	0
RC1H	0	0
RC2	0	0
PC2	0	0
RC3L	205	2.2
RC3M	153	2.2
RC3H	0	0
PC3L	205	2.2
PC3M	153	2.2
PC3H	0	0
W1	0	0
W2	0	0
W3	370	2.3
S1L	0	0
S1M	0	0
S1H	0	0
S2L	0	0
S2M	0	0
S2H	0	0
S3	0	0
URM1_F	1480	2.5
URM1_O	0	0

This project has received funding from the European Union's Horizon 2020 research and innovation programme under grant agreement No 821046

URM2L	153	2.2
URM3L	205	2.2
URM3M_U	153	2.2
URM3M_D	153	2.2
URM3M_B	965	2.5
URM4L	205	2.2
URM5L	205	2.2
URM6L	570	2.4
URM7L	570	2.4
URM8L	570	2.4
URM9L	261	2.3
URM10	0	0

Table 3.33: Weighted average input parameters of chimney vulnerability functions for URM buildings.

Vulnerability class	$\overline{PGA_{chd}}$ [g]	β_{chd} [-]
avgURML:2to10	473.61	2.34
avgURML:3&4	205.00	2.20
avgURM3M	334.98	2.27
avgURM1F	821.50	1.80

This project has received funding from the European Union's Horizon 2020 research and innovation programme under grant agreement No 821046

4 CONCLUDING REMARKS

This document presents exhaustive state-of-the-art compilation of the most representative seismic fragility functions and loss estimation models for the building (various configuration and combinations of masonry, reinforced concrete, and steel structures) and infrastructure components (different railway/roadway bridge typologies and port facilities) in the TBs of the TURNkey project. The fragility and loss models reported in this deliverable for each TB will be implemented within the platform (WP6) developed as the main product of the project. Also, vast majority of the contents of this document may be extrapolated as a useful synthesis of the structural vulnerability standing for the entire European territory. Information presented by the models under consideration are carefully synthesized, unified, homogenized, and reported to exploit their use within and outside of TURNkey project.

This project has received funding from the European Union's Horizon 2020 research and innovation programme under grant agreement No 821046

5 REFERENCES

1. Ahmad N., Crowley H., Pinho R., (2010). Analytical Fragility Functions for Reinforced Concrete and Masonry Buildings and Buildings Aggregates of Euro-Mediterranean Regions – UPAV methodology. *Internal Report, Syner-G Project 2009/2012*.
2. Akansel VH, Yakut A, Gulkan P (2012). Fragility of shear wall buildings with torsional Irregularity. In: Proceedings of the 15th World Conference on Earthquake Engineering (WCEE), Lisbon, Portugal.
3. Akkar S. Sucuoglu H., & Yakut A., (2005). Displacement-based fragility functions for low- and mid-rise ordinary concrete buildings, *Earthquake Spectra*, 21(4), 901-927.
4. API (1993). Recommended practice for planning, design, and constructing fixed offshore platforms. API RP 2A – WSD, 20th ed., American Petroleum Institute.
5. ASCE (2014). Seismic Design of Piers and Wharves. ASCE/COPRI 61-14ISBN (print): 978-0-7844-1348-7ISBN (PDF): 978-0-7844-7834-9
6. ATC (1985). Earthquake damage evaluation data for California. Applied Technology Council, Redwood.
7. Barbat A.H., Pujades L.G. and Lantada N., (2006). Performance of Buildings under Earthquakes in Barcelona, Spain. Computer - *Aided Civil and Infrastructure Engineering*, 21: 573-593. doi:10.1111/j.1467-8667.2006.00450.x.
8. Barbieri DM (2019). Two methodological approaches to assess the seismic vulnerability of masonry bridges. Journal of Traffic and Transportation Engineering, 6(1): 49-64.
9. Basöz NI, Kiremidjian AS, King SA, Law KH (1999). Statistical analysis of bridge damage data from the 1994 Northridge, CA, earthquake. Earthq Spectra, 15(1):25–54.
10. Batilas (2015). Urban Accelerograph Network of Patras (UPAN): Installation, database development and recording process, PhD dissertation, Department of Civil Engineering, Laboratory of Geotechnical Engineering, University of Patras, pp. 1-347 (in Greek)
11. Bellotti D, Famà A, Di Meo A, Borzi B (2019a). Large-scale vulnerability analysis of girder railway bridges. Proceedings of the 7th ECCOMAS Thematic Conference on Computational Methods in Structural Dynamics and Earthquake Engineering, 24–26 June, Crete, Greece.
12. Bellotti D, Famà A, Di Meo A, Borzi B (2019b). Large-scale vulnerability analysis of girder railway bridges. Risk-Based Bridge Engineering: Proceedings of the 10th New York City Bridge Conference, 26-27 August, New York City, USA.
13. Bernardini A, Gori R, Modena C (1990). An Application of Coupled Analysis Models and Experimental Knowledge for Seismic Vulnerability Analysis of Masonry Buildings. In: Koridze A (ed) 3:161-180 Engineering Aspects of Earthquake Phenomena, Omega Scientific, Oxon.
14. Bessason B, Bjarnason JÖ, Guðmundsson A, Sólnes J, Steedman S, (2014). Analysis of damage data of low-rise buildings subjected to a shallow Mw6.3 earthquake. *Soil Dynamics and Earthquake Engineering*, 66;89-101
15. Bessason B, Bjarnason JÖ (2016), Seismic vulnerability of low-rise residential buildings based on damage data from three earthquakes (Mw6.5, 6.5 and 6.3). *Engineering Structures*, 111:64-79. http://dx.doi.org/10.1016/j.engstruct.2015.12.008
16. Bessason B, Bjarnason JÖ, Rupakhety R (2020), Statistical modelling of seismic vulnerability of RC, timber and masonry buildings from complete empirical loss data, *Engineering structures*, 209:109969, doi.org/10.1016/j.engstruct.2019.109969.
17. Bolognini D, Borzi B, Pinho R (2008). Simplified Pushover-Based Vulnerability Analysis of Traditional Italian RC Precast Structures. In: Proceeding of 14th World Conference on Earthquake Engineering, Bejing 2008.
18. Borzi B., Pinho R., Crowley H., (2007). SP-BELA: un metodo meccanico per la definizione della vulnerabilità basato su analisi pushover semplificate, ANIDIS, Pisa.
19. Borzi B, Crowley H, Pinho R (2008a). Simplified Pushover-Based Earthquake Loss Assessment (SPBELA) Method for Masonry Buildings. International Journal of Architectural Heritage, 2(4):353-376.
20. Borzi B, Pinho R, Crowley H (2008b). Simplified pushover-based vulnerability analysis for large scale assessment of RC buildings. Eng Struct, 30(3):804-820.

This project has received funding from the European Union's Horizon 2020 research and innovation programme under grant agreement No 821046

21. Borzi, B, Crowley H. & Pinho R., (2008c). Simplified Pushover-Based Earthquake Loss Assessment (SP-BELA) Method for Masonry Buildings, *International Journal of Architectural Heritage*, 2:4, 353-376, DOI: 10.1080/15583050701828178.
22. Borzi B, Ceresa P, Franchin P, Noto F, Calvi GM, Pinto PE (2015). Seismic vulnerability of the Italian roadway bridge stock. Earthquake Spectra, 31(4): 2137–2161.
23. Borzi B, Di Meo A, Faravelli M, Ceresa P, Monteiro R, Dabeek J (2016). Definition of Fragility Curve for Frame Buildings in Nablus – Palestine. In: 1st International Conference on Natural Hazards & Infrastructure ICONHIC, 28-30 June 2016, Chania, Crete Island, Greece.
24. Boulanger R.W., Curras C.J., Kutter B.L., Wilson D.W., Abghari A. (1999). Seismic soil-pile-structure interaction experiments and analyses. Journal of Geotechnical and Geoenvironmental Engineering, 125 (9): 750-759.
25. Bozzoni F, Famà A, Lai CG, Mirfattah SA (2014). Seismic risk assessment of seaports using GIS: The port of Gioia Tauro in Southern Italy. In PIANC World Congress San Francisco, USA.
26. Bozzoni F, Lai CG, Marsan P, Conca D, Famà A (2018). WebGIS platform for seismic risk assessment of maritime port systems in Italy. In Proc., 4th PIANC Mediterranean Days Congress 2018. Madrid, Spain: Asociaci´on Técnica de Puertos y Costas.
27. Braga F, Dolce M, Liberatore D (1982). A statistical Study on damage buildings and an ensuing review of the M.S.K. – 76 scale. In: Proceedings of the 7th Eur Conference on Earthq. Eng., Athens, Greece.
28. Buratti N, Minghini F, Ongaretto E, Savoia M, Tullini N (2017). Empirical seismic fragility for the precast RC industrial buildings damaged by the 2012 Emilia (Italy) earthquakes. Earthquake Engineering and Structural Dynamics, 46(14):2317-2335.
29. Burden LI, Rix G, Werner S (2016). Development of a Risk Framework for Forecasting Earthquake Losses in Port Systems, Earthquake Spectra, 32(1), 267–284. https://doi.org/10.1193/043013EQS117M
30. Calabrese A, Lai CG (2013). Fragility Functions of Blockwork Wharves Using Artificial Neural Networks. Soil Dynamics and Earthquake Engineering, Vol. 52, pp. 88-102. 2013.
31. Cardone D, Perrone G, Sofia S (2011). A performance-based adaptive methodology for the seismic evaluation of multi-span simply supported deck bridges. Bull. Earthq. Eng., 9(5):1463–1498
32. Casotto C, Silva V, Crowley H, Nascimbene R, Pinho R (2015). Seismic fragility of Italian RC precast industrial structures. Engineering Structures, 94:122-136. doi:10.1016/j.engstruct.2015.02.034.
33. Cattari S., Curti E., Giovinazzi S., Parodi S., Lagomarsino S., & Penna A., (2004). Un modello meccanico per l ' analisi di vulnerabilità del costruito in muratura a scala urbana. *XI Congresso Nazionale "L'Ingegneria Sismica in Italia"* - ANIDIS.
34. CEN (European Committee for Standardization) (2004). Eurocode 8: design of structures for earthquake resistance, part 1: general rules, seismic actions and rules for buildings. EN 1998-1:2004. Brussels, Belgium.
35. CEN (2005). *EN 1991-1, Eurocode 1: Actions on structures - Part 1-4: General actions - Wind actions*. European Committee for standardization (CEN). Engineering Structures 209 (2020) 109969
36. Ceran HB, Erberik MA (2013). Effect of out-of-plane behavior on seismic fragility of masonry buildings in Turkey. Bulletin of earthquake Engineering, 11(5):1775-1795.
37. Cheng Y, Chang J, Wu J (2019). Fragility analysis of a self-anchored suspension bridge based on structural health monitoring data. advances in civil engineering. Volume 3. https://doi.org/10.1155/2019/7467920.
38. Choi E, DesRoches R, Nielson B (2004). Seismic Fragility of Typical Bridges in Moderate Seismic Zones. Engineering Structures, 26(2):187-199. DOI: 10.1016/j.engstruct.2003.09.006
39. Coburn AW, Spence R (1992). Earthquake Protection. John Wiley & Sons Ltd, England.
40. Colombi M., Borzi B., Crowley H., Onida M., Meroni F., & Pinho R., (2008). Deriving vulnerability curves using Italian earthquake damage data. Bulletin of Earthquake Engineering, 6(3), 485–504. https://doi.org/10.1007/s10518-008-9073-6.
41. Conca D, Bozzoni F, Lai CG (2020). Interdependencies in seismic risk assessment of seaport systems: case study at a large commercial port in Italy. ASCE-ASME Journal of Risk and Uncertainty in Engineering Systems, Part A: Civil Engineering, Vol. 6, 2, https://ascelibrary.org/doi/10.1061/AJRUA6.0001043.

This project has received funding from the European Union's Horizon 2020 research and innovation programme under grant agreement No 821046

42. Conte JP, Zhang Y (2007). Performance Based Earthquake Engineering: Application to an Actual Bridge-Foundation-Ground System. Keynote paper, 12th Italian National Conference on Earthquake Engineering, 10-14 June, Pisa, Italy.
43. Cornell CA, Krawinkler H (2000). Progress and challenges in seismic performance assessment. Pacific Earthquake Engineering Research (PEER) Center News Spring, http://peer.berkeley.edu/news/2000spring/.
44. Cosenza E, Manfredi G, Polese M, Verderame GM (2005). A Multi-Level Approach to the Capacity Assessment of Existing RC Buildings. Journal of Earthquake Engineering, 9(1):1–22.
45. Crowley H, Pinho R, Bommer JJ (2004). A Probabilistic Displacement-Based Vulnerability Assessment Procedure for Earthquake Loss Estimation. Bulletin of Earthquake Engineering, 2(2):173–219.
46. Crowley H, Colombi M, Silva S, Monteiro R, Ozcebe S, Fardis M, Tsionis G, Askouni P (2011). Fragility functions for roadway bridges, SYNER-G Report D3.6, www.syner-g.eu.
47. Crowley H. and Pinho R. (2019) Report on the Fragility and Consequence Models for the Groningen Field (Version 6). March 2019. Jan van Elk & Dirk Doornhof Editors
48. Crowley H, Despotaki V, Rodrigues D, Silva V, Toma-Danila D, Riga E, Karatzetzou, Fotopolou S, Zugic Z, Sousa L, Ozcebe S, Gamba P (2020). Exposure model for European seismic risk assessment. Earthquake Spectra, 36(S1): 252-273.
49. Crowley H. and Pinho R. (2020) Report on the Fragility and Consequence Models for the Groningen Field (Version 7). March 2020. Jan van Elk & Dirk Doornhof Editors
50. D'Ayala D., Spence R., Oliveira C., & Pomonis A., (1997). Earthquake Loss Estimation for Europe's Historic Town Centres. *Earthquake Spectra*, 13(4), 773–793. https://doi.org/10.1193/1.1585980.
51. D'Ayala D (2013). Assessing the seismic vulnerability of masonry buildings. In: Tesfamariam S and Goda K (eds) Handbook of Seismic Risk management of civil infrastructure systems, Woodhead publishing.
52. De Felice G, Giannini R (2010). An efficient approach for seismic fragility assessment with application to old reinforced concrete bridges. J. Earthq. Eng., 14(2):231–251.
53. Del Gaudio C, Ricci P, Verderame GM, Manfredi G (2015). Development and urban-scale application of a simplified method for seismic fragility assessment of RC buildings. Eng Struct, 91:40–57, doi:10.1016/j.engst ruct.2015.01.031.
54. Di Ludovico M, Prota A, Moroni C, Manfredi G, Dolce M (2017a). Reconstruction process of damaged residential buildings outside historical centres after the L'Aquila earthquake: part I— "light damage" reconstruction. Bull Earthquake Eng, 15(2):667-692, doi:10.1007/s10518-016-9877-8.
55. Di Ludovico M, Prota A, Moroni C, Manfredi G, Dolce M (2017b). Reconstruction process of damaged residential buildings outside historical centres after the L'Aquila earthquake - part II: "heavy damage" reconstruction. Bull Earthquake Eng, 15(2):693-729, doi:10.1007/s10518-016-9979-3.
56. Di Pasquale G, Orsini G, Pugliese A, Romeo RW (1998). Damage scenario from future earthquakes. In: The 11th Eur. Conference on Earthq. Eng., Rotterdam, Netherlands.
57. Dolce M., Kappos A., Masia A., Penelis G., Vona M. (2006). Vulnerability assessment and earthquake damage scenarios of the building stock of Potenza (Southern Italy) using Italian and Greek methodologies, Engineering Structures, 28, 357–371.
58. Dolce M, Borzi B, Da Porto F, Faravelli M, Lagomarsino S, Magenese G, Moroni C, Penna A, Prota A, Speranza E, Zuccaro G, Verderame GM (2019). Mappe di rischio sismico per il territorio italiano. XVIII Convegno L'Ingegneria Sismica in Italia ANIDIS, 15-19 settembre 2019, Ascoli Piceno, Italy, Paper N. 3549.
59. Duenas-Osorio L, Craig JI, Goodno BJ (2007) Seismic response of critical interdependent networks. Earthq Eng Struct Dyn 36(2):285–306.
60. Dumova-Jovanoska E (2000). Fragility curves for reinforced concrete structures in Skopje (Macedonia) region. Soil Dynamics and Earthquake Engineering, 19(6):455-466, doi:10.1016/S0267-7261(00)00017-8.
61. Elnashai AS, Borzi B, Vlachos S (2004). Deformation-based vulnerability functions for RC bridges. Structural Engineering, 17(2):215-244.

This project has received funding from the European Union's Horizon 2020 research and innovation programme under grant agreement No 821046

62. Enke D, Tirasirichai C, Luna R (2008). Estimation of earthquake loss due to bridge damage in the st. louis metropolitan area: part ii - indirect losses. Natural Hazards Review, ASCE, 9(1):12-19.
63. EPANTYK (2009). Development of GIS software for the representation of the structural wealth of the municipalities of the country and of its structural vulnerability in buildings block level, YP.ES.A, H.D, KEDKE, TEE, pp. 39 (in Greek)
64. Erberik MA, Elnashai AS., (2004). Fragility analysis of flat-slab structures. *Eng Struct*. 26(7):937-948. doi:10.1016/J.ENGSTRUCT.2004.02.012.
65. Erberik MA (2008). Generation of fragility curves for Turkish masonry buildings considering in-plane failure modes. Earthquake Engineering & Structural Dynamics, 37(3):387-405.
66. Fajfar, P. (2000). A nonlinear analysis method for performance-based seismic design. Earthquake Spectra, 16(3), 573–592.
67. Faravelli M, Borzi B, Polli D, Pagano M (2019). Calibration of a mechanics-based method for large-scale vulnerability assessment. Bull Earthquake Eng, 17(5):2485-2508, doi:10.1007/s10518-019-00560-0.
68. Fardis MN, Tsionis G, Askouni P 2009/2012. Analytical fragility functions for reinforced concrete bridges – UPAT methodology, Internal Report, Syner-G Project.
69. Farsangi E.N., Tasnimi A.A., (2016a). The influence of coupled horizontal–vertical ground excitations on the collapse margins of modern RC-MRFs. *International Journal of Advanced Structural Engineering (IJASE)* 8, 169–192. https://doi.org/10.1007/s40091-016-0122-0.
70. Farsangi E. N., Yang T.Y., & Tasnimi A.A., (2016b). Influence of concurrent horizontal and vertical ground excitations on the collapse margins of non-ductile RC frame buildings. *Structural Engineering and Mechanics*, 59(4), 653–669. https://doi.org/10.12989/SEM.2016.59.4.653.
71. FEMA (1999). Hazus 99 technical manual. Federal Emergency Management Agency, Washington, DC, USA.
72. Federal Emergency Management Agency (FEMA) (2003). HAZUS-MH MR4 Technical Manual. Natl Inst Build Sci Fed Emerg Manag Agency (NIBS FEMA) 712.
73. Ferrari SLP, Cribari-Neto F (2004). Beta Regression for Modelling Rates and Proportions. *Journal of Applied Statistics*, 31(7);799–815.
74. Forcellini D (2018). A New Methodology to Assess Indirect Losses in Bridges Subjected to Multiple Hazards. Emerging Science Journal, 2(6):400-409.
75. Franchin P (2013). Methodology for systemic seismic vulnerability assessment of buildings, infrastructures, networks and socio-economic impacts. SYNER-G Reference Report 1. JRC Scientific and Policy Reports. doi:10.2788/69238.
76. Gardoni P, Mosalam KM, Der Kiureghian A (2003). Probabilistic seismic models and fragility estimates for RC bridges. J. Earthq. Eng., 7(1):79–106.
77. Gehl P, Taalab K, D'ayala D, Cheng T (2014). Developing fragility functions for roadway bridges using system reliability and support vector machines. 2nd European Conference on Earthquake Engineering and Seismology, 25-29 Aug, Istanbul, Turnkey.
78. Giannaraki G., I. Kassaras, Z. Roumelioti, D. Kazantzidou–Firtinidou, A. Ganas (2018). Deterministic seismic risk assessment in the city of Aigion (W. Corinth Gulf, Greece) and juxtaposition with real damage due to the 1995 Mw6.4 earthquake, Bulletin of Earthquake Engineering, Springer Nature B.V., pp. 1–32.
79. Giovinazzi S. and Lagomarsino S., (2004). August. A macroseismic method for the vulnerability assessment of buildings. *In 13th World Conference on Earthquake Engineering* , Vol. 896, pp. 1-6.
80. Grünthal, G. (Ed.) (1998) European Macroseismic Scale 1998 (EMS-98) European Seismological Commission, sub commission on Engineering Seismology, Working Group Macroseismic Scales. Conseil de l'Europe, Cahiers du Centre Européen de Géodynamique et de Séismologie, Vol. 15, Luxembourg.
81. Hancilar U, Çaktr E (2015). Fragility functions for code complying RC frames via best correlated IM–EDP pairs. Bull Earthq Eng , 13(11):3381–3400, doi:10.1007/s1051 8-015-9775-5.
82. Hill M., Rossetto T. (2008) Comparison of building damage scales and damage descriptions for use in earthquake loss modelling in Europe, Bulletin of Earthquake Engineering 6(2):335-365
83. Ichii K (2003). Application of performance-based seismic design concept for caisson-type quay walls. Ph.D. dissertation, Kyoto University.

This project has received funding from the European Union's Horizon 2020 research and innovation programme under grant agreement No 821046

84. Ichii K (2004). Fragility curves for gravity-type quay walls based on effective stress analyses. In: 13th WCEE, Vancouver, BC.
85. Icelandic Standards (2010). *Icelandic National Annexes to Eurocodes*, Staðlaráð Íslands.
86. Ioannou I, Bessason B, Kosmidis I, Bjarnason JÖ, Rossetto T (2018). Empirical seismic vulnerability assessment of Icelandic buildings affected by the 2000 sequence of earthquakes, *Bulletin of Earthquake Engineering*, 16(12):5875-5903.
87. Jeong S. H., & Elnashai A. S., (2007). Probabilistic fragility analysis parameterized by fundamental response quantities. *Engineering Structures*, 29(6), 1238–1251. https://doi.org/10.1016/j.engstruct.2006.06.026.
88. Kakderi K, Pitilakis K (2010). Seismic analysis and fragility curves of gravity waterfront structures. In: Fifth international conference on recent advances in geotechnical earthquake engineering and soil dynamics and symposium in Honour of Prof. I. M. Idriss, 6.04a.
89. Kakderi K, Selva J, Fotopoulou S, Argyroudis S, Pitilakis K (2012). Systemic vulnerability and loss for harbors. Deliverable 5.6, SYNER-G Project.
90. Kakderi K, Selva J, Argyroudis S, Pitilakis K, Anastasiadis A, Alexoudi M, Souli A, Fotopoulou S, Rovithis M, Senetakis K (2013). Application and validation study to a harbor system (Thessaloniki, Greece). Deliverable 6.6, SYNER-G Project.
91. Kamath AP (2017). Seismic risk assessment of masonry arch bridges in the United States (M.Sc. Thesis). Clemson University, South Carolina, USA.
92. Kappos A, Pitilakis K, Stylianidis KC (1996). Cost-Benefit Analysis for the Seismic Rehabilitation of Buildings in Thessaloniki, Based on a Hybrid Method of Vulnerability Assessment. In: 5th International Conference on Seismic Zonation, Nice, France, 1:406–413.
93. Kappos A. J., Panagiotopoulos C., Panagopoulos G., Papadopoulos El., (2003). WP4 Reinforce Concrete Buildings (Level 1 and Level 2 analysis). WP4 Report RISK-UE.
94. Kappos A.J., Panagopoulos G., Panagiotopoulos C. et al, (2006). A hybrid method for the vulnerability assessment of R/C and URM buildings. *Bull Earthquake Eng*, 4, 391–413. https://doi.org/10.1007/s10518-006-9023-0.
95. Kappos A, Lekidis V, Panagopoulos G, Sous I, Theodulidis N, Karakostas C, Margaris B (2007). Analytical estimation of economic loss for buildings in the area struck by the 1999 Athens earthquake and comparison with statistical repair costs. Earthquake Spectra, 23(2):333-355, doi:10.1193/1.2720366.
96. Kappos A.J. and Dimitrakopoulos E.G. (2008): Feasibility of pre-earthquake strengthening of buildings based on cost-benefit and life-cycle cost analysis, with the aid of fragility curves. Nat. Hazards, 45, 33-54.
97. Karantoni F, Tsionis G, Lyrantzaki F, Fardis MN (2014). Seismic fragility of regular masonry buildings for in-plane and out-of-plane failure. Earthq. and Structs. 6(6):689-713, doi:10.12989/eas.2014.
98. Karapetrou ST, Fotopoulou SD, Pitilakis KD (2015). Seismic Vulnerability Assessment of RC Building Considering Soil-Structure-Interaction Effects. In: 6th International Conference on Earthquake Geotechnical Engineering, 1-4 November 2015, Christchurch, New Zealand.
99. Karim KR, Yamazaki F (2003). A simplified method of constructing fragility curves for highway bridges. Earthq Eng Struct Dyn, 32(10):1603–1626.
100. Kibboua A, Kehila F, Hemaidi-Zourgui N, Remki M (2017). Comparison between fragility curves of RC bridge piers designed by old and recent Algerian codes. E. J. Engineering Sciences and Technology, 2: 56-67.
101. Kim SH, Shinozuka M (2004). Development of fragility curves of bridges retrofitted by column jacketing. Probab. Eng. Mech., 19(1–2):105–112.
102. Kircil MS, Polat Z (2006). Fragility analysis of RC frame buildings on firm sites. In: Proceedings of the 2nd International Congress Fédération Internationale du Béton, Naples, Italy.
103. Kyriakides N. C., Chrysostomou C. Z., Tantele E. A., & Votsis R. A., (2015). Framework for the derivation of analytical fragility curves and life cycle cost analysis for non-seismically designed buildings. *Soil Dynamics and Earthquake Engineering*, 78, 116–126. https://doi.org/10.1016/J.SOILDYN.2015.07.008-

This project has received funding from the European Union's Horizon 2020 research and innovation programme under grant agreement No 821046

104. Ko Y-Y, Yang H-H, Chen C-H (2010). Seismic fragility analysis for sheet pile wharves – case study of the Hualien harbor in Taiwan. In: Fifth international conference on recent advances in geotechnical earthquake engineering and soil dynamics and symposium in Honor of Prof. I.M. Idriss, 6.05a.
105. Ko Y.Y., Yang H.H. (2019). Deriving seismic fragility curves for sheet-pile wharves using finite element analysis. Soil Dynamics and Earthquake Engineering, 123, 265-277. https://doi.org/10.1016/j.soildyn.2019.05.014
106. Kosbab B (2010) Seismic performance evaluation of port container cranes allowed to uplift. Ph.D. thesis, School of Civil and Environmental Engineering, Georgia Institute of Technology.
107. Kostov M., Vaseva E., Kaneva A., Koleva N., Varbanov G., Stefanov D., Darvarova E., Solakov D., Simeonova S. and Cristoskov L., (2004). Application to Sofia, *Report RISK-UE WP13* - RISK-UE WP13.
108. Kurian SA, Deb SK, Dutta A (2006). Seismic vulnerability assessment of a railway overbridge using fragility curves. Proceedings of the 4th international conference on earthquake engineering, Taipei, Taiwan.
109. Kwon O.S., & Elnashai A., (2006). The effect of material and ground motion uncertainty on the seismic vulnerability curves of RC structure. *Engineering Structures*, 28(2), 289–303. https://doi.org/10.1016/J.ENGSTRUCT.2005.07.010.
110. Kwon O, Sextos AG, Elnashai, AS (2009). Seismic fragility of a bridge on liquefaction susceptible soil. Proceedings of the 10th international conference on structure safety and reliability, Osaka, Japan.
111. Kwon OS, Elnashai AS (2009). Fragility analysis of a highway over-crossing bridge with consideration of soil–structure interactions. Struct. Infrastruct. Eng., 6(1–2):159–178 .
112. Lagomarsino S, Giovinazzi S (2006). Macroseismic and mechanical models for the vulnerability and damage assessment of the current buildings. Bull. Earthq. Eng. 4:415-443, doi:10.1007/s10518-006-9024-z.
113. Lagomarsino S, Cattari S (2014). Fragility functions of masonry buildings. In SYNER-G: Typology definition and fragility functions for physical elements at seismic risk. Springer Science & Business Media Dordrecht, doi:10.1007/978-94-007-7872-6_5.
114. Lang D., Molina-Palacios S., Lindholm C., Balan S. (2012) Deterministic earthquake damage and loss assessment for the city of Bucharest, Romania. J Seismol (2012) 16:67–88.
115. Li J, Spencer BF, Elnashai AS (2012). Bayesian updating of fragility functions using hybrid simulation. ASCE J Struct Eng, 139(7):1160–1171.
116. Liel A. B., & Lynch K. P., (2012). Vulnerability of reinforced-concrete-frame buildings and their occupants in the 2009 L'Aquila, Italy, earthquake. *Natural Hazards Review*, 13(1), 11–23. https://doi.org/10.1061/(ASCE)NH.1527-6996.0000047.
117. Luna R, Hoffman D, Lawrence W (2008). Estimation of earthquake loss due to bridge damage in the St. Louis metropolitan area: part I - direct losses. Natural Hazards Review, 9(1):1-11.
118. Lupoi G, Franchin P, Lupoi A, Pinto PE (2004). Seismic fragility analysis of structural systems. Proccedings of the 13th world conference on earthquake engineering, Vancouver, Canada.
119. Lupoi A, Franchin P, Pinto PE, Monti G (2005). Seismic design of bridges accounting for spatial variability of ground motion. Earthq. Eng. Struct. Dyn., 34(4–5):327–348.
120. Mackie K, Stojadinovic B (2004). Fragility curves for reinforced concrete highway overpass bridges. Proccedings of the 13th world conference on earthquake engineering, Vancouver, Canada.
121. Mackie KR, Stojadinovic B (2005). Fragility basis for California highway overpass bridge seismic decision making. PEER Report No. 2005/02, Pacific Earthquake Engineering Research Center, University of California, Berkeley, USA.
122. Mackie KR, Wong JM, Stojadinovic B (2008). Integrated Probabilistic Performance-Based Evaluation of Benchmark Reinforced Concrete Bridges. Pacific Earthquake Engineering Research Centre. University of California, Berkeley,USA.
123. Mackie KR, Wong JM, Stojadinović B (2009). Post-earthquake bridge repair cost and repair time estimation methodology. Earthquake Engineering & Structural Dynamics, 39(3): 281-301. https://doi.org/10.1002/eqe.942.
124. Martins L. and Silva V., (2018). A global database of vulnerability models for seismic risk assessment - *16ECEE*.

This project has received funding from the European Union's Horizon 2020 research and innovation programme under grant agreement No 821046

125. Maruyama Y, Yamazaki F, Mizuno K, Tsuchiya Y, Yogai H (2010) Fragility curves for expressway embankments based on damage datasets after recent earthquakes in Japan. Soil Dyn Earthq Eng 30:1158–1167.
126. Masi A, Digrisolo A, Manfredi V (2015). Fragility curves of gravity-load designed RC buildings with regularity in plan. Earthq Struct 9(1):1-27, doi:10.12989/eas.2015.9.1.001.
127. McKenna F., Fenves G.L., Scott M.H. (2000). Open system for earthquake engineering simulation. Pacific Earthquake Engineering Research (PEER) Center.
128. Miano A, Jalayer F, De Risi R, Prota A, Manfredi G (2015). Model updating and seismic loss assessment for a portfolio of bridges. Bulletin of Earthquake Engineering, 14 (3):699-719, doi: 10.1007/s10518-015-9850-y.
129. Mirzaeefard H., Hariri-Ardebili M.A., Mirtaheri M. (2021). Time-dependent seismic fragility analysis of corroded pile-supported wharves with updating limit states. Soil Dynamics and Earthquake Engineering, 142, 2021, https://doi.org/10.1016/j.soildyn.2020.106551.
130. Mirfattah SA (2013). Assessment of seismic vulnerability and risk of pile-supported wharves, PhD Thesis, European School of Advanced Studies in Reduction of Seismic Risk (ROSE School, IUSS Pavia), Pavia, Italy. Advisor: Prof. Carlo G. Lai.
131. Mirfattah SA, Lai CG (2015). Effect of Uncertainties in Soil Properties on Probabilistic Seismic Performance of Pile-Supported Wharves Proceedings, 6th International Conference on Earthquake Geotechnical Engineering, Christchurch, New Zealand.
132. Monti G, Nistico N (2002) Simple probability-based assessment of bridges under scenario earthquakes. ASCE J Bridge Eng., 7(2):104–114.
133. Morandi P, Manzini CF, Borzi B, Mauro A, Vecchi A, Tisalvi M, Iacobini F. (2019). Simplified seismic vulnerability assessment of railway masonry arch bridges. E-Proceedings of the 10th New York City Bridge Conference, 26-27 August, New York, USA.
134. Moreno-Gonzalez R. & Bairan J. M., (2013). Seismic Damage Assessment for Waffled-Slabs Reinforced Concrete (RC) Buildings in Barcelona, International Journal of Architectural Heritage: Conservation, Analysis, and Restoration, 7:1, 116-134 http://dx.doi.org/10.1080/15583058.2011.616619
135. Na UJ, Chaudhuri SR, Shinozuka M (2008). Probabilistic assessment for seismic performance of port structures. Soil Dyn Earthq Eng 28(2):147–158.
136. Na UJ and Shinozuka M (2009). Simulation-based seismic loss estimation of seaport transportation system, Reliability Engineering and System Safety 94, 722–731.
137. Na UJ, Chaudhuri SR, Shinozuka M (2009). Performance evaluation of pile supported Wharf under seismic loading. In: Tang A, Werner S (eds) 2009 TCLEE conference: lifeline earthquake engineering in a multihazard environment, ASCE, pp 1032–1041.
138. National Institute of Building Sciences NIBS (2004). HAZUS-MH: users's manual and technical manuals. Report prepared for the FEMA.
139. Nguyen DD, Park D, Shamsher S, Nguyen VQ, Lee TH. (2019) Seismic vulnerability assessment of rectangular cut-and-cover subway tunnels. Tunnelling and Underground Space Technology 86 (2019) 247–261
140. Nielson BG, Desroches R (2007). Analytical Seismic Fragility Curves for Typical Bridges in the Central and Southeastern United States. Earthquake Spectra, 23(3): 615-633. DOI: 10.1193/1.2756815.
141. Ntritsos N (2015). A State-Dependent Approach for Seismic Fragility Analysis of Wharves Supported in Liquefiable Soil, Master Thesis, European School of Advanced Studies in Reduction of Seismic Risk (ROSE School, IUSS Pavia), Pavia, Italy. Advisor: Carlo G. Lai.
142. Ntritsos N, Lai CG (2016). Seismic vulnerability of pile–supported wharves considering recurrent liquefaction–induced damage. Editor: Quake CoRE. URI: http://hdl.handle.net/10092/12778
143. Nuti C., Vanzi I., & Santini S., (1998). Seismic risk of Italian hospitals. *11th European Conference on Earthquake Engineering*, 39(085).
144. Olteanu P., Coliba V., Vacareanu R., Pavel F., Ciuiu D. (2016) Analytical seismic fragility functions for dual RC structures in Bucharest. In: The 1940 Vrancea earthquake. Issues, insights and lessons learnt, Springer Natural Hazards, 463-479.

This project has received funding from the European Union's Horizon 2020 research and innovation programme under grant agreement No 821046

145. Oropeza M, Michel C, Bigler M, Lestuzzi P (2010). New analytical fragility curves for existing URM buildings in regions with moderate seismicity. In: Proceedings of the 8th International Masonry Conference. Dresden, Germany.
146. Ospina R, Ferrari SLP (2012). A general class of zero-or-one inflated beta regression models, *Computational Statistics and Data Analysis*, 56:1609–1623.
147. Ozmen H. B., Inel M., Meral E., & Bucakli M., (2010). Vulnerability of Low and Mid-Rise Reinforced Concrete Buildings In Turkey. *14Ecee*.
148. Pachakis D, Kiremidjian AS (2004). Estimation of downtime-related revenue losses in seaports following scenario earthquakes, Earthquake Spectra 20, 427–449.
149. Padgett JE, DesRoches R (2009). Retrofitted bridge fragility analysis for typical classes of multispan bridges. Earthq. Spectra, 25(1):117–141.
150. Pang Y, Wu L (2018). Seismic fragility analysis of multispan reinforced concrete bridges using mainshock-aftershock sequences. Mathematical Problems in Engineering, Volume 2018. https://doi.org/10.1155/2018/1537301.
151. Park J, Choi E (2011). Fragility analysis of track-on steel-plate-girder railway bridges in Korea. Engineering Structures, 33(3): 696–705.
152. Pavel F., Vacareanu R. (2016) Scenario-based earthquake risk assessment for Bucharest, Romania. International Journal of Disaster Risk Reduction 20: 138-144.
153. Pavel F., Calotescu I., Stanescu D., Badiu A. (2018) Life-Cycle and Seismic Fragility Assessment of Code-Conforming Reinforced Concrete and Steel Structures in Bucharest. Int J Disaster Risk Sci (2018) 9:263–274.
154. Pelà L, Aprile A, Benedetti A (2009). Seismic assessment of masonry arch bridges. Engineering Structures, 31(8): 1777-1788. DOI: 10.1016/j.engstruct.2009.02.012.
155. PIANC (2001). Seismic Design Guidelines for Port Structures, International Navigation Association, Balkema, 474pp.
156. POLA (2012). Port of Long Beach Wharf Design Criteria, WDC Version 3.0.
157. POLB (2010). The Port of Los Angeles Code for Seismic Design, Upgrade and Repair of Container Wharves, California, City of Los Angeles, Harbour Department.
158. Polese M., Verderame G. M., Mariniello C., Iervolino I., & Manfredi G., (2008). Vulnerability Analysis for Gravity Load Designed RC Buildings in Naples – Italy. *Journal of Earthquake Engineering*, 12(sup2), 234–245. https://doi.org/10.1080/13632460802014147.
159. Polese M, Di Ludovico M, Marcolini M, Prota A, Manfredi G (2015). Assessing reparability: simple tools for estimation of costs and performance loss of earthquake damaged reinforced concrete buildings. Earthquake Engineering and Structural Dynamics, 44:1539-1557, doi:10.1002/eqe.2534.
160. Pomonis A., Gaspari M., Karababa F.S. (2014). Seismic vulnerability assessment for buildings in Greece based on observed damage data sets, Bollettino di Geofisica Teorica ed Applicata Vol. 55, n. 2, pp. 501-534; June 2014, DOI 10.4430/bgta0069
161. Qi'ang W, Ziyan W, Shukui L (2012). Seismic fragility analysis of highway bridges considering multi-dimensional performance limit state. Earthq Eng Eng Vib, 11(2):185–193.
162. RISK-UE An Advanced approach to earthquake risk scenarios with applications to different European towns. WP4: Vulnerability of current buildings Risk-UE 2003. UTCB Hybrid Approach
163. Rossetto T., & Elnashai A., (2003). Derivation of vulnerability functions for European-type RC structures based on observational data. *Engineering Structures*, 25(10), 1241–1263. https://doi.org/10.1016/S0141-0296(03)00060-9.
164. Rossetto T, Elnashai A (2005). A New Analytical Procedure for the Derivation of Displacement-Based Vulnerability Curves for Populations of RC Structures. Engineering Structures, 7(3):397–409.
165. Rosti A., Rota M., Penna A. (2020). Empirical fragility curves for Italian URM buildings. Bulletin of Earthquake Engineering, https://doi.org/10.1007/s10518-020-00845-9
166. Rota M, Penna A, Strobbia CL (2008). Processing Italian damage data to derive typological fragility curves. Soil Dynamics and Earthquake Engineering, 28:933-947.
167. Rota M, Penna A, Magenes G (2010). A methodology for deriving analytical fragility curves for masonry buildings based on stochastic nonlinear analyses. Engineering Structures, 32(5):1312-13-23.

This project has received funding from the European Union's Horizon 2020 research and innovation programme under grant agreement No 821046

168. Sabetta F, Goretti A, Lucantoni A (1998). Empirical fragility curves from damage surveys and estimated strong ground motion. In: 11th European Conference on Earthquake Engineering, Paris, France, 1-11.
169. Sarabandi P., Pachakis D. D., King S. A. & Kiremidjian A. S., (2004). Empirical Fragility Functions From Recent Earthquakes. *13th World Conference on Earthquake Engineering*, (1211), Paper No. 1211.
170. Saxena V, Deodatis G. Shinozuka M, Feng MQ (2000). Development of fragility curves for multi-span reinforced concrete bridges. Proceedings of the International Conference on Monte Carlo Simulation, Principality of Monaco, Balkema Publishers.
171. Seo J, Park H (2015). Seismic restoration cost curve of curved steel bridges. Forensic Engineering 2015. doi:10.1061/9780784479711.070
172. Shafieezadeh A (2011). Seismic vulnerability assessment of wharf structures. Ph.D. thesis, School of Civil and Environmental Engineering, Georgia Institute of Technology.
173. Shinozuka M, Murachi Y, Dong X, Zhou Y, Orlikowski MJ (2003). Effect of seismic retrofit of bridges on transportation networks. Earthquake Engineering and Engineering Vibration, 2(2): 169–179. doi:10.1007/s11803-003-0001-0
174. Shinozuka M, Feng MQ, Lee J, Naganuma T (2000a). Statistical analysis of fragility curves. ASCE J. Eng . Mech., 126(12):1224–1231.
175. Shinozuka M, Feng MQ, Kim HK, Kim SH (2000b). Nonlinear static procedure for fragility curve development. ASCE J Eng Mech, 126(12):1287–1295.
176. Shirazian S, Ghayamghamian MR, Nouri GR (2011). Developing of fragility curve for two-span simply supported concrete bridge in near-fault area. World Acad .Sci. Eng. Technol. 5(3):140–144.
177. Silva V, Crowley H, Pinho R, Varum H (2014). Investigation of the characteristics of Portuguese regular moment-frame RC buildings and development of a vulnerability model. Bull Earthq Eng, 13(5):1455–1490.
178. Simões A, Milošević J, Meireles H, Bento R, Cattari S, Lagomarsino S (2015). Fragility curves or old masonry building types in Lisbon. Bull Earthq Eng, 13:3083–3105, doi:10.1007/s1051 8-015-9750-1.
179. Singhal A, Kiremidjian AS (1996). Method for Probabilistic Evaluation of Seismic Structural Damage. ASCE Journal of Structural Engineering, 122(12):1459–67.
180. Spence R, So E, Scawthorn C (2011). Human Casualties in Earthquakes: Progress in Modelling and Mitigation. Advances in Natural and Technological Hazards Research. Springer, Netherlands.
181. SRM-LIFE (2007). Development of a global methodology for the vulnerability assessment and risk management of lifelines, infrastructures and critical facilities. Application to the metropolitan area of Thessaloniki. Research project, G. Secretariat for Research and Techniques, Greece.
182. Stewart J.P., Klimis N., Savvaidis A., Theodoulidis N., Zargli E., Athanasopoulos G., Pelekis P., Mylonakis G., and Margaris B. (2014). Compilation of a Local VS Profile Database and Its Application for Inference of VS30 from Geologic- and Terrain-Based Proxies, Bulletin of the Seismological Society of America, Vol. 104, No. 6, pp. 1–15, doi: 10.1785/0120130331
183. Tanaka S, Kameda H, Nojima N, Ohnishi S (2000). Evaluation of seismic fragility for highway transportation systems. Proceedings of 12th world conference on earthquake engineering, Auckland, New Zealand.
184. Tecchio G, Donà M, Da Porto F (2016). Seismic fragility curves of as-built single-span masonry arch bridges. Bull. Earthq. Eng., 14(11): 3099–3124, doi:10.1007/s10518-016-9931-6.
185. Thomopoulos C, Lai CG (2012). Preliminary Definition of Fragility Curves for Pile-Supported Wharves. Journal of Earthquake Engineering, Vol. 16, Supplement 1, 2012, pp. 83-106.
186. Tirasirichai C., Enke D. (2007). Case study: applying a regional cge model for estimation of indirect economic losses due to damaged highway bridges. The Engineering Economist, 52(4): 367-401.
187. Toma-Danilă D., Cioflan C., Ionescu C., Tiganescu A. (2018) The near real-time system for estimating the Seismic Damage in Romania (SeisDaRo) - recent upgrades and results. Proceedings of the 16ECEE (Tessaloniki, Greece)
188. Tran QH, Huh J, Doan NS, Mac VH Ahn J-H (2019). Fragility Assessment of a Container Crane under Seismic Excitation Considering Uplift and Derailment Behavior. Appl. Sci. 2019, 9(21), 4660.

This project has received funding from the European Union's Horizon 2020 research and innovation programme under grant agreement No 821046

189. Tsionis G., A. Papailia, M.N. Fardis., (2011). Analytical Fragility Functions for Reinforced Concrete Buildings and Buildings Aggregates of Euro-Mediterranean Regions UPAT methodology. *Internal Report, Syner-G Project* 2009/2012.
190. Tsionis G, Fardis MN (2014). Seismic fragility curves for reinforced concrete buildings and bridges in Thessaloniki. In: 2nd European conference on earthquake engineering and seismology, Istanbul, Turkey.
191. UTCB (Technical University of Civil Engineering, Bucharest) (2006) Study on early earthquake damage evaluation of existing buildings in Bucharest, Romania. Draft report prepared for Building Research Institute and International Institute for Seismology and Earthquake Engineering, Tsukuba, Japan.
192. Vacareanu R., Radoi R., Negulescu C., Aldea A., (2004). Seismic Vulnerability Of Rc Buildings In Bucharest, Romania. *13th World Conference on Earthquake Engineering*, (1250).
193. Vacareanu R., Chesca A.B., Georgescu B., Seki M. (2007) Case study on the expected seismic losses of soft and weak groundfloor buildings. Proceedings of the International Symposium on Strong Vrancea Earthquakes and Risk Mitigation (Oct. 4-6, 2007, Bucharest, Romania).
194. Vargas Y. F., Pujades L.B. and Barbat A.H., (2010). Probabilistic assessment of the global damage in reinforced concrete structures, *14ECEE, Ohrid*.
195. Villar-Vega M., Silva V., Crowley H., Yepes C., Tarque N., Acevedo A. B., María H. S., (2017). Development of a Fragility Model for the Residential Building Stock in South America. *Earthquake Spectra*, 33(2), 581–604. https://doi.org/10.1193/010716EQS005M.
196. Vona M (2014). Fragility Curves of Existing RC Buildings Based on Specific Structural Performance Levels. Open Journal of Civil Engineering, 4:120-134, doi:10.4236/ojce.2014.42011.
197. Werner SD, Taylor CE (2004). Final Report, Seismic Risk Reduction Planning for Wharf and Embankment Strengthening Program, Port of Oakland, Oakland, CA.
198. Werner SD, Cook WC (2010). Wharf repair estimates for use in demonstration seismic risk analysis of port systems. Seismic Systems & Engineering Consultants, Oakland.
199. Whitman RV (1973). Damage probability matrices for prototype buildings, Report 8, R73-57. Structures Publication 380.
200. Yamazaki F, Motomura H, Hamada T (2000). Damage assessment of expressway networks in Japan based on seismic monitoring. Proceedings of the 12th world conference on earthquake engineering, Auckland, New Zealand.
201. Yang Z., Elgamal A., Parra E (2003). Computational model for cyclic mobility and associated shear deformation. Journal of Geotechnical and Geoenvironmental Engineering, 129 (12): 1119-1127.
202. Zampieri P (2014). Simplified seismic Vulnerability Assessment of Masonry Arch Bridges. PhD thesis, University of Trento, University of Padua, Italy.
203. Zampieri P, Zanini MA, Faleschini F (2016). Derivation of analytical seismic fragility functions for common masonry bridge types: methodology and application to real cases. Engineering Failure Analysis, 68: 275-291.
204. Zhang J, Huo Y, Brandenberg SJ, Kashighandi P (2008). Effects of structural characterizations on fragility functions of bridges subject to seismic shaking and lateral spreading. Earthq. Eng. Eng. Vib., 7(4):369–382.
205. Zhou Y, Banerjee S, Shinozuka M (2010). Socio-economic effect of seismic retrofit of bridges for highway transportation networks: a pilot study. Struct Infrastruct Eng, 6:145–157. https://doi.org/10.1080/ 15732470802663862.
206. Zuccaro G, Cacace F (2011). Seismic Casualty Evaluation: the Italian Model, an Application to the L'Aquila 2009 Event. In R. Spence et al. (eds.), Human Casualties in Earthquakes, Advances in Naturaland Technological Hazards Research 29, doi:10.1007/978-90-481-9455-1_12, c Springer Science+Business Media B.V.

This project has received funding from the European Union's Horizon 2020 research and innovation programme under grant agreement No 821046

6 ANNEX

Table 6.1: Vulnerability index for the exposure databases in Luchon area (per municipality).

			SERA		**INSEE**		**field measurement**	
Number	**Commune**	**Name**	Buildings	Vi	Buildings	Vi	Buildings	Vi
1	**31010**	ANTIGNAC	59.34	0.72	70.31	0.68	69.24	0.62
2	**31015**	ARGUT-DESSOUS	62.07	0.67	74.53	0.66	76.55	0.62
3	**31017**	ARLOS	107.73	0.72	114.14	0.7	113.83	0.63
4	**31019**	ARTIGUE	27.3	0.72	35.18	0.77	39.35	0.69
5	**31040**	BACHOS	33.82	0.74	33.97	0.7	30.81	0.64
6	**31042**	BAGNERES-DE-LUCHON	999.79	0.67	1787.08	0.7	1860.71	0.64
7	**31046**	BAREN	12.9	0.65	20.1	0.6	14.08	0.67
8	**31064**	BENQUE-DESSOUS-ET-DESSUS	37.33	0.72	39.25	0.65	44.45	0.62
9	**31067**	BEZINS-GARRAUX	61.2	0.67	69.09	0.66	66.98	0.65
10	**31068**	BILLIERE	24.17	0.72	23.62	0.68	27.93	0.67
11	**31081**	BOURG-D'OUEIL	37.77	0.72	32	0.68	35.32	0.62
12	**31085**	BOUTX	496.05	0.71	542.47	0.71	520.76	0.65
13	**31092**	BURGALAYS	99.42	0.72	110.07	0.68	105.68	0.61
14	**31123**	CASTILLON-DE-LARBOUST	55.34	0.72	83.19	0.67	74.02	0.62
15	**31125**	CATHERVIELLE	47.99	0.73	52.51	0.71	64.33	0.65
16	**31127**	CAUBOUS	14.27	0.74	16.5	0.79	17.94	0.62
17	**31129**	CAZARIL-LASPENES	23.3	0.71	27.42	0.69	23.43	0.62
18	**31132**	CAZAUX-LAYRISSE	38.86	0.73	43.74	0.68	46.75	0.62
19	**31133**	CAZEAUX-DE-LARBOUST	80.74	0.72	85.66	0.7	77.75	0.62
20	**31139**	CHAUM	143.07	0.73	164.94	0.67	179.28	0.62
21	**31142**	CIER-DE-LUCHON	169.57	0.7	193.44	0.67	188.19	0.62
22	**31144**	CIERP-GAUD	502.23	0.72	574.22	0.68	603.57	0.62
23	**31146**	CIRES	32.36	0.71	37.58	0.65	35.6	0.62
24	**31176**	ESTENOS	119.95	0.73	135.84	0.69	127.02	0.62
25	**31177**	EUP	115.03	0.72	123.07	0.68	118.63	0.62
26	**31190**	FOS	381.08	0.74	388.19	0.72	401.09	0.6
27	**31199**	FRONSAC	157.41	0.72	172.51	0.72	187.68	0.62
28	**31213**	GARIN	123.17	0.7	143.97	0.64	127.37	0.64
29	**31221**	GOUAUX-DE-LARBOUST	57.17	0.69	62	0.72	71.38	0.69
30	**31222**	GOUAUX-DE-LUCHON	58.83	0.71	64	0.68	71.49	0.69
31	**31235**	GURAN	66.62	0.73	73	0.72	75.12	0.62
32	**31242**	JURVIELLE	30.62	0.72	22.75	0.78	23.83	0.62
33	**31244**	JUZET-DE-LUCHON	163.82	0.68	232.81	0.62	227.8	0.65
34	**31290**	LEGE	38.9	0.74	42.81	0.75	46.3	0.62
35	**31298**	LEZ	64.22	0.74	71.45	0.68	69.53	0.62
36	**31316**	MARIGNAC	299.97	0.72	336.94	0.68	356.29	0.64

This project has received funding from the European Union's Horizon 2020 research and innovation programme under grant agreement No 821046

37	**31335**	MAYREGNE	53.96	0.72	60	0.72	62.09	0.62
38	**31337**	MELLES	183.85	0.74	193.72	0.73	174.25	0.65
39	**31360**	MONTAUBAN-DE-LUCHON	157.99	0.67	248.94	0.65	253.42	0.62
40	**31394**	MOUSTAJON	72.82	0.69	88.94	0.62	97.59	0.61
41	**31404**	OO	84.03	0.7	98.68	0.7	109.8	0.67
42	**31432**	PORTET-DE-LUCHON	27.66	0.72	30.53	0.74	31.79	0.62
43	**31434**	POUBEAU	55.3	0.7	61.69	0.64	53.23	0.67
44	**31465**	SACCOURVIELLE	22.59	0.72	26.29	0.71	27.03	0.62
45	**31470**	SAINT-AVENTIN	131.55	0.72	142.89	0.72	147.44	0.66
46	**31471**	SAINT-BEAT	409.87	0.71	368.36	0.7	375.4	0.62
47	**31500**	SAINT-MAMET	287.57	0.66	411	0.66	485.64	0.66
48	**31508**	SAINT-PAUL-D'OUEIL	60.63	0.72	73	0.72	80.13	0.67
49	**31524**	SALLES-ET-PRATVIEL	72.22	0.72	81.91	0.65	88.33	0.62
50	**31548**	SIGNAC	47.82	0.71	53.4	0.75	58.38	0.62
51	**31549**	SODE	20.73	0.73	21.65	0.76	22.34	0.62
52	**31559**	TR5BONS-DE-LUCHON	12.87	0.71	13.89	0.7	14.37	0.62
53	**31590**	BINOS	27.3	0.71	28.6	0.71	36.68	0.64
			Total	**Avg**	**Total**	**Avg**	**Total**	**Avg**
			6572.15	0.71	8103.84	0.69	8338	0.63